

KINETICS AND MORPHOLOGICAL DEVELOPMENT OF THE SULPHIDE
SCALE ON A NICKEL - 20 w/o CHROMIUM ALLOY AT 700°C AND LOW
SULPHUR POTENTIALS

TO MY PARENTS

and

PADDY

KINETICS AND MORPHOLOGICAL DEVELOPMENT OF THE SULPHIDE
SCALE ON A NICKEL - 20 w/o CHROMIUM ALLOY AT 700°C AND LOW
SULPHUR POTENTIALS

By

JOHN ANTHONY CHITTY, B. Met.

A Thesis

Submitted to the School of Graduate Studies
in Partial Fulfilment of the Requirements
for the Degree
Master of Engineering

McMaster University

October 1972

MASTER OF ENGINEERING (1972)
(Metallurgy)

McMASTER UNIVERSITY
Hamilton, Ontario

TITLE: Kinetics and Morphological Development of the
Sulphide Scale on a Nickel - 20 w/o Chromium
Alloy at 700^oC and Low Sulphur Potentials

AUTHOR: John Anthony Chitty, B. Met. (Sheffield University)

SUPERVISOR: Professor W. W. Smeltzer

NUMBER OF PAGES: (x); 129.

ABSTRACT

The kinetics for the sulphidation of a Ni-20 wt. % Cr alloy at 700°C and sulphur potentials below 10^{-9} atmospheres have been studied using a thermogravimetric technique. The morphology of the reaction product was studied using optical microscopy, electron probe microanalysis and X-ray techniques. The kinetics were observed to be parabolic at sulphur potentials below 5×10^{-10} atmospheres with rates much slower than those reported for pure chromium under similar conditions. The parabolic kinetic reaction rate constant was found to vary as a semilogarithmic function of sulphur potential. The reaction product consisted of an external scale, identified as mainly Cr_3S_4 , with dissolved nickel up to 5% and a subscale with morphological break-down of the alloy/external scale interface. Approximate determinations of the diffusivity of chromium in the alloy and the scale as well as sulphur diffusivity in the alloy have been made. Tentative mechanisms have been proposed to explain the diffusion control of the reaction and the stabilization of the external scale by dissolved nickel.

ACKNOWLEDGMENTS

The author wishes to express his sincere gratitude to his supervisor, Dr. W. W. Smeltzer, for his continued guidance and interest throughout the course of this study.

Many thanks are also due to Drs. J. S. Kirkaldy and D. J. Young for their helpful comments and discussion. The author also appreciates the invaluable assistance provided by Horst Neumayer, Tom Bryner, Martin van Oosten and Fred Smith. The drawings were carefully prepared by David Studley Hodgson and the thesis was typed with accuracy and patience by Mrs. Anita Miltimore to both of whom the author is gratefully indebted.

The materials were supplied through the good offices of Dr. L. A. Morris, Falconbridge Nickel Mines Research Laboratories, and the research was financed by a National Research Council grant to Dr. W. W. Smeltzer.

Lastly, the author wishes to thank the rest of the faculty, staff and graduate students of the Department of Metallurgy and Materials Science for making his stay at McMaster enjoyable and rewarding.

TABLE OF CONTENTS

	<u>Page</u>	
CHAPTER I	INTRODUCTION	1
CHAPTER II	REVIEW OF SULPHIDATION THEORY	3
	2.1 Introduction	4
	2.2 Sulphidation of Pure Metals	4
	2.2.1 Thermodynamics	4
	2.2.2 Defect Structures of Metal Sulphides	6
	2.2.3 Rate Laws Applicable to Sulphidation	11
	2.2.4 Effect of Gas Flow, Temperature and Pressure	13
	2.2.5 Sulphidation Mechanisms	14
	2.3 Alloy Sulphidation	19
	2.3.1 Classification and Modes of Alloy Sulphidation	21
	2.3.2 Alloy Sulphidation Rates	24
	2.3.3 Alloy Sulphidation Mechanisms	24
CHAPTER III	THE SULPHIDATION BEHAVIOUR OF NICKEL, CHROMIUM AND NICKEL-CHROME ALLOYS	36
	3.1 Introduction	36
	3.2 The Sulphidation of Nickel	37
	3.3 The Sulphidation of Chromium	41
	3.4 The Sulphidation of Nickel-Chromium Alloys	48
	3.5 Summary	52
CHAPTER IV	EXPERIMENTAL APPARATUS AND PROCEDURE	55
	4.1 Introduction	55
	4.2 Specimen Preparation	55
	4.3 Sulphidation Apparatus	57
	4.3.1 The Reaction Gas Production Apparatus	57
	4.3.2 The Reaction Chamber	60
	4.3.3 The Spring	62
	4.4 The Sulphidation Procedure	62

		<u>Page</u>
4.5	Gas Analysis	63
	4.5.1 Theory	63
	4.5.2 Procedure	66
4.6	Metallography	67
	4.6.1 Preparation	67
	4.6.2 Examination	70
4.7	Analytical Methods	72
	4.7.1 X-ray Techniques	72
	4.7.2 Electron Microprobe Analysis	72
CHAPTER V	EXPERIMENTAL RESULTS	74
5.1	Sulphidation Kinetics	74
5.2	Metallography	77
5.3	Phase Identification	93
	5.3.1 Electron Microprobe Analysis	95
	5.3.2 X-ray Analysis	101
CHAPTER VI	DISCUSSION	104
6.1	Introduction	104
6.2	Reaction Kinetics	105
	6.2.1 Parabolic Kinetics	105
	6.2.2 Linear Reaction Kinetics	110
6.3	Morphology	111
	6.3.1 The External Scale	111
	6.3.2 Morphological Breakdown	115
	6.3.3 Internal Sulphidation	116
	6.3.4 External Scale Stringers	119
CHAPTER VII	SUMMARY	121
CHAPTER VIII	FUTURE WORK	123
APPENDIX	X-RAY ANALYSIS DATA	124
REFERENCES		125

LIST OF FIGURES

		<u>Page</u>
Figure 2.1	Summary of various mechanisms leading to formation of sulphide scales on metals involving (a) An outward diffusion of cations and (b) inward diffusion of anions.	8
Figure 2.2	A: Model for p-type semiconducting sulphide B: Model for n-type semiconducting sulphide	9
Figure 2.3 ⁽²⁴⁾	Typical oxidation curves for formation of protective scales plotted in parabolic form.	20
Figure 2.4	Sulphidation modes of alloys.	22
Figure 2.5	(a) Interface stability model ⁽²²⁾ . (b) Fully developed depleted alloy spikes.	30
Figure 2.6 ⁽³¹⁾	A calculated diffusion path for internal sulphidation in Fe-Mn-S system.	33
Figure 3.1 ⁽⁴⁰⁾	Plot of H_2S/H_2 v's $1/T$ for the system nickel-sulphur (compositions of alloys are in wt. % of sulphur).	38
Figure 3.2 ⁽⁵¹⁾	The chromium-sulphur phase diagram.	44
Figure 3.3 ⁽⁵²⁾	Equilibrium studies of chromium sulphide stoichiometry as a function of sulphur potential.	45
Figure 3.4 ⁽⁵⁸⁾	700°C isotherm of the Ni-Cr-S phase diagram.	49
Figure 4.1	Schematic of kinetic assembly.	58
Figure 4.2	Plot of the measured P_{H_2S}/P_{H_2} atmosphere ratio against the sulphur bath temperature in °K by several workers.	68
Figure 5.1	Plot of weight gain per unit area against time for the sulphidation of a Ni - 20 w/o Cr alloy at 700°C and different sulphur potentials. The values of sulphur potential are in atmospheres.	75

		<u>Page</u>
Figure 5.2	Parabolic plot of weight gain per unit area against time for the sulphidation of a Ni - 20 w/o Cr alloy at 700°C and different sulphur potentials. Values of sulphur potential are given in atmospheres.	76
Figure 5.3	Semilogarithmic plot of sulphur potential against parabolic rate constant, k_p .	79
Figure 5.4	Photomicrographs of specimens sulphidized for various periods of time at a sulphur potential of 5.5×10^{-12} atmospheres.	81
Figure 5.5	Photomicrographs of specimens sulphidized for various periods of time at a sulphur potential of 1.6×10^{-11} atmospheres.	83
Figure 5.6	Photomicrographs of specimens sulphidized for various periods of time at a sulphur potential of 6.5×10^{-11} atmospheres.	85
Figure 5.7	Photomicrographs of specimens sulphidized for various periods of time at a sulphur potential of 2.3×10^{-10} atmospheres.	87
Figure 5.8	Micrograph of specimen sulphidized at sulphur potential of 5.5×10^{-12} atm. for 16 hours showing possible porosity at alloy/scale interface. Mag. 2000X.	90
Figure 5.9	(a) Micrograph of specimen sulphidized at sulphur potential of 1.6×10^{-11} atm. for 15 1/2 hours showing a series of fine stringers. Mag. 2000X.	91
	(b) Micrograph of specimen sulphidized at sulphur potential of 2.3×10^{-10} atm. for 8 hours showing a single large stringer. Mag. 2000X.	91
Figure 5.10	Micrograph of sample sulphidized for 12 hours at $P_{S_2} = 2.3 \times 10^{-10}$ atm. and etched with Vilella's reagent. Mag. 600X.	92
Figure 5.11	Micrograph of specimen sulphidized for 1/2 hours at $P_{S_2} = 8.8 \times 10^{-10}$ atm. Mag. 2000X.	92

		<u>Page</u>
Figure 5.12	Plot of external layer growth and subscale penetration against time for specimens sulphidized at $P_{S_2} = 6.5 \times 10^{-11}$ atmospheres.	94
Figure 5.13	Distribution profile after sulphidation at a sulphur potential of 5.5×10^{-12} atmospheres for 24 hours.	96
Figure 5.14	Distribution profile after sulphidation at a sulphur potential of 1.6×10^{-11} atmospheres for 15 hours.	97
Figure 5.15	Distribution profile after sulphidation at a sulphur potential of 6.5×10^{-11} atmospheres for 8 hours.	98
Figure 5.16	Distribution profile after sulphidation at a sulphur potential of 2.3×10^{-10} atmospheres for 13 hours.	99
Figure 5.17	Distribution profile after sulphidation at a sulphur potential of 8.8×10^{-10} atmospheres for 2 hours.	100
Figure 6.1	Plot of external scale stoichiometry against sulphur potential compared with Young's ⁽⁵²⁾ equilibrium studies.	112
Figure 6.2	Plot of sulphur potential ($\log_{10} P_{S_2}$) against alloy composition as a mole fraction to give a tentative phase diagram for the Ni-Cr-S system at 700°C .	114
Figure 6.3	Plot of subscale penetration against the square root of time for specimens sulphidized at a sulphur potential of 6.5×10^{-11} atm.	117
Figure 6.4	700°C isotherm of Ni-Cr-S phase diagram showing tentative composition path.	120

LIST OF TABLES

		<u>Page</u>
Table 3.1	Phases found in the range Cr-CrS _{1.5} at room temperature after Jellinek ⁽⁵⁰⁾ .	42
Table 3.2	Phases found on sulphurized chromium samples after Lifshin ⁽⁷⁾ .	47
Table 3.3	Summary of past sulphidation studies.	53
Table 4.1	Analysis of the NiCr alloy used.	56
Table 4.2	Computer program used to calculate sulphur partial pressure from gas analysis data.	69
Table 4.3	Nickel sulphamate plating bath composition and conditions.	71
Table 5.1	Parabolic rate constants as a function of gas composition and the sulphur potential.	78
Table 5.2	External scale thickness, subscale penetration, weight gain and volume fraction of subscale as a function of time.	80
Table 5.3	Phase analysis of the external scale by x-ray and electron microprobe techniques.	102

CHAPTER I

INTRODUCTION

Investigation of the corrosion behaviour of materials in sulphur-containing environments has been neglected in comparison to the work done in the field of oxidation with air, pure oxygen or oxygen-supplying atmospheres. It is only in recent years that an increased interest has developed in sulphur corrosion. This is due to the natural occurrence of sulphur and sulphur compounds in fuels and the difficulty in purifying these fuels. Sulphur is the cause of aggressive corrosion of materials that come into contact with hot combustion atmospheres derived from these fuels and also creates contamination problems in petroleum plants and chemical industries.

Although sulphidation, i. e. the reaction between sulphur and metal without specifying the source of sulphur, is termed as an oxidation process, the behaviour of sulphur is somewhat different from oxygen. As a result very little of the wealth of information collected on oxygen corrosion applies to sulphidation. Thus the fundamental mechanism(s) behind sulphidation phenomena is not completely understood and there is a drastic lack of fundamental data concerning metal-sulphur systems e. g. sulphide defect structures, metal-sulphur phase diagrams, diffusion data, etc.

The strength and the high-temperature corrosion resistance of nickel-base type alloys make them suitable for turbine, jet engine and heat-exchanger applications. They are also the subject of academic interest since fundamental studies of their sulphidation properties should lead to the understanding of the processes involved

and the development of improved sulphidation resistance.

Several workers⁽¹⁻⁷⁾ have investigated the kinetic behaviour of nickel-chromium alloys of varying compositions in various sulphidizing environments at elevated temperatures. Romeo et al⁽⁵⁾ studied the sulphidation of a Ni-20 wt. % Cr alloy at 700°C in hydrogen sulphide-hydrogen atmospheres with sulphur partial pressures ranging from 8×10^{-8} to 2×10^{-2} atmospheres. The present study is a continuation of the above work using the same alloy composition and temperature but under extremely low sulphur pressures ($P_{S_2} < 10^{-10}$ atmospheres). It is known⁽⁷⁾ that under these conditions only chromium sulphide is formed as the product scale. However the purpose of the study is to establish the precise morphology of the scale and to ascertain the dependence of the nature of the chromium sulphide and the reaction kinetics on sulphur partial pressure. Also the concentration gradients of nickel and chromium in the chromium-nickel sulphide phases and alloy are investigated.

The kinetic results were obtained by a thermogravimetric method in the form of weight-gain time continuous recordings. Parabolic kinetics were observed at all sulphur partial pressures where chromium sulphide is the sole corrosion product. At a pressure where the formation of nickel sulphide is thermodynamically possible predominantly linear kinetics were observed. The scale morphology was studied on samples from static experiments using metallographic, X-ray and electron probe techniques.

The following sections present an outline of theory applicable to sulphidation, a literature survey, a description of experimental and analytical techniques, experimental results and a discussion of them.

CHAPTER II

REVIEW OF SULPHIDATION THEORY

2.1 . Introduction

The thermodynamic properties of metals are such that when they are exposed to a gaseous environment a complex chemical system exists. Most metals will react to form stable films or scales depending on the conditions but interpretation of the reaction behaviour has proved to be very difficult.

The reaction between metals and sulphur in any form is considered an oxidation process. Thus the general principles of oxidation mechanisms apply quite readily to sulphidation. Unfortunately, the behaviour of a specific metal with sulphur is not necessarily the same as with oxygen since the physico-chemical properties of these two elements differ significantly. Many factors may influence the reaction process such as thermodynamics, diffusion of reactants in the scale and metal, structures of metal and scale, scale composition, gas solution in the metal phase, nucleation and mechanical properties of the scales. The above properties of the sulphides and oxides of a specific metal can also differ enough for the reaction behaviour to be different.

It is the purpose of this chapter to summarize the oxidation theory that is relevant to sulphidation. Many standard works⁽⁸⁻¹²⁾ exist that give a complete description of most aspects of oxidation and a recent comprehensive review of sulphidation has been written by Strafford⁽¹³⁾.

2.2 Sulphidation of Pure Metals

2.2.1 Thermodynamics

Elementary thermodynamic principles provide an initial guide to the likelihood of interaction between the metal and sulphur in its elemental form or combined in gases, e. g. hydrogen sulphide. The equation for the reaction between sulphur vapour and a divalent metal (M) to form metal sulphide (MS) may be simply written as:



N.B. Sulphur has several molecular species, i. e. it may exist as $S_2 \rightarrow S_8$ in the vapour as discussed by Berkowitz⁽¹⁴⁾, but diatomic molecular sulphur is predominant. Even so this will affect the sulphur activity in the vapour as discussed later.

The driving force for sulphide formation is the change in free energy (ΔG°) accompanying the reaction and if this is negative, i. e. $\Delta G^\circ < 0$, the reaction should be spontaneous. Many sulphur containing environments are at elevated temperatures where the standard free energy of formation of most metal sulphides is often negative⁽¹⁵⁾ so corrosion must be expected.

A more precise theoretical approach is to apply the van't Hoff reaction isotherm to equation (2.1):

$$\Delta G^\circ = - RT \ln k \quad (2.2)$$

where ΔG° is the standard free energy change for the reaction

R is the gas constant

T is the temperature in $^{\circ}\text{K}$ for the reaction
 and k is the equilibrium constant for the reaction
 For the formation of sulphide, k is given by the law of mass action
 as:

$$k = \frac{A_{\text{MS}}}{A_{\text{M}} \cdot (P_{\text{S}_2})^{1/2}} \quad (2.3)$$

where A_{MS} is activity of sulphide

A_{M} is activity of metal

P_{S_2} is partial pressure of diatomic sulphur vapour.

Assuming the activities of metal and metal sulphide are unity, i. e.
 M is insoluble in MS, then (2.3) reduces to

$$k_{\text{p}} = 1/(P_{\text{S}_2})^{1/2} \quad (2.4)$$

where k_{p} is the equilibrium constant in terms of partial pressure.
 Applying equation (2.4) to equation (2.2) gives

$$\Delta G^{\circ} = -RT \ln k_{\text{p}} = RT \ln (P_{\text{S}_2})^{1/2} \quad (2.5)$$

Similarly for dissociation of the sulphide

$$\Delta G^{\circ} = -RT \ln (P_{\text{S}_2})^{1/2} \quad (2.6)$$

Thus formation of the metal sulphide as given by equation (2.1) will occur only if the partial pressure of the sulphur in the reaction environment is greater than the dissociation pressure of the bulk sulphide at reaction temperature. The sulphur activities discussed are obtained only under true thermodynamic conditions of reversible

chemical equilibrium between the various species involved in expression (2.3) but these are rarely attained in practical situations.

In his review Strafford⁽¹³⁾ gives a comprehensive free energy vs temperature diagram for the formation of various sulphides. Ellingham⁽¹⁶⁾ and Richardson and Jeffes⁽¹⁷⁾ discuss the theory and use of these diagrams to summarize the thermodynamic properties of binary sulphides reviewed by Freeman⁽¹⁵⁾ and Kubaschewski et al⁽¹⁸⁾. Thermodynamics can only act as a guide to possible reaction and are of limited use. The corrosion product eventually covers the metal surface completely so that any subsequent reaction is controlled by the physical and chemical properties of the sulphide scale. Equation (2.1) no longer determines the course of the reaction and the problem is one of diffusion and phase boundary processes for which the mechanisms are complex.

2.2.2 Defect Structures of Metal Sulphides

After the initial step of adsorption of the gas on the metal surface, sulphur may dissolve in the metal and sulphide form on the surface either as a film or as discrete sulphide nuclei. These steps are functions of surface orientation, crystal defects on the surface, impurities in the metal and gas, and surface preparation. The sulphide then usually grows as a compact phase with reactants spatially separated. Now further reaction is only possible if at least one of the reactants passes through this superficial layer. In fact the reaction becomes a combination of several partial processes involved with the different regions of activity.

There is a distinct mechanism associated with each phase boundary. At the sulphide/sulphur interface there is chemisorption and dissociation of sulphur molecules into atoms and subsequent

formation of sulphide by incorporation of these atoms into the solid. At the metal/sulphide interface there is ionization of metal atoms into ions and electrons. Precipitation of sulphide is also possible under certain conditions at this boundary leading to internal sulphidation. The third and possibly most important process is the diffusion of either cations, M^{n+} , or anions, $S^{=}$, and migration of electrons through the sulphide lattice. The slowest of these three steps is the rate determining mechanism and the processes are summarized in Fig. 2.1⁽¹³⁾. They only apply to a sulphide layer which is compact, dense and pore free.

Before discussing the above mechanisms any further it is necessary to describe the defect structures of sulphides and rate laws involved with each mechanism. The defect nature of the sulphide, which is commonly a semiconductor, determines which of the reactants diffuse through the scale. Semiconductors are of two types, namely, metal excess or n-type and metal deficit or p-type. Models for both are shown in Fig. 2.2. Wagner⁽¹⁹⁾ proposed that both oxides and sulphides are not of exact stoichiometric composition. The non-stoichiometry is equivalent to the presence of point defects and in order to maintain electrical neutrality complementary valence or electronic defects are simultaneously created. The defects can be cation or anion vacancies or ions in interstitial positions in the lattice depending on the type of semiconductor. Sulphide conductivity has been shown to be several orders of magnitude lower than that of metals and is predominantly electronic due to movement of electronic defects, i. e. electron holes or electrons.

Many sulphides are p-type semiconductors e. g. NiS ^(20, 21). They contain a deficit of metal ions on the lattice and diffusion transport of metal cations is via these vacancies with conductivity occurring by transport of electron holes. An alternative p-type defect model involving an excess of anions in the interstitial position is unlikely because of the

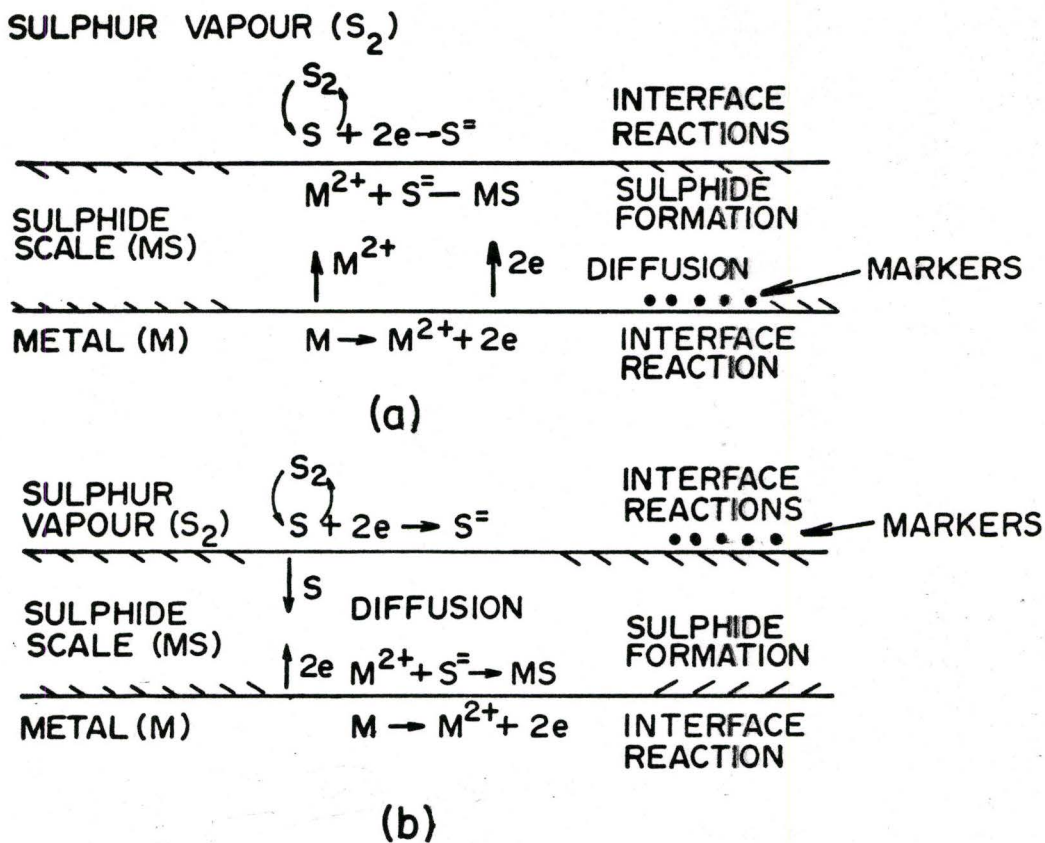
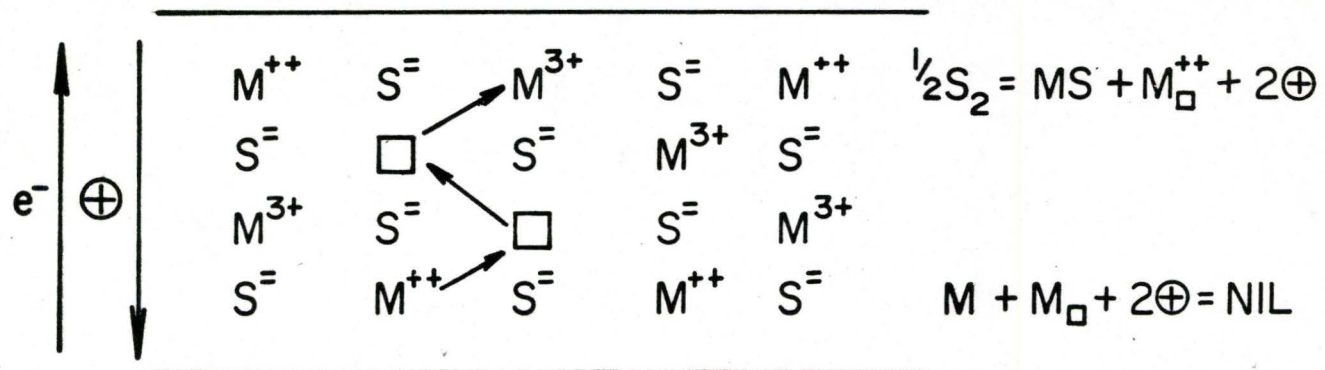


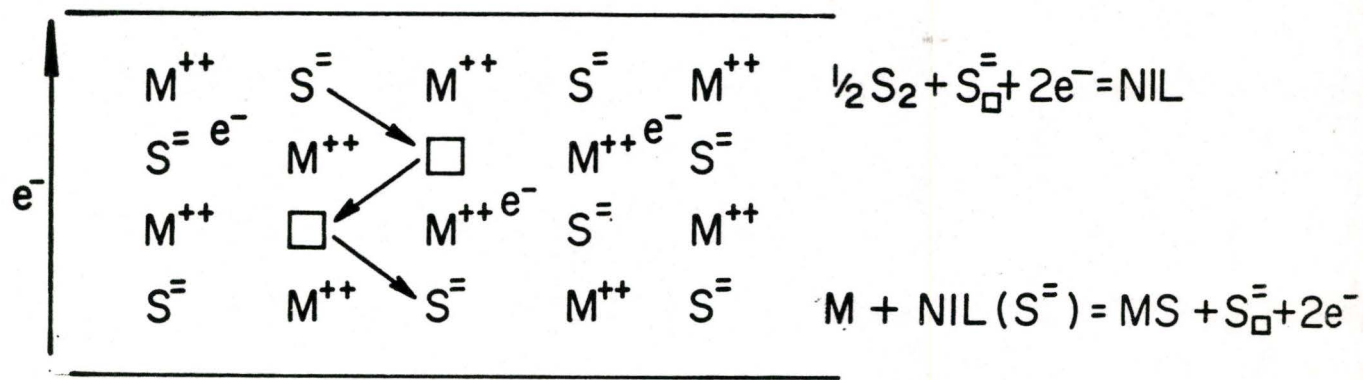
Fig. 2.1 Summary of various mechanisms leading to formation of sulphide scales on metals involving (a) An outward diffusion of cations and (b) inward diffusion of anions.

A.



(MODEL FOR P-TYPE SEMICONDUCTING SULPHIDE)

B.



(MODEL FOR N-TYPE SEMICONDUCTING SULPHIDE)

Fig. 2.2 A: Model for p-type semiconducting sulphide.
 B: Model for n-type semiconducting sulphide.

large ionic radius of the sulphur anion compared with the usually smaller cation and has not yet been observed in sulphides. N-type sulphides have also been observed. They have an excess of cations in the interstitial lattice positions which are free to diffuse and conductivity is via electron transport. The alternative n-type model of sulphur anion vacancies is theoretically possible but has not yet been reported. The conductivity or electron transport is necessary to create sulphur ions at the sulphide/sulphur interface.

Temperature and partial pressure of sulphur in the surroundings affect the extent and type of non-stoichiometry. It increases with decreasing sulphur pressure for n-type sulphide and this dependence varies from $P_{S_2}^{-1/2}$ to $P_{S_2}^{-1/6}$ depending on valency of the species. Conversely p-type sulphides display an inverse relationship to sulphur pressure i. e. non-stoichiometry increases with increasing sulphur pressure to the power of $1/2$ to $1/6$. The above relationships have been theoretically predicted from the defect models for sulphides and verified by measuring electrical conductivity of the sulphide as a function of sulphur pressure but not as successfully as for oxides. The importance of defect concentration dependence on sulphur pressure manifests itself in the sulphide scale where a sulphur pressure gradient exists. A defect gradient results from this and a concentration gradient in a single solid phase causes diffusion of ions via the defects.

Information concerning the defect nature of sulphides may be obtained by studying certain properties and reactions which depend on the concentration of the ionic and electronic defects. Individual experiments alone are inadequate but the collective consideration of physical and chemical data obtained from different investigations will yield the complete picture of the defect structure. Unfortunately, data from this field of investigation are still very sparse.

2.2.3. Rate Laws Applicable to Sulphidation

The formation and growth of compact, dense, pore-free sulphide scales is due to the three partial processes described, one of which is the slowest and hence rate controlling. Normally reaction kinetics reflect the rate-controlling process and are related to a number of empirical rate laws. If an empirical rate equation can be determined from kinetic studies of a reaction, it should be possible to match theoretical equations based on physical theory to explain the kinetics of the reaction.

The rate laws observed in the sulphidation of metals may take various forms since the processes involved are very complex but only two are predominant. They are linear and parabolic and refer to determination of changes in scale thickness, specimen weight or volume of sulphur consumed from the atmosphere as a function of time. The simplest, most reliable and most used quantitative technique is to measure changes in weight (ΔM) per unit surface area (A) which, provided the density is constant throughout the scale layer, are directly proportional to the scale thickness so

$$\frac{\Delta M}{A} = \frac{\text{mol. wt. of sulphur}}{\text{mol. wt. of sulphide}} \cdot \rho \cdot x \quad (2.7)$$

where ρ is density of sulphide
 x is thickness of sulphide layer

The linear rate law is expressed simply as

$$\frac{dx}{dt} = \frac{d}{dt} \left(\frac{\Delta M}{A} \right) = k_L \quad (2.8)$$

which on integration yields

$$\frac{\Delta M}{A} = k_L \cdot t + B \quad (2.9)$$

where k_L is the linear rate constant

t is the time

B is a constant

Ideally $B = 0$ when $t = 0$ but due to mixed reaction control during the initial stages of the reaction the linear portion of the kinetic curve may not necessarily go through the origin. Linear kinetics are observed when the scale is non-protective, i. e. porous or cracked, allowing direct contact between metal and gas. They are also observed when diffusion of species in the scale is sufficiently rapid that a phase boundary reaction is rate controlling. According to the principles of Pilling and Bedworth⁽²²⁾ if the volume ratio of sulphide to metal consumed is less than unity, a porous non-protective layer will be formed, and if greater than unity, a compact protective sulphide will be formed. Of course, there are exceptions to the rule e. g. large scales can break down mechanically due to internal stresses causing spalling and porosity thus enhancing the reaction rate.

The most common rate law observed is parabolic and is based on rate control by either cation or anion diffusion. It is best described theoretically (see section 2.2.5.). The rate of sulphidation is inversely proportional to film thickness:

$$\frac{dx}{dt} = \frac{k}{x} \quad (2.10)$$

which on integration and substitution into (2.7) yields the parabolic relationship

$$\left(\frac{\Delta M}{A}\right)^2 = k_p t + C \quad (2.11)$$

where k_p is the parabolic rate constant.

Other rate law relationships that have been formulated are cubic:

$$\left(\frac{\Delta M}{A}\right)^3 = k_c t \quad (2.12)$$

logarithmic:

$$\left(\frac{\Delta M}{A}\right) = k_l \cdot \log(a.t. + t_o) \quad (2.13)$$

and finally inverse logarithmic:

$$1/\left(\frac{\Delta M}{A}\right) = B - k_i \log t \quad (2.14)$$

which are usually applied to thin film formation at lower temperatures.

It is quite common for two or more rate laws to be combined in a single kinetic curve e.g. an initial linear region followed by a parabolic curve.

2.2.4 Effect of Gas Flow, Temperature and Pressure

Gas flow will increase the supply of reactant gas and remove gaseous reaction products. It affects the transition between interface control and gaseous diffusion control.

The effects of gas pressure may aid the interpretation of the reaction mechanism. No or very small pressure effect at high pressure (> 1 mm) is usually observed for stable sulphides but at low

pressure an effect is often observed. The flux of gaseous molecules is directly proportional to the pressure and the rate of gaseous diffusion to the reaction surface may be rate controlling. For an interface reaction such as the dissociation of diatomic sulphur molecules the rate would increase with the square root of the gas pressure. Again, in a diffusion process the sulphidation rate-pressure relationship can vary depending on defect structure and metal valency as previously discussed.

The temperature has an effect on rate equations since surface reactions are expected to obey an Arrhenius relation

$$K = K_0 e^{-Q/RT} \quad (2.15)$$

where K is rate constant

K_0 is constant with same units as K

Q is activation energy for the reaction

Rates of both phase boundary and diffusion controlled reactions are expected to vary exponentially with temperature.

2.2.5 Sulphidation Mechanisms

2.2.5 (a) Initial Sulphide Formation

Once the thermodynamic considerations for the sulphidation reaction are satisfied initial sulphide formation takes place by the following steps.

Initially gas molecules accumulate on the metal surface and since the impingement rate of gas is proportional to gas pressure it has been found that a monolayer of gas forms in less than 2 seconds at pressures greater than 10^{-6} torr. This means that there is no

problem in getting sulphur to be adsorbed on the metal surface but ultra high vacuum conditions would be preferred to prevent oxygen contamination. An actual detailed mechanism for chemisorption is not yet understood but the sticking probability of the gas is unity and decreases as gas is adsorbed as there is a repulsion mechanism between the gas ions. Dissociative chemisorption will occur if a gas atom adjacent to an adsorbed molecule changes place with the underlying metal atom in a place exchange process. Thus a sulphide nucleus is formed and this will coalesce with other nuclei to form one or more sulphide layers probably by surface diffusion processes. Initially the heat of chemisorption (ΔH) is about the same as the heat of formation of sulphide and the rate is fast. ΔH drops after the initial rapid sulphidation to a value characteristic of physical adsorption. A model has been suggested⁽²³⁾ in which both metal and sulphide bonds are broken during place exchange which has net activation energy ΔE . When this value is positive the process becomes temperature activated and a stable film forms and an electrical potential builds across it. Depending on environmental conditions further sulphidation can proceed in one of two ways.

2.2.5 (b) Film Formation

At low temperatures, especially below 100°C , further growth of the initially formed film of sulphide is essentially influenced only by the electrical potential gradient because of the high field built up across it. As the film grows the potential gradient decreases and the rates of ion and electron migration decrease rapidly until further growth is almost negligible.

Many theories of low and intermediate temperature sulphidation exist and are based on ion or electron migration as the rate-limiting

process. These theories are divided into two groups based on film thickness i. e. for thin films $< 100 \text{ \AA}$, and thick films of $10^2 - 10^4 \text{ \AA}$. Since the conditions investigated in this thesis are not related to this type of mechanism the reader is referred to Hauffe⁽¹⁰⁾ and Fehlner and Mott⁽²³⁾ for a detailed presentation of the major theories.

2.2.5 (c) Scale Formation

Under conditions of isothermal sulphide scale formation both linear and parabolic reaction kinetics have been observed. Electron field effects can be neglected in scales greater than $1 \mu\text{m}$ thick and provided the scale is compact and dense its growth usually follows a parabolic time dependence and can be considered protective. Parabolic kinetics are observed in most cases for metal sulphidation.

Wagner⁽¹⁹⁾ postulated a phenomenological theory to account for parabolic scale growth based on ambipolar diffusion of the reactants as the rate-controlling process provided the reaction product is a semiconductor. The semiconductor defects are a prerequisite for ionic species to be mobile. Now under conditions of interfacial equilibria transport of reactants across a sulphidation reaction product layer proceed by the independent migration of ions and electrons under the influence of an electro-chemical potential gradient. This is set up both by the dependence of defect concentration on variation of gas pressure across the layer and the fact that ionic mobility is less than electron mobility. The electrons move rapidly through the film to ionize chemisorbed gas atoms at the outer scale surface and the slower ions diffuse independently via defects to an interface depending on the type of defect to form fresh reaction product.

The current of the species 'i' in equivalents per cm^2 is given by:

$$J_i = Z_i V_i C_i = Z_i C_i B_i \left(\frac{d\mu_i}{dx} + Z_i F \frac{d\psi}{dx} \right) \quad (2.16)$$

where $Z_i C_i$ represents the concentration in equivalents per cm^3

V_i is particle velocity

B_i is particle mobility

μ_i is chemical potential

$Z_i F \psi$ is electrical potential (F is Faraday)

Parabolic rational rate constant expressions can be derived from the above relationship^(10, 11). The original form of the parabolic scaling rate constant was in terms of electrical conductivity and transport numbers of ions and electrons but a later and more popular form makes use of the more easily determined ion diffusivities. For a scale exhibiting transport by one component and predominantly electronic conductivity the parabolic rational rate constant, k_r , may be expressed as:

$$k_r = C_{eq} \int_{a_1(o)}^{a_1(i)} \left(D_2^* \left(\frac{Z_2}{Z_1} \right) + D_1^* \right) d \ln a_1 \quad (2.17)$$

or

$$k_r = C_{eq} \int_{a_2(i)}^{a_2(o)} \left(D_1^* \left(\frac{Z_1}{Z_2} \right) + D_2^* \right) d \ln a_2 \quad (2.18)$$

where k_r is in equivalents $\text{cm}^{-2} \text{sec}^{-1}$.

$a_{1,2}(o)$ is activity of metal, gas respectively at the scale-gas interface.

Z_1 and Z_2 are valence of metal and gas respectively.

D_1^* and D_2^* are self diffusion coefficients of cation and anion respectively.

$C_{eq.} = C_1 Z_1$ or $C_2 Z_2$ and is equivalent concentration of ions in equivalents cm^{-3} .

Thus according to the Wagner theory the scaling rate depends upon the difference in activity of the migrating species across the scale and large diffusivities give increased metal attack. Also if the defect concentrations in the scale are known as functions of the thermodynamic variables along with their mobilities then it is possible to predict the scaling rate of a metal provided phase boundary reactions are not rate-controlling and no irregularities in scale formation take place. Conversely, information concerning defect structure of the reaction product can be obtained from observed scaling kinetics. Many metal-oxygen systems have been found to verify Wagner's predictions but due to the lack of fundamental data such as defect structures and diffusivities fewer sulphide systems have been found. Several aspects of Wagner's model have been questioned in recent years since it is felt that defect structures are much more complex than originally suggested yet it still remains as the basic theory to parabolic oxidation kinetics.

Phase boundary reactions can control the scaling rate if interfacial reactions proceed more slowly than the diffusion processes. Linear kinetics are then observed, the amount of gas consumed being directly proportional to time. If the linear relationship is maintained indefinitely the scale is volatilizing, porous, cracked or spalled thus enabling gas to be rapidly transferred to the reaction front. If the scale is compact then the linear relationship is only followed for a period of time before diffusion controlled kinetics are obeyed.

Curves typical of those obtained in sulphidation experiments are shown in Fig. 2.3⁽²⁴⁾. Curve (a) represents ideal parabolic kinetics. Curve (b) which is often experimentally encountered shows a region of rapid scaling before onset of parabolic kinetics. The model for this is a combination of short circuit and lattice diffusion of reactants. Low resistance diffusion paths such as grain boundaries and line defects give rise to short circuit paths in scales. Their effect is minimized with increasing scale thickness. Curve (c) shows a region of slow kinetics governed by a constant reaction rate of some type before onset of parabolic kinetics. This is due to some type of phase boundary reaction. It could be adsorption control of the gas at the scale/gas interface or reaction control at the metal/scale interface.

Occasionally sulphidation reactions have been observed to be initially parabolic followed by linear kinetics (paralinear). The transition in behaviour appears to be associated with the development of mechanically imperfect, porous or partially fused scales.

2.3 Alloy Sulphidation

In general pure metals are not suitable for high temperature structural engineering applications due to lack of strength. Alloying additions must be made to the base metal to overcome this deficiency but in doing so the selected additions must, if possible, improve the sulphidation resistance of the material. Since alloys contain two or more sulphidizable constituents the situation becomes more complex with the addition of more factors and parameters. For example, one component will sulphidize preferentially to the others since the components have different affinities for sulphur as illustrated by the Ellingham diagram for sulphide formation. Other factors that must be taken into account are the solubility limits of the phases, the

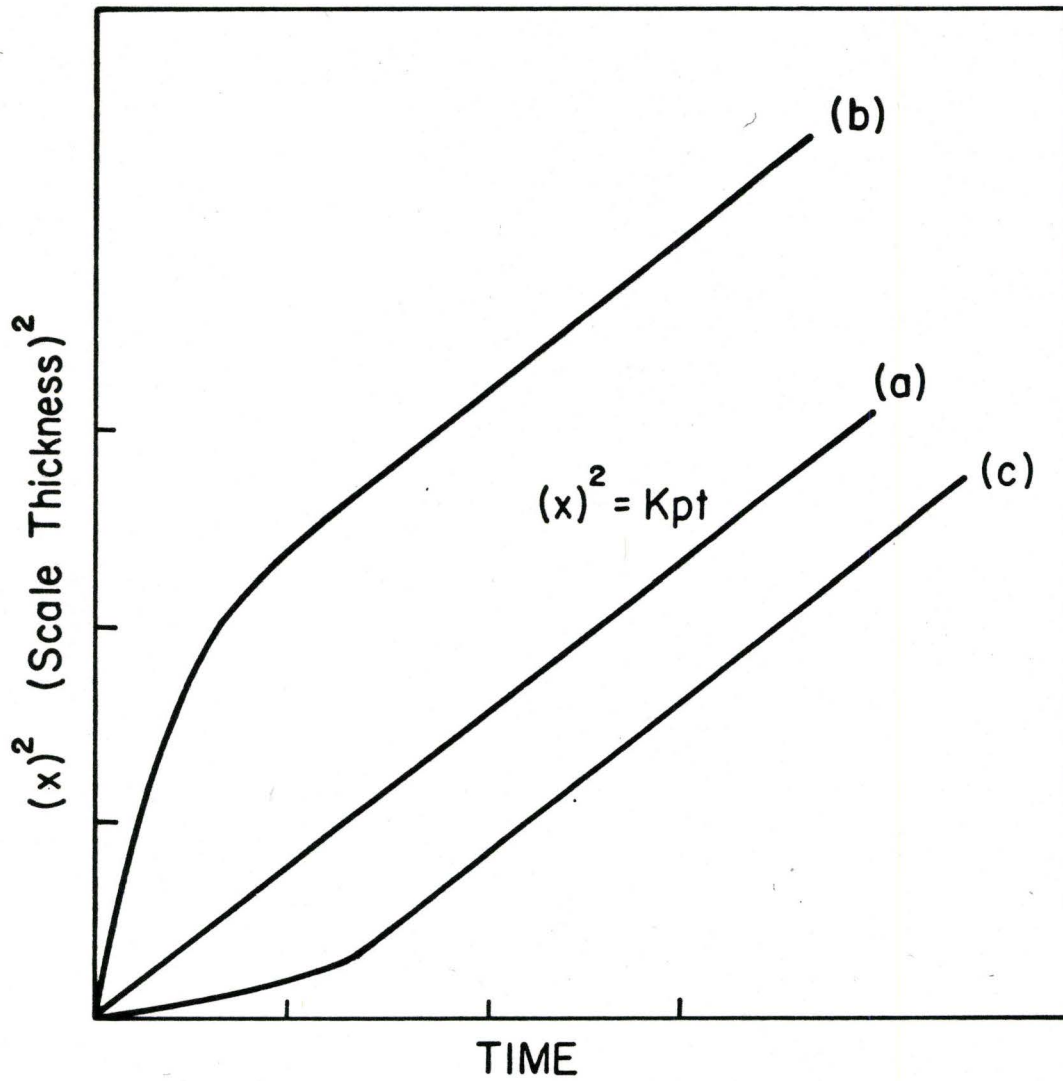


Fig. 2.3⁽²⁴⁾ Typical oxidation curves for formation of protective scales plotted in parabolic form.

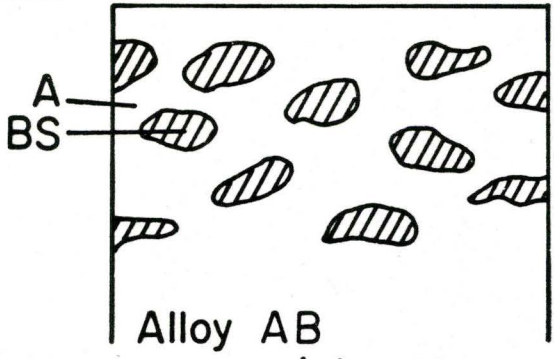
diffusion rates of atoms in both the alloy and the scale, possible formation of ternary compounds, the effect of alloy additions on the defect structure of the base metal sulphide, internal precipitation of sulphide in the alloy, and relative volumes of the various phases which will affect porosity and cracking.

Owing to the complexity of the situation no unified theory exists to predict the sulphidation behaviour to be expected. The general sulphidation principles plus the known pure metal behaviour of the alloying elements offer two possible approaches to the problem of developing sulphidation resistant alloys. Firstly Wagner⁽²⁵⁾ has established principles according to which it should be possible to reduce the number of defects present in a semiconducting sulphide scale by the incorporation into that scale of a suitable alloying element with a different valency from the base metal. This effect should reduce the rate of a diffusion controlled reaction. Unfortunately certain practical limitations severely restrict the application of this alloying theory. The second approach is to consider an alloying element that sulphidizes preferentially to the base metal at a slower rate and forms a protective layer. The preferentially formed sulphide must have a lower defect concentration than the base metal sulphide. Thermodynamics, usually in the form of ternary phase diagrams for a binary alloy AB and sulphur, provide useful information in predicting the alloying element likely to be preferentially sulphidized and possible phases formed.

2.3.1 Classification and Modes of Alloy Sulphidation

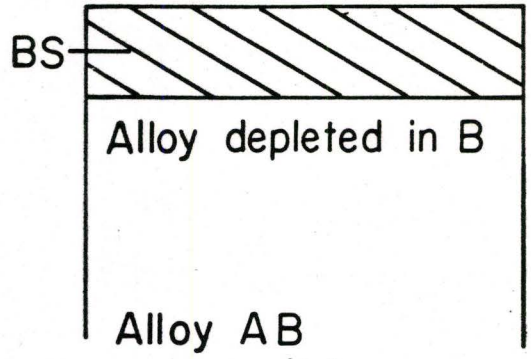
Once the existence of a more noble element has been determined, it is usually beneficial to consider the possible modes of sulphidation as classified by Moreau and Benard⁽²⁶⁾ and Wood⁽²⁷⁾ based on experimental observations. They are illustrated diagrammatically in Fig. 2.4.

CLASS I Atmosphere



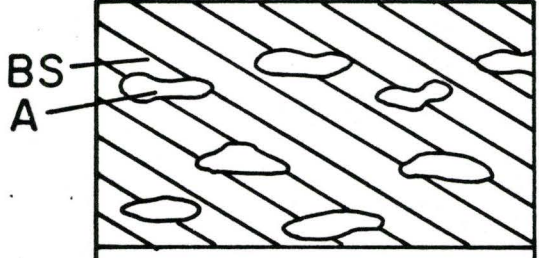
(a)

Atmosphere



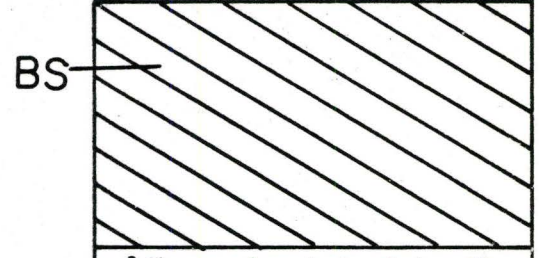
(b)

Atmosphere



(c)

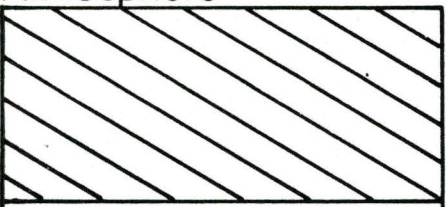
Atmosphere



(d)

CLASS II Atmosphere

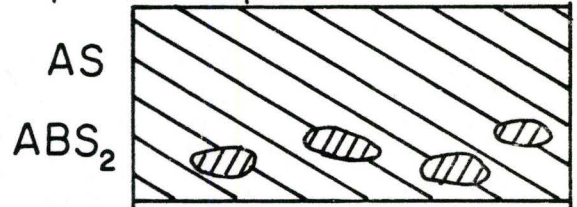
(A,BS)



(e)

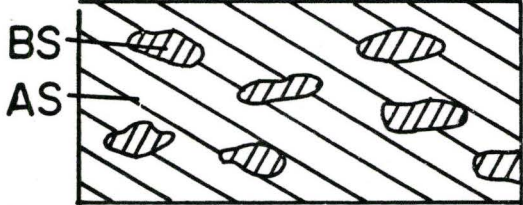
AS
ABS₂

Atmosphere



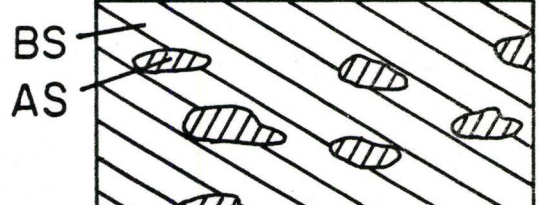
(f)

Atmosphere



(g)

Atmosphere



(h)

Fig. 2. 4 Sulphidation modes of alloys.

An alloy, AB, represents the general alloy under consideration in which A is the more noble metal.

Class I refers to the case of selective sulphidation. In (a) and (b) the addition B is the minor constituent. B may sulphidize internally as in (a) forming particles of BS in a matrix of A, the sulphur pressure in the atmosphere being less than the dissociation pressure of AS. Again under these conditions an exclusive external scale, BS, can form as in (b) with or without internal sulphidation. In situations (c) and (d) the alloy addition B is now the major component. In (c) B sulphidizes exclusively leaving the unreacted metal A dispersed in BS. Situation (d) shows external BS with the enrichment of A in a zone at the alloy surface.

Class II deals with the simultaneous sulphidation of both elements, the sulphur pressure in the atmosphere being greater than the equilibrium dissociation pressures of both sulphides. In (e) sulphides of A and B give a solid solution (A, B)S with the possibility of some internal (A, B)S richer in B than the surface scale. A double sulphide is formed in (f), often as a spinel, which may give a complete surface layer of variable composition or particles incorporated into a matrix of AS if the reaction is incomplete. In (g) and (h) the sulphides are virtually insoluble in each other. B is the minor component in (g) and BS lies internally beneath a mixed layer of AS and BS. When B is the major component there is no internal sulphide as in (h).

This classification is only general and provides some clarity to alloy sulphidation. There are variations from these simple cases as a result of mechanical stresses, coalescence of sulphides and other factors characteristic of particular systems. The case of multilayered scales also exists in two variations. Firstly, a minor addition of less noble metal may sulphidize initially before the more noble metal begins to sulphidize at a faster rate on top of the first layer. Also, if a metal that sulphidizes preferentially exhibits several stable sulphides, they may appear in various proportions depending on conditions of temperature

and pressure. The sulphide richest in metal will be located adjacent to the alloy surface and the phase richest in sulphur adjacent to the gas phase. Even under conditions of high sulphidation potentials where only the most stable sulphide is expected the potentials at the alloy-sulphide interface will be low enough to favour formation of the other sulphides and they will grow.

2.3.2. Alloy Sulphidation Rates

The empirical relationships put forward in section (2.2.3) apply equally as well to alloy sulphidation but experimental kinetic data obtained often deviates from the ideal rate laws owing to the increased complexity of the mechanisms. The following conditions are necessary for the parabolic rate law to hold in alloy systems. There must be no change in the sequence of reaction layers with time. The scale structure must not alter i. e. no cracking or phase transformations. The interface reactions must be sufficiently rapid for the establishment of local thermodynamic equilibrium. Finally, in order to define boundary conditions, the composition of the alloy at some point must be the initial composition, and the diffusivities of the various species should not be a function of concentration.

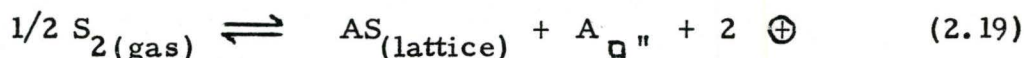
2.3.3 Alloy Sulphidation Mechanisms

There are a large number of kinetic factors to be considered in any theoretical description of alloy sulphidation. Several models have been suggested for a few limiting cases and those relevant to this study are discussed here.

2.3.3 (a) Variation of Defect Concentration in Mixed Sulphides Forming Continuous Ideal Solid Solutions

For the purpose of this discussion the formation of a single phase divalent p-type semiconducting sulphide (AS) on the surface of alloy AB is considered. The alloy element B has a different valency from A, is present as a minor addition (i. e. in amounts insufficient to form a separate sulphide phase) and is freely soluble in the parent sulphide. Both nickel and chromium fit these conditions being divalent and trivalent respectively.

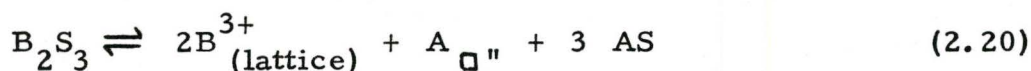
The metal deficit sulphide has a formula of the type $M_{(1-\delta)}S$ due to vacancies in the cation lattice, the anion lattice considered being almost perfect. To maintain electrical neutrality an equivalent number of defect electrons must be introduced. The formation of defects proceeds by the following reaction:



where A_{\square} represents cation vacancy

and \oplus is an electron hole or cation of higher valency on the lattice

The addition of a small amount of trivalent metal sulphide, B_2S_3 , results in an increase in the number of cation vacancies and decrease in electron holes by the following equation:



Thus if the formation of AS displays parabolic kinetics i. e. diffusion controlled, then an increase in cation vacancies would result in an increase in sulphidation rate. The total conductivity decreases since electron holes are destroyed. This situation would be expected for

nickel with very small additions of chromium. The converse effect of a decrease in rate would be given by small additions of lower valency sulphide to the higher valency sulphide as with small amounts of nickel in chromium sulphide. The complete opposite is found for n-type semiconductors. Small alloy additions may prove useful in providing defect data of the parent sulphide but do not enhance sulphidation resistance to a large degree.

2.3.3 (b) Preferential Sulphidation Mechanisms

There are two distinct models discussed in this section. Both concern the case where one constituent, A, of the alloy AB is more noble than the other. In the first case the more noble element can be in fact noble, i.e. it will not react with the corrosive atmosphere, or it can be made essentially noble in that the partial pressure of the gas is less than the dissociation pressure of the sulphide of this element. For this situation Wagner⁽²⁸⁾ showed that the steady state, diffusion controlled growth of BS on the alloy AB follows a parabolic rate lower than that of the pure metal B given by

$$\frac{k}{k_o} = \frac{P_a^{1/n} - P^{1/n}}{P_a^{1/n} - P_s^{1/n}} \quad (2.21)$$

where k and k_o are the parabolic rate constants for BS growing on alloy and pure B respectively,

P_a is applied pressure of sulphur

P is dissociation pressure of sulphide in equilibrium with the alloy composition at the alloy-sulphide interface

P_s is dissociation pressure of sulphide in equilibrium with pure B.

n is a constant determined by the defect equilibrium established locally within sulphide BS.

Internal sulphidation and mutual solubilities of sulphides have been neglected and it is assumed a p-type sulphide has been formed. Now if the alloy is nearly an ideal solid solution the equation can be written

$$\frac{k}{k_o} = \frac{1 - (X_{eq}/X)^{2/n}}{1 - X_{eq}^{2/n}} \quad (2.22)$$

where X is mole fraction of B in the alloy at the alloy-sulphide interface
 X_{eq} is mole fraction of B in alloy that would be in equilibrium with BS at applied pressure P_a , and is $\ll 1$ for a very stable sulphide.

When $X \gg X_{eq}$ there is very little decrease in the sulphide growth rate determined by diffusion through the sulphide, but as X approaches X_{eq} the growth rate must decrease and it will then be determined by the interdiffusion process in the B depleted alloy layer. The model was applied fairly successfully to Ni-Pt alloy oxidation. It was found from this that the more noble alloying element must diffuse slowly in the alloy phase to effectively reduce the scaling rate. Also the alloy must not readily dissolve the reaction gas in order to remain effective against subscaling by an internal sulphidation mechanism.

The second case under discussion concerns competitive sulphidation where the thermodynamic conditions are such that both elements in the alloy can sulphidize but one is more stable than the other. Depending on the relative diffusivities of the elements in both the alloy and scales and their compositions several different situations may arise. Wagner⁽²⁹⁾ examined the case in which BS has a lower dissociation pressure than AS but AS grows faster on pure A than BS grows on pure B i. e., the rate of diffusion of B in BS is significantly smaller than A in AS and provides a stable protective scale.

For BS to form alone initially and to be maintained the alloy

must be rich in B and the diffusion rate of B in the alloy must be reasonably high to avoid depletion at the alloy surface. Formation of AS will then not be thermodynamically possible. If both the concentration and rate of diffusion of B in the alloy are very low only the formation of AS may be possible with an enhanced sulphidation rate. At intermediate alloy compositions and diffusion rates, the attack of both components may occur allowing the formation of a complex scale consisting either of two insoluble sulphides (AS and BS) often as alternate layers, or some kind of compound sulphide of the type (A, B)S. The reader is referred to these considerations in section (2.3.1) and Fig. 2.4.

From the above it is desirable to know the minimum concentration of B required for exclusive formation of the highly protective scale BS. The diffusion rate for supply of B to the alloy-scale interface must be greater than the consumption of metal. Wagner⁽²⁹⁾ has derived an expression for this minimum concentration ($X_{B(\min)}$) by setting the diffusive flux equal to rate of consumption as follows.

$$X_{B(\min)} = \frac{V}{Z_B M} \left(\frac{k_o}{D_B} \right)^{1/2} \quad (2.23)$$

where V is volume/g.mol. of alloy and/or sulphide

Z_B is valency of B

D_B is diffusivity of B in the metal and alloy

k_o is parabolic rate constant for pure BS on B

Several systems have been found to agree with this expression.

2.3.3 (c) Morphological Breakdown of Alloy/Sulphide Interface

The models discussed so far are based on the premise that a planar metal-sulphide interface is stable in noble-base metal alloy

systems. In fact under certain conditions this is not true. For a system where only one component sulphidizes and the interdiffusion in the alloy is fast compared with the rate at which the component is consumed by scale growth ($D_{AB} \gg k_o$) the component cannot become depleted in the alloy to any great extent. If the interface is assumed to be slightly perturbed and take the form of a sine wave profile as shown in Fig. 25(a)⁽²⁹⁾ then the points (1) of the alloy most advanced into the scale react most rapidly because the concentration gradient through the scale is steepest at these points. Thus the perturbation decays and planarity is restored. With the restriction that diffusion of the sulphidizing component is much slower in the alloy than in the scale the perturbations grow at the points (2) deepest into the alloy since the concentration gradient of component in the alloy is steepest at these points. Thus columns of scale can penetrate into the alloy (Fig. 25(b) and are separated by regions rich in the non-reacting component. This is not internal sulphidation but can be found in conjunction with it. Wagner⁽²⁹⁾ found that the necessary but not sufficient condition for instability of a planar interface is given by

$$\left(\frac{X_A}{1 - X_A} \right) \frac{(D/V)_{\text{alloy}}}{(D^*/V)_{\text{sulphide}}} < 1 \quad (2.24)$$

where X_A is mole fraction of reacting component in alloy
 D^* is self diffusion coefficient of cation in scale at alloy interface.

V is molar volume.

Thus spike formation is favoured by dilute reaction component as well as slow diffusivity in the alloy compared with the scale. The more extended tips of the alloy spikes may spheroidize and give rise to isolated particles embedded in the external scale.

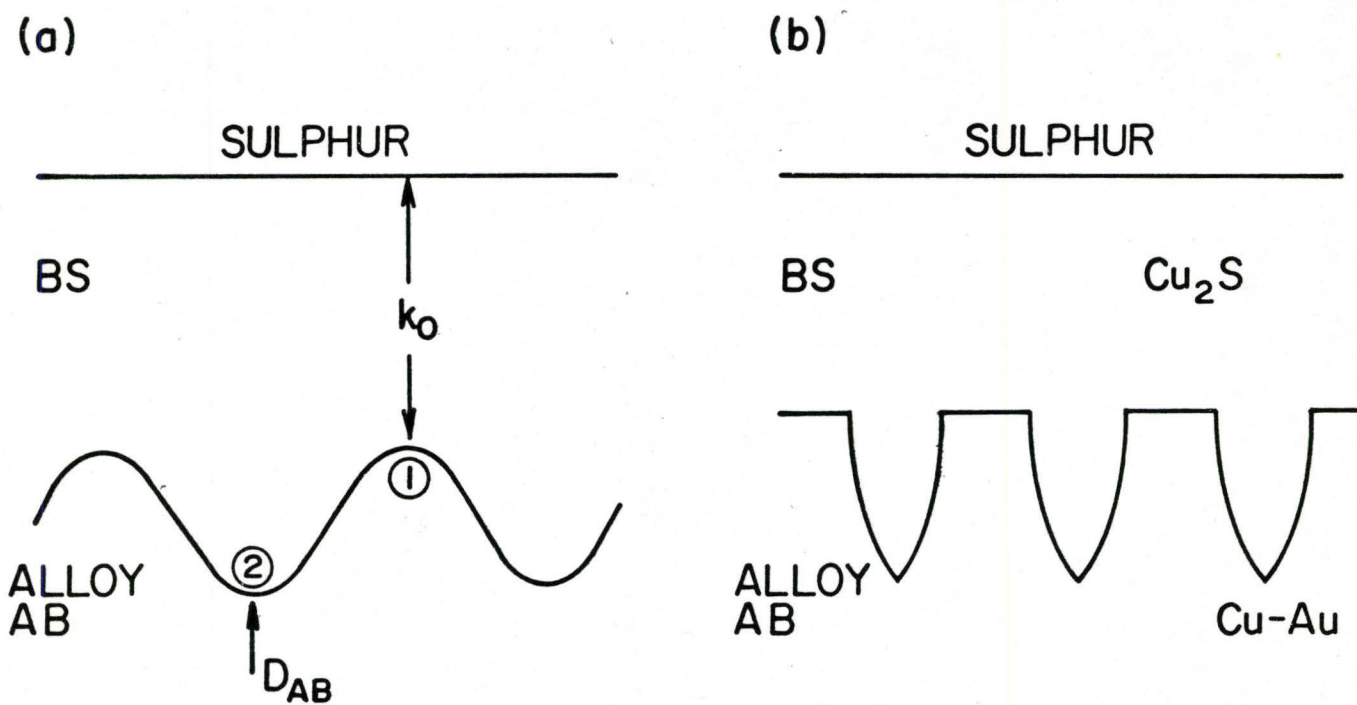


Fig. 2.5 (a) Interface stability model⁽²²⁾.

(b) Fully developed depleted alloy spikes.

2.3.3 (d) Internal Sulphidation

This is the process by which sulphur diffuses into an alloy and causes subsurface precipitation of the sulphides of one or more alloying elements which are less noble than the solvent metal. At one time it was believed that a large number of different variables had to be satisfied for initial sulphidation but these have since been questioned and the conditions and description may be given generally.

If the sulphur diffusion coefficient in the alloy is much greater than the alloy interdiffusion coefficient i.e., $D_S \gg D_{AB}$, sulphur, if soluble, will diffuse so rapidly that the less noble component, B, of the binary alloy AB will be effectively precipitated in situ as sulphide. The mole fraction of the sulphide will be the same as the initial mole fraction of B in the alloy. Assuming diffusion as the rate controlling mechanism, since experiment has shown that the process follows parabolic kinetics, Wagner⁽³⁰⁾ defined the parabolic rate constant as follows:

$$k = \frac{2 X_S^A}{V X_B^S} D_S^{1/2} \quad (2.25)$$

where X_S^A is the solubility of sulphur in A given by the concentration of sulphur at metal/scale interface.

X_B^S is the solubility of B in sulphide

and V is the stoichiometric ratio of sulphur to metal atoms in the sulphide precipitate.

Thus depth of subscale penetration depends only on D_S . By applying Fick's second law to the sulphur diffusion through the subscale and solving for boundary conditions expressions have been derived for the

parabolic rate constant under different limiting conditions. When the counterdiffusion of the component B is significant D_S is of the order of D_{AB} but $D_S \ll \frac{X_B^S}{X_S^A} \cdot D_{AB}$ so

$$k = \frac{\pi^{1/2}}{V} \frac{X_S^A}{X_B^S} \left(\frac{D_S}{D_B}\right)^{1/2} \quad (2.26)$$

Kirkaldy⁽³¹⁾ has treated the problem using a ternary diffusion model based on the thermodynamics of irreversible processes as introduced by Onsager⁽³²⁾ and developed by himself among many others⁽³³⁾. Using the 'virtual path' concept^(34, 35) the matrix diffusion profiles and precipitate distribution have been obtained in closed form for systems of arbitrary constitution. Fig. 26⁽³¹⁾ shows a 'virtual path' calculated for the reaction between MnS and an Fe-1.08% Mn alloy. It is a ternary diffusion path for an infinite or semi-infinite diffusion couple calculated on the basis of a planar interface for all phases appearing in the couple. These paths may reveal the existence of supersaturated regions of the couple which can lead to internal precipitation. The 'virtual path' of the type shown is not expected to last since precipitation occurs and presumably the actual diffusion path runs close to the phase boundary.

Kirkaldy has made several assumptions. The internal precipitate must be small, finely dispersed uniformly and equilibrated with the immediate surroundings. Also parabolic kinetics must be obeyed, but there are no restrictions on the magnitude and variability of kinetic parameters and constitution. Binary interaction equations have been used and solved for parabolic conditions. From these equations for concentration of components, 1 and 2, have been developed in terms of diffusivities and position. The amount precipitated per unit volume at any position x in time t is given by:

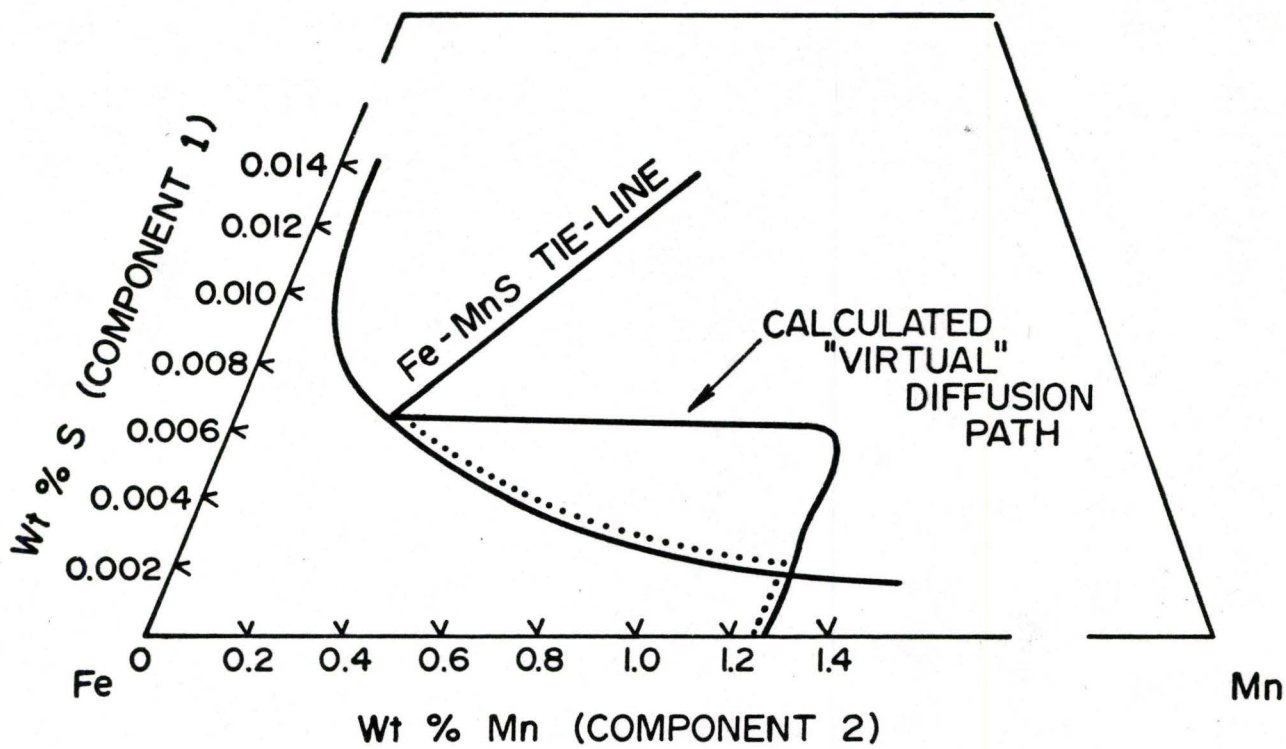


Fig. 2.6⁽³¹⁾ A calculated diffusion path for internal sulphidation in Fe-Mn-S system.

$$P = \int_0^t \dot{p} t = \int_0^t \frac{1}{t} \left(D_1 \frac{d^2 C_1}{d\lambda^2} + \left(\frac{\lambda}{2} + \frac{dD_1}{d\lambda} \right) \frac{dC_1}{d\lambda} \right) dt \quad (2.27)$$

where the normalized co-ordinate $\lambda = x/\sqrt{t}$.

The expression for C_1 has been modified for the limiting conditions $D_1 > D_2$, $\frac{d^2 C_1}{d\lambda^2} \gg 1$, i. e., diffusivity of gas in the alloy is greater than diffusivity of reaction component in the alloy but $D_{1 \text{ eff}} \approx D_{2 \text{ eff}} \approx D_2$, and substituted into equation 2.27 which becomes

$$P(x, t) = \frac{D_1 - D_2}{D_2} C_1(1) \operatorname{erf} c \frac{\lambda}{2 \frac{D_1}{D_2}} \quad (2.28)$$

This expression has been experimentally verified by applying data to predict P and matched against observations.

Wagner⁽³⁰⁾ also developed an equation for the volume fraction of sulphide ϕ in the subscale region as follows:

$$\phi = \frac{2\gamma}{\pi} \frac{x_B^S}{x_S^A} \cdot \frac{D_{AB}}{D_S} \quad (2.29)$$

When the precipitating sulphide is very stable the subscale particles are very fine. If the sulphide is more easily dissociated the particles tend to coalesce and are coarser. Also the size depends on the gas partial pressure so particle size will decrease with distance into the alloy. Particle coarsening is by an Ostwald ripening mechanism. There can also be preferential penetration along grain boundaries where the diffusion of sulphur may be more rapid. Also grain boundaries especially if they contain inclusions act as preferential nucleation sites.

A situation also exists where formation of internal and external scale of the same metal sulphide, i. e., that of the less noble component,

occurs simultaneously. Two models have been put forward to explain this. The first by Thomas⁽³⁶⁾ proposes that the presence of a small amount of noble metal dissolved in the external scale increases the dissociation pressure of the sulphide. Thus at the interface the partial pressure of sulphur is greater than the dissociation pressure of the sulphide which would normally be expected. Thus the penetrating sulphur ions are capable of forming internal sulphide of the less noble metal. There would not be dissolved noble metal in the internal particles.

The second approach by Wagner⁽³⁷⁾ states that the formation of external scale of the less noble component sulphide leads to depletion of this component in the alloy at the scale interface especially if its diffusivity in the alloy is slow. Assuming the sulphur diffusivity in the alloy is high then at the alloy-scale interface where the reacting metal activity is low the concentration of dissolved sulphur atoms is greater than in the interior of the alloy where the metal activity is high.

The sulphur activity in the alloy + sulphide is given by the equilibrium

$$BS_{(s)} = B_{(alloy)} + S_{(alloy)} \quad (2.30)$$

Consequently there will be a steep sulphur concentration gradient in the alloy due to inward diffusion of the sulphur and precipitation of the internal sulphide. Thus the sulphur activity at the interface rises well above the dissociation pressure of the sulphide so it is possible for external scale to grow.

CHAPTER III

THE SULPHIDATION BEHAVIOUR OF NICKEL, CHROMIUM AND NICKEL-CHROME ALLOYS

3.1 Introduction

The following review discusses the experimental observations found so far for the reaction between sulphur and nickel, chromium and Ni-Cr alloys resulting in the formation of sulphide scales. The field of 'hot corrosion' is not covered as this involves complex phenomena observed using multicomponent gases at high temperature in the presence of impurities such as sodium and vanadium. The experimental data collected so far on the sulphidation behaviour of the metals and alloys in question is not very substantial. The interpretation of the data that does exist is confused by uncertainties and contradictory opinions due to the lack of basic information and experience.

Two main sulphidizing environments have been used. One method is to vapourize sulphur from a melt, the sulphur pressure being controlled by the melt temperature according to the Clausius-Clapeyron equation. The other is to use gas mixtures of hydrogen sulphide and hydrogen. On the basis of the equilibrium $\text{H}_2\text{S} \rightleftharpoons \text{H}_2 + 1/2 \text{S}_2$ the sulphur partial pressure P_{S_2} is defined at every temperature by the ratio of $P_{\text{H}_2\text{S}}/P_{\text{H}_2}$. Zelouf and Simkovich⁽³⁸⁾ have argued that the presence of hydrogen in the gas mixture possibly affects the defect structure of the sulphide scale. They propose that if hydrogen is soluble in a p-type semiconducting sulphide then additional cation

vacancies will be created. Calculation of P_{S_2} involves the assumption that at temperatures in the order of 1000°K the sulphur vapour is diatomic⁽³⁹⁾ but it has already been pointed out⁽¹⁴⁾ that higher molecular weight species exist to a lesser extent. Thus measurement of sulphur pressure dependence of the parabolic rate constant to determine the defect structure of the scale involves precise determination of partial pressure of diatomic molecules.

In general the formation of nickel and chromium sulphides is diffusion controlled i. e., parabolic kinetics are observed after initial linear kinetics due to adsorption and nucleation phenomena. Unfortunately the interpretation of parabolic kinetics for nickel, chromium and its alloys is hindered by the formation of inner porous layers and lack of diffusivity data. The interpretation for the binary alloys is especially complicated by the inherent complexity of the ternary diffusion occurring in a heterogeneous system. As a result a quantitative diffusion model for the sulphidation process has not yet been advanced.

3.2 The Sulphidation of Nickel

Thermodynamic data on the Ni-S system have been illustrated by Rosenqvist⁽⁴⁰⁾ and more recently by Kellerud and Yund⁽⁴¹⁾. It is shown in Fig. 3.1⁽⁴⁰⁾ that at above 800°C a liquid sulphide is to be expected for a wide range of sulphur pressures. Solid nickel sulphide of bulk stoichiometry Ni_3S_2 and NiS can be obtained below 800°C in a restricted range of sulphur pressure. Also the liquid eutectic Ni_3S_2 - Ni can exist at temperatures as low as 645°C .

The defect structures of nickel sulphides have still to be accurately determined. In most cases structures have been postulated only in order to fit experimental data. X-ray diffraction and density measurements^(20, 21) showed NiS to have a p-type defect structure.

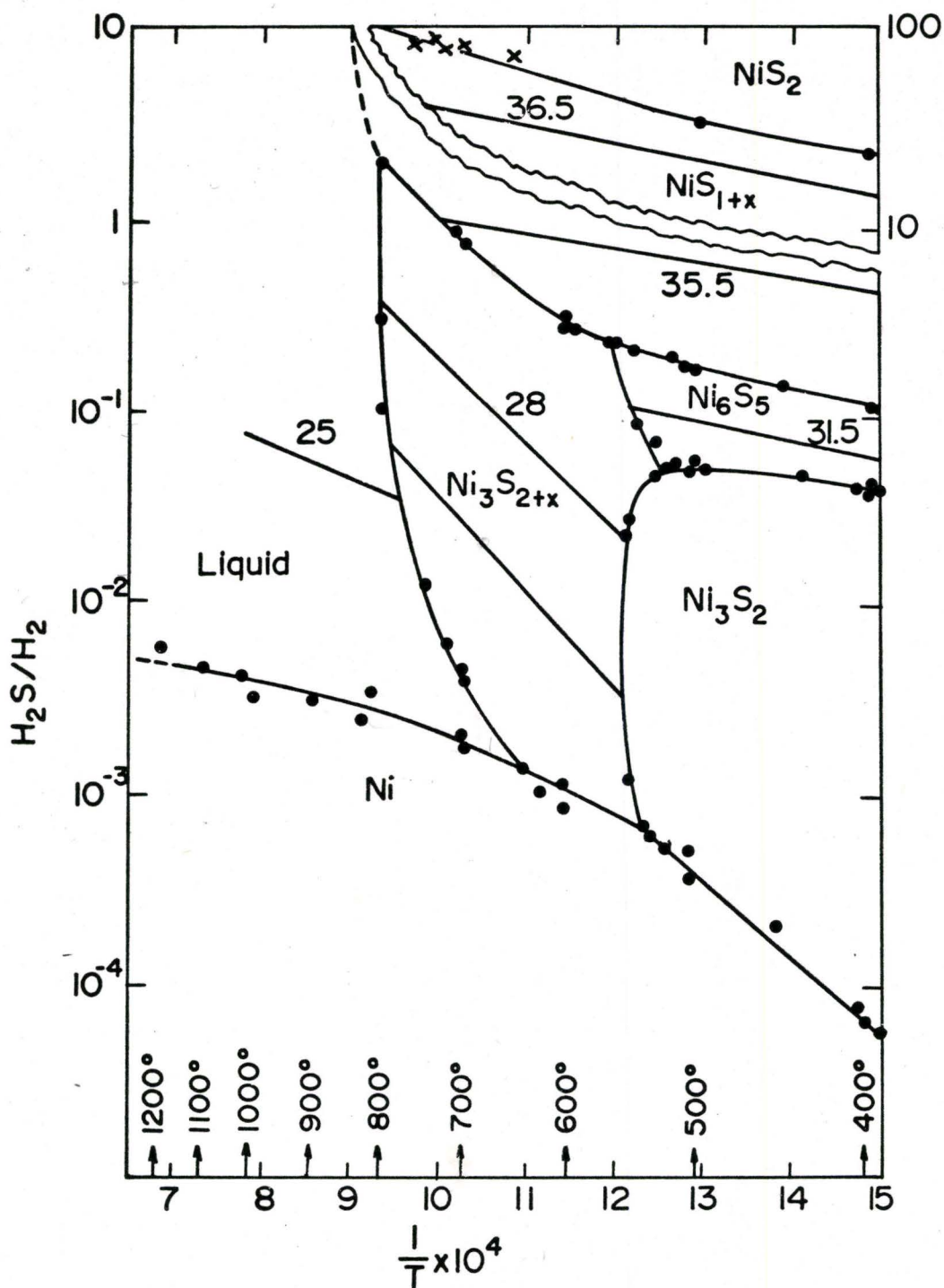


Fig. 3.1⁽⁴⁰⁾ Plot of H_2S/H_2 v's $1/T$ for the system nickel-sulphur (compositions of alloys are in wt. % of sulphur).

Hauffe and Flindt⁽⁴²⁾ have shown by both electrical conductivity measurements on doped sulphide and thermoelectric power measurements at 700°C that NiS is an n-type conductor although all these measurements are independent of P_S in the range 10^{-2} - 100 torr, which is characteristic of an intrinsic semiconductor. On the other hand, Ni_3S_2 appears to be a p-type semiconductor. From observation of sulphidation kinetics by many workers^(1, 43, 44) NiS behaves as a p-type material. Romeo⁽⁶⁾, using inert and radioactive marker techniques, observed p-type behaviour for the formation of both NiS and Ni_3S_2 .

The first kinetic studies were carried out by Hauffe and Rahmel⁽⁴⁵⁾ on pure nickel at 630°C with sulphur pressure varying in the range 10^{-2} - 1 torr. Linear kinetics were observed for the formation of a double layered scale considered to be NiS although no composition analysis was carried out. The inner layer was porous and the outer layer more compact but prone to cracking. The reaction was considered to be phase boundary controlled by the dissociation of sulphur into atoms at the metal-scale interface as it was thought that sulphur could reach the metal across the scale via the pores before being dissociated. The reaction between sulphur atoms and metal was considered to be fast. The proposed rate controlling mechanism was supported by the fact that the linear rate constant varied linearly with the square root of sulphur partial pressure. This was later supported by Pfeiffer⁽⁴⁶⁾ under similar conditions. Most recently Dutrizac and Ingraham⁽⁴⁷⁾, using temperatures ranging from 300°C to 507°C and sulphur vapour pressure from 0.1 to 70 torr, observed linear kinetics and similar scale morphology to the previous studies although at 400°C and 70 torr a change to parabolic kinetics was observed. A point to note is that the reaction rate varied from fast to slow during the same run depending upon formation and healing of cracks respectively.

Both 'fast' and 'slow' reaction rates varied linearly with the square root of sulphur pressure. The mechanism was interpreted as a surface controlled process where the fast rate (cracked scale) was related to dissociation of sulphur onto the metal surface and the slow rate (compact scale) to sulphur dissociation at the outer surface of the scale.

All other studies on nickel sulphidation have displayed parabolic kinetics. Czerski et al⁽⁴³⁾ used sulphur vapour at atmospheric pressure and temperatures in the range 480° to 640°C. Although the kinetics were parabolic rather than linear the scale morphology and compositions were similar to those reported by Hauffe and Rahmel⁽⁴⁵⁾. The relative thickness of the two layers obtained were found to vary with temperature, reaction time and specimen geometry. Dravnieks⁽⁴⁴⁾ studied the reaction between nickel and molten sulphur and a comparison between his observed parabolic kinetics and those of Czerski et al⁽⁴³⁾ led to the assumption that the aggregation state of sulphur does not influence the mechanism of nickel sulphide scale formation. Also the mechanism of parabolic scale growth was believed to be based on the outward diffusion of nickel ions and electrons to react with sulphur at the gas/scale interface. This was supported by radioactive sulphur (³⁵S) studies⁽⁴⁸⁾. The nickel sulphide was considered to be a p-type semiconductor, an assumption that was also used to explain the linear kinetics of Hauffe and Rahmel⁽⁴⁵⁾. Czerski et al⁽⁴³⁾ proposed that these linear kinetics at the low sulphur pressures were controlled by the chemisorption and reaction rate of sulphur with nickel at the scale/sulphur interface rather than at the metal/scale interface as previously thought.

An interesting mechanism was also proposed for the porous layer formation that can be generalized to other systems. Assuming that the cohesive force between sulphide scale and metal is progressively reduced during scale growth it is possible for a gap to form at the

metal scale interface. If the surface of the metal sulphide region of the gap dissociates the sulphur produced will in turn react with the exposed metal again forming new nuclei of metal sulphide. Meanwhile the nickel ions and electrons generated by the dissociation process migrate towards the gas phase interface. The contact between scale and metal is partially maintained so that the primary process of outward migration of metal ion continues to form the compact outer layer and the secondary dissociation process results in the formation of the porous inner layer.

From the few studies made it is seen that high temperature and sulphur pressure favour parabolic kinetics with the formation of more protective, compact scale and linear kinetics and non-protective scales result at lower temperatures and pressures. Formation of a liquid sulphide phase gives linear kinetics as shown by Hancock⁽²⁾ using conditions of 900°C with nickel in contact with sulphur and hydrogen in a closed quartz vessel. A liquid nickel sulphide eutectic was formed. This product is also found to be associated with the failure of Ni-base superalloys used in gas turbines when sulphur is the major fuel impurity.

Finally, the comparison of the interpolated values for parabolic oxidation and sulphidation constants shows that nickel sulphidation is generally a faster process than oxygen oxidation.

3.3 The Sulphidation of Chromium

There is even less information available about the Cr-S system. El Goresy and Kellerud⁽⁴⁹⁾ have proposed a partially schematic diagram of the system on the basis of Jellinek's⁽⁵⁰⁾ crystallographic study of the system at room temperature plus their own data. Jellinek⁽⁵⁰⁾ has established the existence of six phases in the approximate stoichiometric range CrS-Cr₂S₃. Each phase has a narrow homogeneity range and they are listed in Table 3.1. Smith⁽⁵¹⁾ has constructed a

TABLE 3.1

Phases Found in the Range Cr-CrS_{1.5} at Room Temperature after Jellinek⁽⁵⁰⁾

Phase	Symmetry	Homogeneity Range
<i>a</i> -Cr	Cubic b. c.	Very narrow
CrS	Monoclinic	Probably CrS _{0.97}
Cr ₇ S ₈	Trigonal	Cr _{0.88} S - Cr _{0.87} S
Cr ₅ S ₆	Trigonal	Cr _{0.85} S
Cr ₃ S ₄	Monoclinic	Cr _{0.79} S - Cr _{0.76} S
Cr ₂ S ₃ tr.	Trigonal	Cr _{0.69} S
Cr ₂ S ₃ rh	Rhombohedral	Cr _{0.67} S

Cr-S phase diagram, Fig. 3.2, based on the little data that exists at present. Young⁽⁵²⁾ is at present working on diffusion couple studies using binary couples of the form Cr/CrS_x in an attempt to identify the homogeneity ranges of the sulphide phases at elevated temperature (700°C). His results are shown in Fig. 3.3.

At present defect data for chromium sulphides is also sparse. Thermoelectric power measurements⁽⁵³⁾ have been carried out on sulphides of variable stoichiometry CrS_x. In the range $1.00 \leq x \leq 1.12$ chromium sulphide appears to be p-type but for $1.12 < x < 1.20$ it behaves as an n-type. The range 1.20 to 1.50 has yet to be examined so no direct evidence exists for the defect structure of Cr₂S₃ although sulphidation kinetic studies by Mrowec⁽¹⁾ suggest that it may be p-type.

Kinetic studies of chromium sulphidation have also received little attention. Unlike the Ni-S system the reaction should not be complicated by the presence of liquid phases as the melting point of the eutectic CrS-Cr is 1350°C. Hancock⁽²⁾ has made some qualitative observations on the reaction between chromium and sulphur at 900°C under the same conditions reported for his nickel studies. He concluded that the unidentified chromium sulphide scale provided some degree of protection to the underlying metal.

Arkorov et al⁽⁵⁴⁾ have reported parabolic sulphidation of pure chromium in sulphur vapour at 12 torr, in the temperature range 700°C to 1000°C. A double-layered scale was observed and sulphides in the range Cr₅S₆ to Cr₂S₃ were identified. Davin and Coutsouradis⁽⁵⁵⁾ also observed parabolic kinetics using an H₂S/H₂ mixture at temperatures varying from 800°C to 1000°C. The rate constant varied from 0.22 to 2.8 mg.² cm.⁻⁴ sec.⁻¹ and these results have recently been confirmed and expanded by Strafford and Hampton⁽⁵⁶⁾ using temperatures of 850°C, 925°C and 1000°C and various H₂S/H₂ mixtures. Neither set of workers reported the scale morphology or identity.

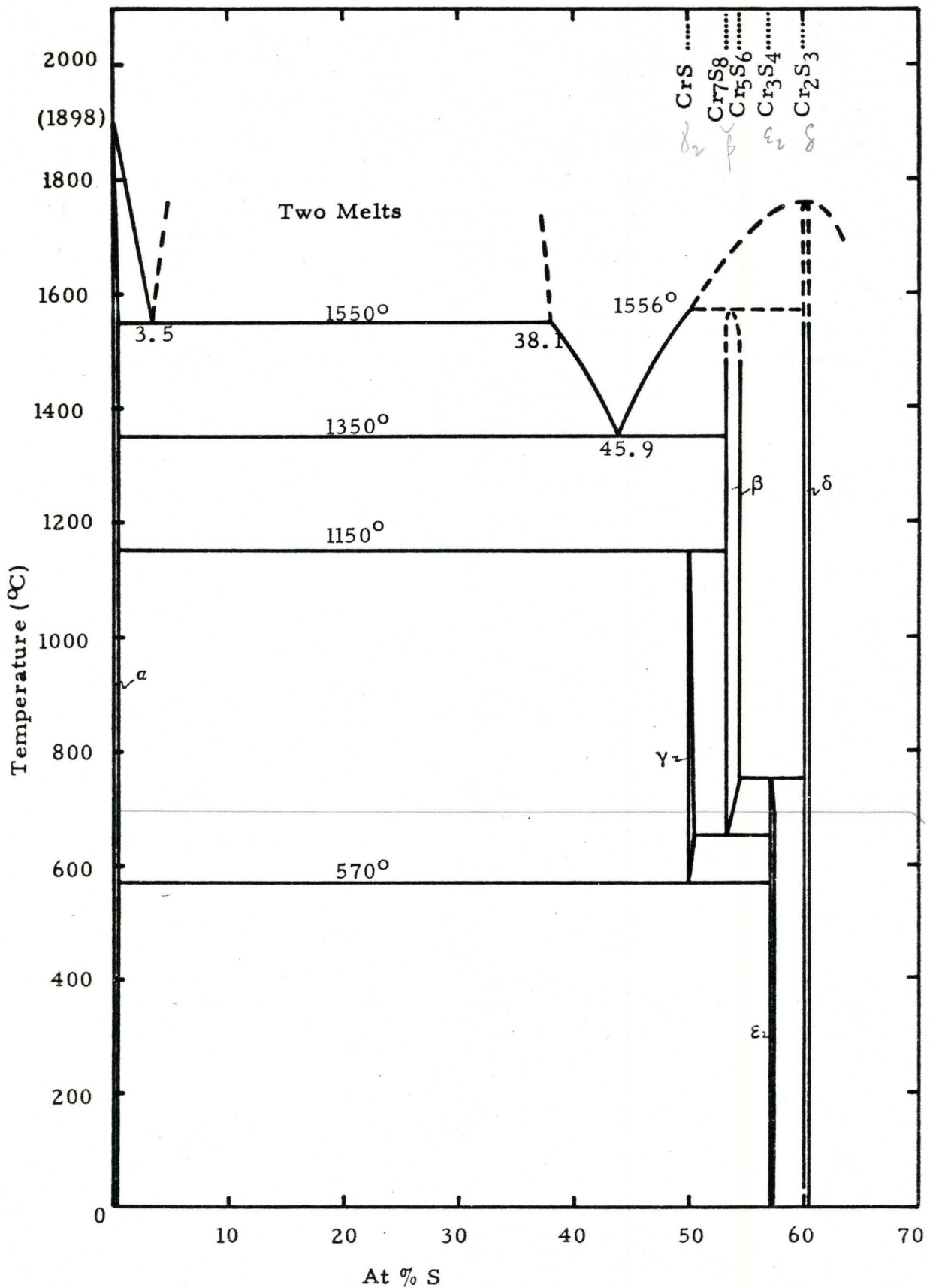


Fig. 3.2⁽⁵¹⁾ The chromium-sulphur phase diagram

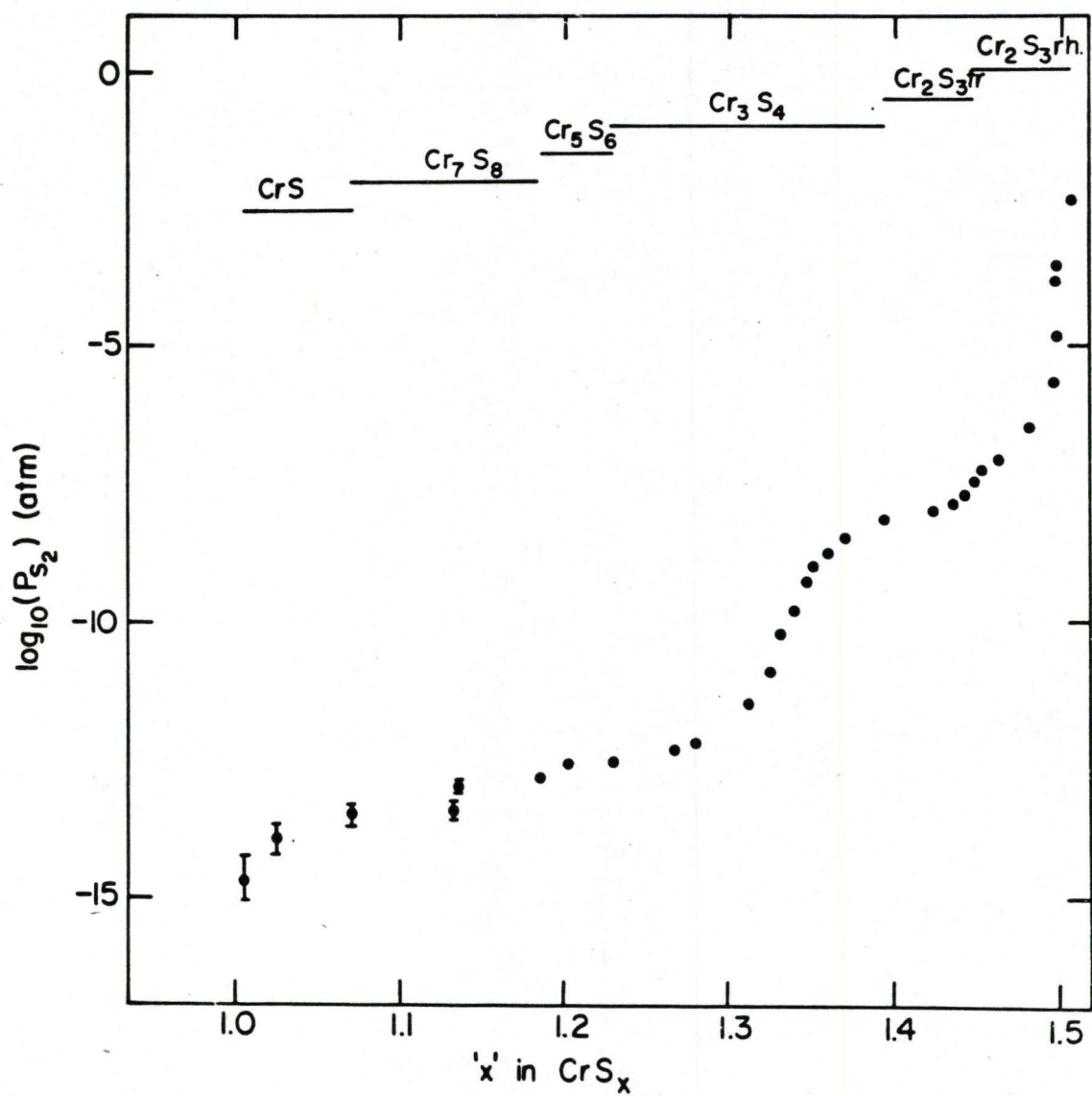


Fig. 3.3⁽⁵²⁾ Equilibrium studies of chromium sulphide stoichiometry as a function of sulphur potential.

Mrowec et al⁽¹⁾, in a comprehensive study of the kinetics and mechanism of the solid state reaction in the nickel-chromium-sulphur system, observed parabolic kinetics for sulphidation of pure chromium at a slower rate than that observed for pure nickel. They used sulphur vapour at one atmosphere pressure and temperatures ranging from 700° to 900°C. They observed a double layered scale and identified both layers as Cr₂S₃ by X-ray methods. Inert marker studies showed that the marker tends to the interface between the two layers. No definite conclusions could be drawn from this. Romeo and Spacil⁽⁵⁷⁾ found both parabolic kinetics and a duplex scale using a 10% H₂S/H₂ gas mixture at 900°C. The inner layer of this scale was compact and the outer layer porous. It was impossible to identify the scale compositions as the X-ray methods proved unreliable. The Debye-Scherrer patterns were incomplete and difficult to compare with standards.

Finally Lifshin et al⁽⁷⁾ attempted to identify the structure of the chromium sulphide scales in their kinetic studies of pure chromium at temperatures from 550° to 1000°C with H₂S/H₂ mixtures such that P_{S₂} varied from 10⁻⁷ to 10⁻¹² atmospheres. A duplex layer structure was observed under all conditions, the composition of which is given in Table 3.2. Parabolic kinetics were observed at the lower temperatures but there were deviations from a diffusion controlled process at higher temperatures. This could be due to the fact that at these very low sulphur pressures outward diffusion of chromium is faster than adsorption of reaction gas onto the scale outer surface which then becomes rate controlling. Also the variation of rate constant with sulphur pressure gave a relationship that would be expected for the formation of a p-type sulphide.

TABLE 3.2Phases Found on Sulphurized Chromium Samples After Lifshin⁽⁷⁾

Temp. (°C)	Inner	Outer	Plated
550	-	Cr ₃ S ₄ -	-
600	(Cr ₅ S ₆) Cr ₃ S ₄	Cr ₃ S ₄	-
650	(CrS) Cr ₇ S ₈ (Cr ₅ S ₆)	(Cr ₅ S ₆) Cr ₃ S ₄	Cr ₃ S ₄
700	(CrS) Cr ₇ S ₈ (Cr ₅ S ₆)	Cr ₅ S ₆ (Cr ₃ S ₄)	Cr ₃ S ₄
750	(CrS) Cr ₇ S ₈	Cr ₇ S ₈	Cr ₃ S ₄
800	-	-	Cr ₃ S ₄
834	-	-	Cr ₅ S ₆
850	-	-	Cr ₅ S ₆
900	(CrS) Cr ₇ S ₈	(CrS) Cr ₇ S ₈	Cr ₇ S ₈
1000	-	-	Cr ₇ S ₈

(Parentheses indicate phases present in lesser amounts.)

Chromium samples and platinum samples plated with chromium were sulphurized in $H_2S/H_2 = 10^{-3}$ atmosphere. The former samples exhibited an "inner" and "outer" scale.

3.4 The Sulphidation of Nickel-Chromium Alloys

As yet ternary phase diagrams of the Ni-Cr-S system have not been published. Bolze et al⁽⁵⁸⁾ using literature thermal data and analysis of diffusion couples have compiled a series of tentative isotherms in the range 600° to 850°C. The 700°C isotherm which is relevant to this study is shown in Fig. 3.4. Due to the lack of thermodynamic data for the ternary system plus the lack of basic data for the individual components it is very difficult to predict the sulphidation behaviour of the alloys.

Probably the most comprehensive investigation of the sulphidation properties of Ni-Cr alloys has been carried out by Mrowec et al⁽¹⁾. These authors, using sulphur vapour at 1 atmosphere pressure, examined the entire range of alloy compositions from pure nickel through to pure chromium at various temperatures in the range 600° to 900°C. They observed parabolic kinetics under all experimental conditions. The data was summarized by plotting the parabolic rate constants as a function of chromium content from which the sulphidation behaviour could be classified in a general manner into four stages according to alloy composition. The mechanisms were then interpreted in terms of scale defect structure. For chromium concentrations up to 0.1 wt. % the reaction rate increased above that for pure nickel. Since the scale was NiS containing up to approximately 0.4% Cr in solid solution and, assuming NiS is a p-type semiconductor, the mechanism was explained as a substitution of trivalent Cr ions on the NiS sublattice thus increasing the vacancy concentration in the scale. With further increase in chromium content up to 20% the reaction rate steadily decreased. A duplex scale was observed, the outer layer being entirely NiS while the inner layer contained particles of Cr₂S₃ in a NiS matrix. The amount of Cr₂S₃ increased with the chromium content of the alloy

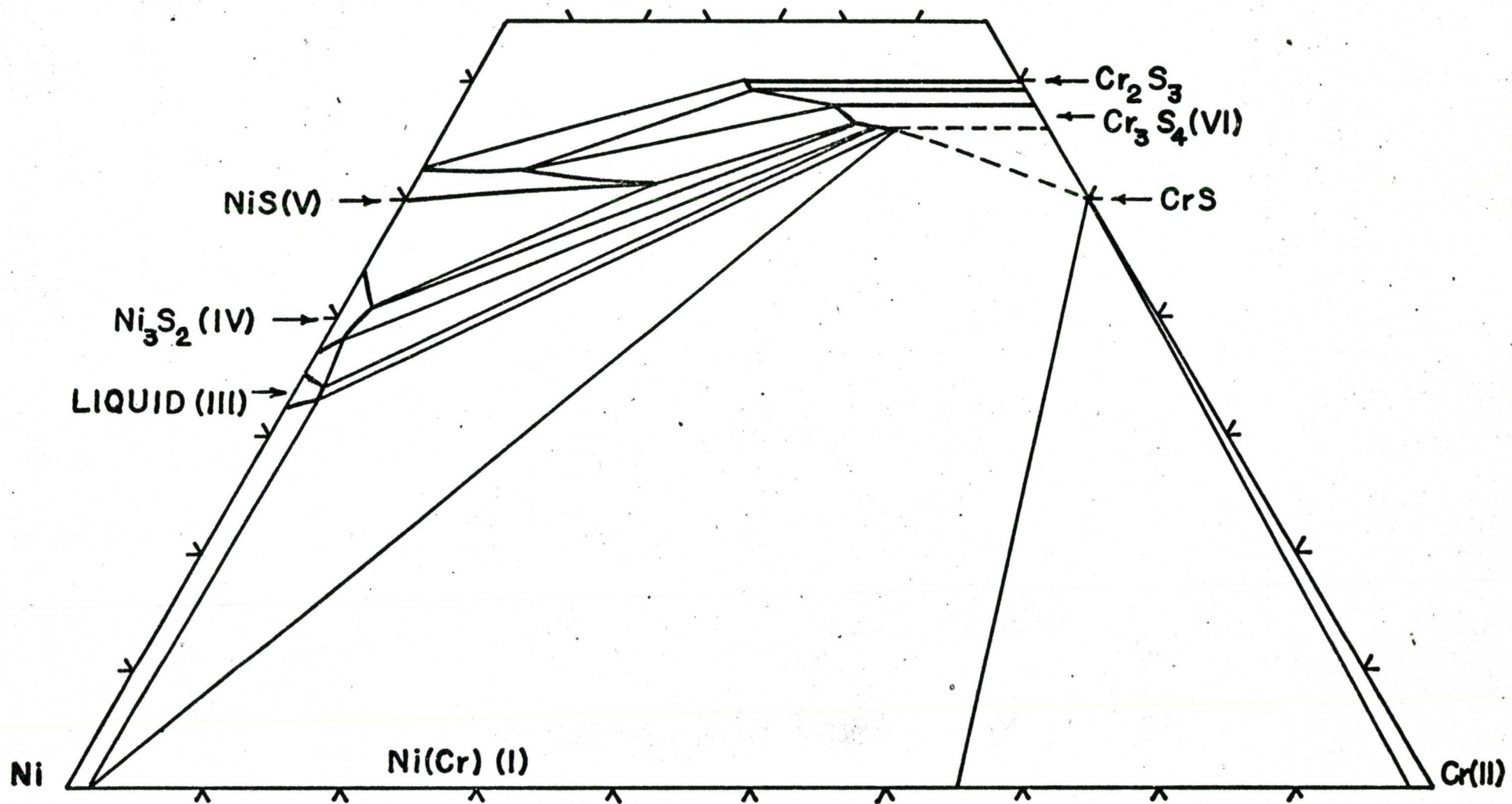


Fig. 3.4⁽⁵⁸⁾ 700°C isotherm of the Ni-Cr-S phase diagram.

until it became the major portion of the inner layer. The proposed mechanism is complex and is out of the scope of this review so the reader is best referred to the reference. From 20% to about 50% chromium content the reaction rate continued to decrease to a minimum below that for pure chromium. The scale was still duplex with NiS as the outer layer but the inner layer was Cr_2S_3 with NiS as the dispersed phase in the form of needles or stringers. The mechanism proposed was similar to the one for the second stage. Above 50% chromium content the reaction rate gradually increased. The duplex scale observed was entirely Cr_2S_3 with the inner layer porous and the outer layer compact. Outward diffusion of metal accounted entirely for the scale growth and assuming that Cr_2S_3 is p-type the presence of divalent Ni ions on the scale sublattice would decrease the reaction rate below that for pure chromium as observed.

Although these results are very relevant to an understanding of the sulphidation process they are open to some criticisms. At temperatures as high as 900°C the sulphidation product is expected to be liquid nickel sulphide as observed by Romeo et al^(5,6) for the Ni-20% Cr alloy. The formation of liquid nickel sulphide may in fact account for the presence in the inner chromium sulphide layer of stringers identified by Romeo and Smeltzer⁽⁵⁹⁾ as nickel sulphide. They proposed that when the molten nickel sulphide has formed as the reaction product it wets the solid chromium sulphide layer dissolving it preferentially at grain boundaries and thus penetrating inwards.

Sulphidation experiments on nickel-chromium alloys have also been carried out by Hancock⁽²⁾ at 600° , 700° and 900°C with hydrogen sulphide as the corrosive environment. At 600° and 700°C the Ni-20% Cr alloy displayed parabolic kinetics with the formation of a duplex scale with an inner layer of various stoichiometric chromium sulphides and an outer layer of Ni_3S_2 . However at 900°C the kinetics

were linear and scale examination showed it to consist of dark spheroidal particles of chromium sulphide in a matrix of Ni_3S_2 and metallic nickel. Furthermore, the matrix appeared to have been liquid at the reaction temperature. Alloys richer in chromium were found to be more resistant to corrosion by H_2S at all temperatures. Even at 900°C a stable scale of chromium sulphide was formed with an outer layer of Ni_3S_2 . Also the total scale thickness decreased with increasing chromium content. Hancock repeated the experiments with sulphur in oxidizing conditions instead of reducing conditions and found that the reaction rate was greater under the latter conditions.

Davin and Coutsouradis⁽⁵⁵⁾ reported results similar to those of Hancock using $\text{H}_2\text{S}/\text{H}_2$ mixtures, alloy compositions of 20 and 35% Cr. and temperatures of 800° , 900° and 1000°C . An interesting part of their study was evidence that Co-Cr alloys possess sulphidation resistance superior to that of the Ni-Cr alloys which is of use for application to gas turbine blade materials.

Romeo et al^(5, 6) have studied the kinetics and morphology of the sulphidation of Ni-20% Cr alloys at 700°C in $\text{H}_2\text{S}/\text{H}_2$ atmospheres with sulphur pressure varying from about 10^{-7} to 10^{-2} atmospheres. At all pressures the scale growth was parabolic indicating a diffusion controlled process. The growth kinetics were found to be almost independent of sulphur partial pressure when the reaction products were solid i. e. when $P_{\text{S}_2} > 10^{-8}$ atm. A duplex scale consisting of nickel sulphide overlying chromium sulphide was observed. The outer layer was identified as principally NiS when $P_{\text{S}_2} > 10^{-5}$ atm. and Ni_3S_2 at $P_{\text{S}_2} < 10^{-5}$ atm. and at 10^{-5} atm. both compounds coexisted. The precise stoichiometry of the inner layer could not be identified and its average composition of CrS was reported. Marker experiments indicated that metal diffusion is responsible for mass transport in both scale layers and sulphur did not diffuse inwards at all. A tentative

diffusion model was proposed in which the outer nickel sulphide layer grows at the gas/scale interface, while the inner chromium sulphide layer grows at the expense of nickel sulphide according to the schematic displacement reaction, $\text{NiS} + \text{Cr} \rightarrow \text{CrS} + \text{Ni}$. This can only be confirmed by a knowledge of relative diffusion constants, the defect nature of the solid sulphides and a thermodynamic description of the system, most of which is at present inadequate.

Finally Lifshin et al⁽⁷⁾ have worked with sulphur pressures below those of Romeo and co-workers. They used P_{S_2} of 10^{-11} atm. with temperatures varying from 700° to 1100°C and chromium contents of 10, 20 and 30 wt. %. The scales consisted of tight, adherent chromium sulphide formed selectively accompanied by a subscale. The kinetics observed were parabolic and the rates increased with chromium content of the alloy. After an initial reaction rate increase with increasing temperature a decrease was observed at temperatures above 800°C . The latter phenomenon was attributed to the effect of sulphur pressure dependence on a term in the Arrhenius equation for the parabolic rate constant.

3.5 Summary

Nickel, chromium and their binary alloys sulphidize parabolically under most experimental conditions. This indicates that the mechanism is diffusion controlled but detailed quantitative mechanisms have yet to be assessed owing to the lack of basic thermodynamic, defect structure and diffusion data. Difficulty has also been encountered in identifying the chromium sulphide scales obtained. A brief summary of past results is shown in Table 3.3.

A certain degree of protection is offered by these scales although porosity, cracking and spalling have been observed especially after long periods of time. A serious limitation of the binary Ni-base

TABLE 3.3

Experimenter	Material	Atmosphere	Temp. (°C)	Scale	Kinetics	
Davin and Coutsouradis 1965	Cr 80 Ni-20 Cr 65 Ni-35 Cr	H ₂ S-30% H ₂	800-1000	CrS 'CrS' + Ni ₃ S ₂ + Ni	Parabolic linear 800° catastrophic 900° failure 1000	
Hancock 1961	Cr Ni 80 Ni-20 Cr 80 Ni-20 Cr	H ₂ S	900 900 600-700 900	'CrS' Ni ₃ S ₂ + Ni 'CrS' + Ni ₃ S ₂ 'CrS' + Ni ₃ S ₂	linear parabolic linear	
Seybolt 1967	Cr 80 Ni-20 Cr 35 Ni-65 Cr	H ₂ - .001 H ₂ S	800-1000	Cr ₇ S ₈		
Mrowec, Werber and Zastawnick 1966	Ni Ni-0.11 Cr Ni-4.5 Cr	1 atm. S ₂	600-700	Inner NiS Outer NiS + Ni ₃ + X + Ni ₃ + X	parabolic	
	Ni-13.8 Cr Ni-32.8 Cr	S ₂	750-850	NiS	Cr ₂ S ₃	parabolic
	Ni-63 Cr Ni-82 Cr Cr	S ₂	750-900	Cr ₂ S ₃	Cr ₂ S ₃	parabolic
Arkorev Konev 1959	Cr	S ₂ at 12 mm Hg press.	700 800-1000	Cr ₅ S ₆ Cr ₅ S ₆	Cr ₃ S ₄ Cr ₂ S ₃	parabolic
Czerski Mrowec Werber 1962	Ni	1 atm. S ₂	480-640	NiS	NiS	Parabolic
Romeo Smeltzer Kirkaldy 1970	80 Ni-20 Cr	H ₂ S + H ₂ P _{S₂} 10 ⁻⁷ - 10 ⁻²	700	'CrS'	Ni ₃ S ₂ < 10 ⁻⁵ NiS > 10 ⁻⁵	parabolic
Lifshin Seybolt Hudson 1970	Cr Ni- 10 Cr Ni- 20 Cr Ni- 30 Cr	H ₂ - .001 H ₂ S	550-1000 700-900 1100	See Table 3.2 Cr ₃ S ₄ - Cr ₅ S ₆ Cr ₇ S ₈	paralinear parabolic	

alloys is the formation of molten nickel sulphide eutectics at relatively low temperatures resulting in catastrophic failure of the material. As a result Strafford and Hampton⁽⁶⁰⁾ have questioned the role of chromium as an inhibitor of high temperature sulphidation. The addition of a third element such as aluminum or titanium has been suggested as a possible method of enhancing resistance to sulphur corrosion.

CHAPTER IV

EXPERIMENTAL APPARATUS AND PROCEDURE

4.1 Introduction

Various experimental techniques are available to determine the kinetics of the type of reaction under study. The most common methods in use measure the growth of scale by gravimetric, volumetric, manometric and electrometric techniques. The gravimetric method was employed for this study as it is simple and reliable. The specimens were exposed to hydrogen sulphide-hydrogen atmospheres at a total pressure of 1 atmosphere at 700°C.

Thermodynamic studies⁽⁵⁸⁾ show that the formation of a liquid phase in the Ni-Cr-S system is possible at temperatures above 600°C especially when the sulphur partial pressure is less than 10^{-8} atm. Preliminary experiments at 700°C with sulphur partial pressure less than 5×10^{-10} atm. showed that the reaction was of the gas-solid type. Thermodynamic considerations show that at sulphur pressures below 5×10^{-10} atm. only chromium sulphide formation is possible which was experimentally supported by Lifshin et al⁽⁷⁾. Thus this study follows on directly from those of Romeo et al⁽⁵⁾ but utilizes sulphur pressures several orders of magnitude lower.

4.2 Specimen Preparation

The Ni - 20 wt. % Cr alloy composition was selected because it consists of a solid solution over a large range of temperatures as

shown by the binary phase diagram for the Ni-Cr system⁽⁶¹⁾. Alloys with higher chromium contents may correspond to a two-phase structure. The impurity contents of the alloy are recorded in Table 4.1 below.

TABLE 4.1

Analysis of the NiCr alloy used. The Cr content is given in weight percent. All others are in p. p. m. by wt.

Element	Cr	Si	Mn	Co	Fe	Al	C	S
Analysis	19.9	500	10	50	50	100	22	6

Cold rolled sheets of approximately 1 mm thickness were supplied direct by Falconbridge Laboratories. The test specimens were obtained by shearing the sheets into plates approximately 1.5 x 0.5 x 0.1 cm. These are dimensional requirements suggested by Romanski⁽⁶²⁾ for a "specific area" of the specimen. It was not considered necessary to apply the corrections for the area consumed by the reaction as proposed by the same author, since the overall consumption in all experiments was well below 10% of the initial specimen area. A suspension hole of approximately 1 mm radius was drilled in each specimen and they were then batch annealed in vacuo for 3 days at 1000^oC for stress relief. The specimens were then metallographically polished on all sides through 220, 320, 400 and 600 grit silicon carbide grinding papers under water as lubricant. Final polishing was carried out on selvyt cloths impregnated with 6 μ and 1 μ diamond abrasive using kerosene as lubricant before storing under acetone. Prior to each experiment the specimen to be used was dried, weighed and the surface area computed by measuring its

dimensions with a micrometer.

4.3 Sulphidation Apparatus

The apparatus used for the sulphidation experiments is shown schematically in Fig. 4.1. It consists of essentially two parts, i. e. the reaction gas producer and the reaction chamber, both of which are described below. The numbers in the brackets in the following text represent the corresponding parts of the experimental apparatus in Fig. 4.1.

4.3.1 The Reaction Gas Production Apparatus

This is the apparatus depicted to the right in Fig. 4.1 and similar to that used by Rosenqvist and Dunicz⁽⁶³⁾ and Brigham et al⁽⁶⁴⁾. Matheson ultra high purity hydrogen (99.999 vol. % pure) was passed through a chamber of silica gel before being bubbled through the molten sulphur (5) held at a constant temperature between 115°C and 180°C in an oil bath (4). The flow of hydrogen was regulated by a Rotameter (1) with a R-2-15 AA tube and stainless steel float all supplied by Brooks Instrument Division. The rotameter was carefully calibrated by measuring the rate of movement of a soap bubble in a calibrated burette. A flow rate of approximately 100 cc per minute was used which was rapid enough to prevent thermal segregation of the gas in the reaction chamber but slow enough to allow sulphur saturation of the hydrogen on passing through the sulphur bath. Dow Corning 210H fluid, a silicone oil, was used for the oil bath as it is very slow to evaporate and the level and temperature of the bath remained constant. A heating element (3) connected to a Fisher proportional temperature control (6) was used to regulate the bath and thus sulphur temperature.

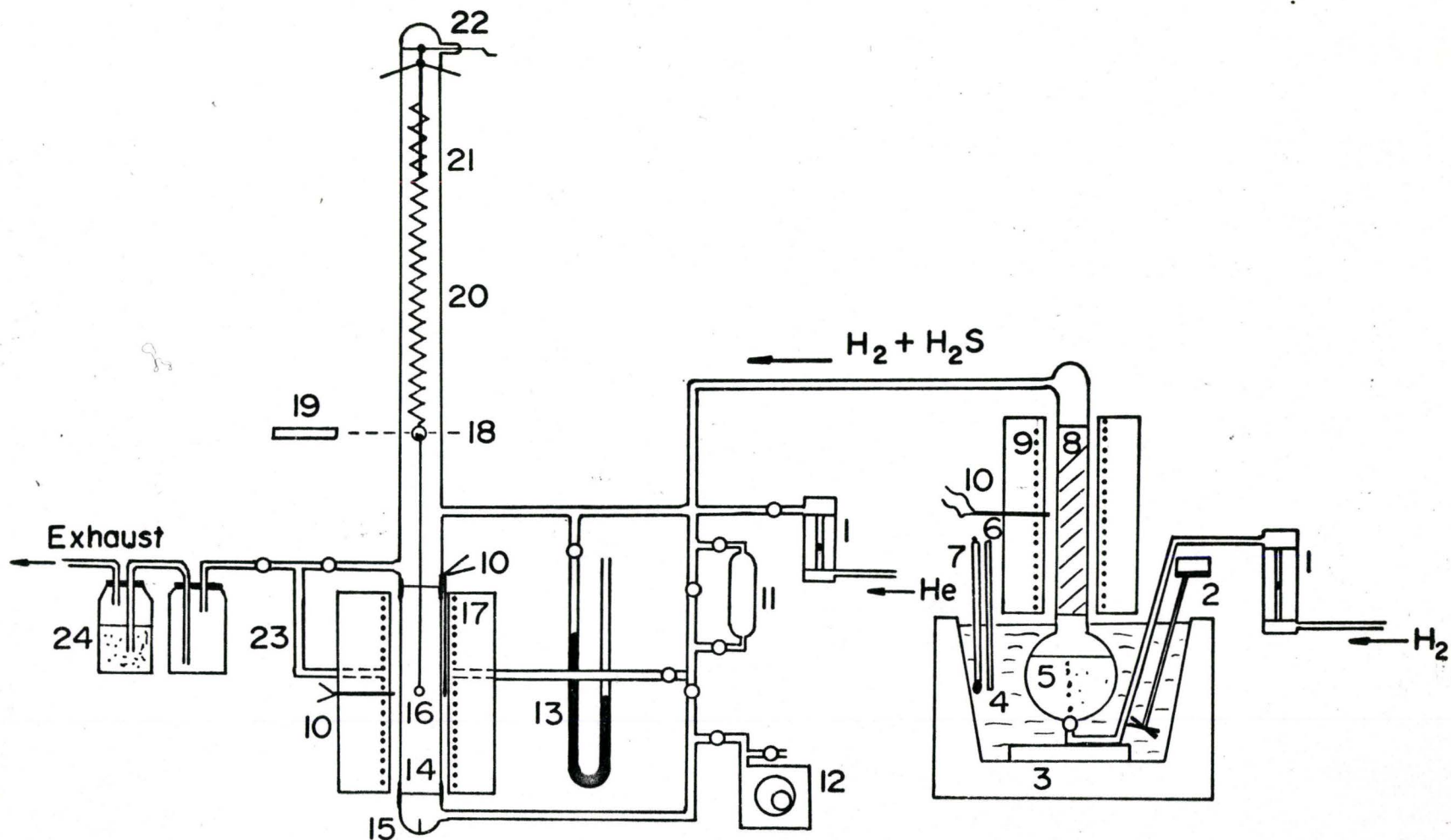


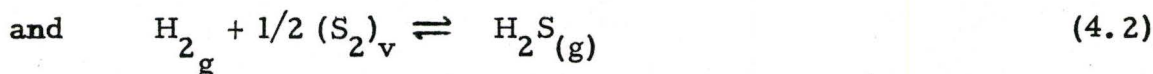
Fig. 4.1 Schematic of kinetic assembly.

- | | | |
|----------------------------------|---------------------|---|
| 1. Rotameter | 9. Furnace 500°C | 17. Furnace 700°C |
| 2. Stirrer | 10. Thermocouple | 18. Target |
| 3. Heating Element | 11. Gas Sampler | 19. Cathetometer |
| 4. Constant Temperature Oil Bath | 12. Vacuum Pump | 20. Spring Chamber |
| 5. Sulphur Bath | 13. Manometer | 21. Marker |
| 6. Temperature Control | 14. Mullite Tube | 22. Winch and Forks for positioning specimen |
| 7. Thermometer | 15. Alignment Spike | 23. Gas Bypass |
| 8. Porcelain Packing | 16. Specimen | 24. Ballast and adsorption flask with CaCl_2 |

The bath temperature was measured with a 0 to 360°C mercury thermometer (7) .

The hydrogen on passing through the molten sulphur became saturated with sulphur vapour but chemical reaction did not occur until these gases were heated to 500°C in a reaction column (8) packed with porcelain saddles. An atmosphere of hydrogen sulphide and hydrogen was produced in the reaction column and the H_2S/H_2 ratio of the atmosphere was directly related to the sulphur or oil bath temperature as shown below.

Two equations represent the reactions taking place:



The equilibrium constant for reaction 4.1 is given by

$$k_1 = (P_{S_2})^{1/2} \quad (4.3)$$

and for reaction 4.2 by

$$k_2 = \frac{P_{H_2S}}{P_{H_2} (P_{S_2})^{1/2}} \quad (4.4)$$

Thus the gas ratio is given by (4.3) and (4.4) as

$$\frac{P_{H_2S}}{P_{H_2}} = k_2 (P_{S_2})^{1/2} = k_2 \cdot k_1 \quad (4.5)$$

The equilibrium constant k_2 is obtained from known thermodynamic data for reaction (4.2) and k_1 is obtained from values of sulphur

vapour pressure reported by West and Menzies⁽⁶⁵⁾. By varying the temperature of the sulphur bath between 115° and 180° C the H_2S/H_2 ratio can be varied between 3×10^{-4} and 10^{-2} atm. which gives a sulphur partial pressure range of 2×10^{-12} to 3×10^{-9} atm. in the reaction chamber (14). The temperature of the equilibrium column (8) does not require precise control so the furnace was controlled by a variac and its temperature measured with a chromel-alumel thermocouple (10) connected directly to a calibrated meter.

The H_2S/H_2 gas atmosphere was then passed through a gas sampler (11) of known volume (207.5 cc) before entering the main reaction chamber (14).

4.3.2 The Reaction Chamber

This is the apparatus shown on the left of Fig. 4.1 and is similar to apparatus described previously by Morris and Smeltzer⁽⁶⁶⁾ with modifications by Romeo et al⁽⁵⁾. The furnace chamber was a 26" x 1 3/4" O.D. mullite tube (14) surrounded by a Kanthal element furnace (17). Power was supplied to the heating element from the 230v. line through a 2500 V.A. transformer. The temperature of the furnace was controlled to $\pm 2^\circ$ C by a Honeywell controller using a Pt-Pt/13% Rh. thermocouple (10) placed through the furnace wall to a point between the mullite tube and the furnace windings at the hot zone. The reaction temperature was measured by a chromel-alumel reference thermocouple (10) situated between the mullite tube and the furnace windings at the hot zone. This thermocouple was calibrated against another chromel-alumel thermocouple which was lowered in steps down the center of the reaction chamber against a flow of inert gas simulating reaction conditions in order to find the hot zone.

For a continuous gravimetric measurement of the reaction kinetics the specimen was supported in the reaction chamber from a

McBain balance. This consisted of a winch and positioning forks (22) , a metal spring (20) (described later) connected to the winch by .005" molybdenum wire, a reference marker (21) , and a target (18) attached to the bottom of the spring. The specimen was attached to the target with a length of .005" platinum wire. The weight gain on sulphidation was measured by following the spring extension via the target movement with a cathetometer until the sample passed through the reaction hot zone which was about 2 cm. in length. The specimen was lowered in and out of the reaction chamber by means of the winch. Helium was used to purge the upper portion of the reaction column to avoid condensation of sulphur in the spring chamber although this is not now thought to be necessary. The flow rate was controlled by another rotameter (1) with a R-2-15 AAA tube and sapphire float. The rate was low so as not to dilute the H_2S/H_2 atmosphere.

A vacuum pump (12) was used to evacuate the assembly to about 10^{-2} torr. while the furnace was brought to temperature, hence the bypass (23) for the reaction gas mixture. The assembly was then filled with helium before the reaction gas was passed. Helium was also used to flush the assembly after the experiment was completed. The gas, on leaving the chamber, was passed through sintered glass bubblers containing caustic soda to remove the hydrogen sulphide.

A modification to the assembly, in place of the spring chamber, was used to carry out static gravimetric experiments for the purpose of collecting specimens at various stages of scale growth for morphological studies. The modification consisted of a column similar to the spring chamber (20) but was equipped with four winches and four quartz rods. A specimen was attached to each of these rods and then lowered into the reaction zone once the furnace was at temperature. The four specimens can be lifted out of the reaction chamber and quenched after different, convenient periods of time.

4.3.3 The Spring

The spring (20) was manufactured from Ni-Span "C"⁽⁶⁷⁾ wire as described by Morris⁽⁶⁸⁾. This material is an age hardening alloy containing Cr, Ti, Ni and Fe and possesses a constant modulus of elasticity and rigidity over a useful range of temperatures above and below ordinary room temperature. The combination of zero thermoelastic coefficient, which eliminates temperature change effects of the elastic moduli, and the high elastic and strength properties obtainable through heat treatment make it an ideal spring material.

The wire was wound onto a 5/8" stainless steel rod using the slowest speed possible on a lathe. The ends were fastened with wire onto the rod and the whole thing was annealed at 1350^oF for 4 to 5 hours in either vacuo or argon. About 15 windings produced a spring of suitable length for the spring chamber. The spring was then calibrated with the target and a specimen attached to it by adding a series of small nichrome wire weights of approximately 10 milligrams (\pm 2 micrograms) to the specimen and measuring the extension with the cathetometer. A straight line plot was obtained for an extension time graph with a slope of 0.0415 g cm^{-1} , which remained constant throughout the course of the investigation.

4.4 The Sulphidation Procedure

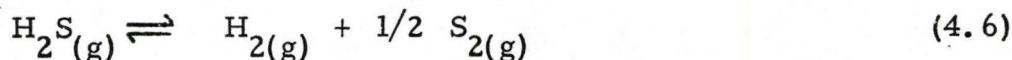
At the onset of an experimental run the oil bath was set at a temperature that yielded the required $\text{H}_2\text{S}/\text{H}_2$ ratio. Hydrogen was passed through the molten sulphur for several hours to allow the system to stabilize. The specimen was loaded onto the end of the spring and the reaction assembly was sealed and evacuated. The system was then filled with helium and the furnace was brought up to temper-

ature. The H_2S/H_2 atmosphere was passed in the bottom of the reaction chamber and allowed to flow for five minutes to allow the equilibrium pressure of sulphur in the hot zone to be reached. The specimen was lowered into position. Weight gain was followed for a maximum extension of 0.5 cm which is the distance over which all of the specimen was in the hot zone. At the end of the run the specimen was raised out of the reaction zone into the upper portion of the column where the temperature drop was sufficient to quench it. The reaction gas was diverted and the system flushed with helium before the specimen was removed.

4.5 Gas Analysis

4.5.1 Theory

It has been shown in section 4.3.1 that for a fixed temperature of the sulphur bath a certain hydrogen and hydrogen sulphide atmosphere is produced and all of the sulphur vapour is considered to have reacted with the hydrogen. The gas atmosphere then proceeds to the reaction chamber where the hydrogen sulphide dissociates to form sulphur gas by the reaction:



The equilibrium constant for this reaction is given by

$$k_3 = \frac{(P_{S_2})^{1/2} P_{H_2}}{P_{H_2S}} \quad (4.7)$$

Thus if k_3 and the P_{H_2S}/P_{H_2} ratio are known it is possible to calculate the sulphur partial pressure in the reaction chamber.

Several expressions are available for calculating the value of k_3 at the reaction temperature. The usual method is to express k_3 in terms of standard free energy for the reaction (ΔG_3°) by the van't Hoff relationship where

$$\Delta G_3^{\circ} = -RT \ln k_3 \quad (4.8)$$

A value for ΔG_3° at reaction temperature is then given by⁽⁶⁹⁾

$$\Delta G_3^{\circ} = 21,570 - 11.79T \text{ cal.mole}^{-1} \quad (4.9)$$

At 700°C ΔG_3° has a value of 10,090 cal.mole⁻¹ which on substituting in equation (4.8) gives a value of 5.36×10^{-3} for k_3 . Yuan and Kroger⁽⁷⁰⁾ using emf as a function of sulphur partial pressure have derived the following expression for the equilibrium constant of reaction (4.6) as a function of temperature.

$$\log k_3(T) = - \frac{4.57 \times 10^3}{T} + 2.35 \quad (4.10)$$

At 700°C a value of 5.30×10^{-3} is obtained for k_3 . In the temperature range 1000° to 1400°K the following expression for standard free energy ΔG_3° has been obtained from J. A. N. A. F.⁽⁷¹⁾:

$$\Delta G_3^{\circ} = 21,268 - 0.6878 T \log T - 9.364 T \quad (4.11)$$

which at 700°C gives a value of 10157 cal mole⁻¹. This in turn yields a value of 5.22×10^{-3} for k_3 . Since it is uncertain which value of k_3 is closest to the true value and all three differ by insignificant amounts compared to the values of the H_2S/H_2 ratios experimentally obtained it was decided to use an average of the above three values for k_3 .

Thus at 700°C the equilibrium constant k_3 for reaction 4.6 was found to be 5.29×10^{-3} .

Bale and Toguri⁽⁷²⁾ have discussed the possibility of the following reactions changing the equilibrium conditions:



Free energy data have been listed^(73, 17) which shows that the polymerization of S_2 according to (4.12) is insignificant. Variable data also exist for the dissociation of S_2 ^(17, 74, 75) but even the most favourable does not provide enough monoatomic sulphur to significantly affect the gas mixture composition. The variable data that exist for HS formation by (4.14) shows that it has a significant affect on the equilibrium above 1000°C. Although the reaction temperature is close to this figure reaction (4.14) has not been taken into account as it is assumed only H_2S is present in the reacting gas and the sulphur arising from its dissociation reacts with the alloy specimen.

The H_2S/H_2 ratio is obtained by the iodide method of sulphur analysis as reported by Dunicz and Rosenqvist⁽⁷⁶⁾. The H_2S in a known volume of the gas atmosphere is adsorbed in an alkaline sodium hypochlorite solution which is titrated against a standard thiosulphate solution as described later. The difference between thiosulphate used for this titration and that used for a blank solution is equivalent to a known amount of sulphur. In fact 1 ml. of 0.01M sodium thiosulphate solution is equivalent to 4×10^{-5} g of sulphur. The hydrogen sulphide partial pressure is given by

$$P_{H_2S} = \frac{A \cdot 4 \times 10^{-5} \cdot R \cdot T}{M_s \cdot V} \quad (4.15)$$

where A is no. of ml. thiosulphate used
 M_s is molecular weight of sulphur
 V is volume of gas sampler.

The hydrogen partial pressure is the difference between atmospheric pressure and P_{H_2S} , hence the P_{H_2S}/P_{H_2} ratio is easily calculated.

4.5.2 Procedure

The reaction gas atmosphere was flushed through the known volume gas sampler (11) for at least an hour before isolation. At this point the air pressure and room temperature were measured. Into each of three 100 ml flasks 25 ml of an alkaline sodium hypochlorite solution were pipetted. The alkaline sodium hypochlorite solution consists of 10 ml of a 6% by weight sodium hypochlorite solution added to 1 litre of 2.5N sodium hydroxide solution corresponding to a pH of about 14.4. Two of the flasks were fitted with fine sintered glass bubblers and connected in series to the gas sampler. The gas in the sampler was slowly bubbled through the solutions using helium for 1 hour, the flow rate being controlled by a micrometer needle valve. The solutions were stirred by means of small magnetic stirrers during the adsorption process. The first solution should have adsorbed all the sulphur present in the gas and the second solution was merely a precautionary measure.

Both flasks were removed after adsorption was complete and, along with the blank, were each treated with 1 g. of crystalline sodium iodide and 10 ml. of 50% acetic acid. Each solution was titrated against 0.01N sodium thiosulphate solution with two drops of starch indicator

added towards the end of the titration. The end point was given when the blue indicator turned colourless. There was a problem with starch solution as its colour returns. It was decided that if the colour did not return after a period of 5 minutes the end point was reached. The difference in the titration results for the blank and the adsorption solutions was equivalent to a certain amount of sulphur as described in the theory in the previous section.

The P_{H_2S}/P_{H_2} ratio and P_{S_2} values were calculated from the titration data using the computer program given in Table 4.2. The results obtained for any specific sulphur bath temperature at such low sulphur partial pressures fluctuated so much due to such reasons as oxidation of the thiosulphate solution, difficulty in reading the end point with starch indicator, and fluctuations within the gas itself. As a result the gas analysis was carried out separately from the sulphidation experiments and the results plotted along with those of Rosenqvist and Dunicz⁽⁶³⁾ and Brigham et al⁽⁶⁴⁾. The sulphur pressures quoted for the experiments were obtained from the resulting curve given in Fig. 4.2.

4.6 Metallography

4.6.1 Preparation

The specimens obtained from the static sulphidation experiments were examined metallographically. A select number of specimens were cold mounted vertically in epoxy resin within 1" O.D. plastic rings. They were polished through 220, 320, 400 and 600 silicon carbide grinding papers with final polishing on 6μ and 1μ diamond impregnated cloths. Kerosene was used as the lubricant at all stages to minimize the sulphide porosity due to chipping out of the oxide. On microscopic

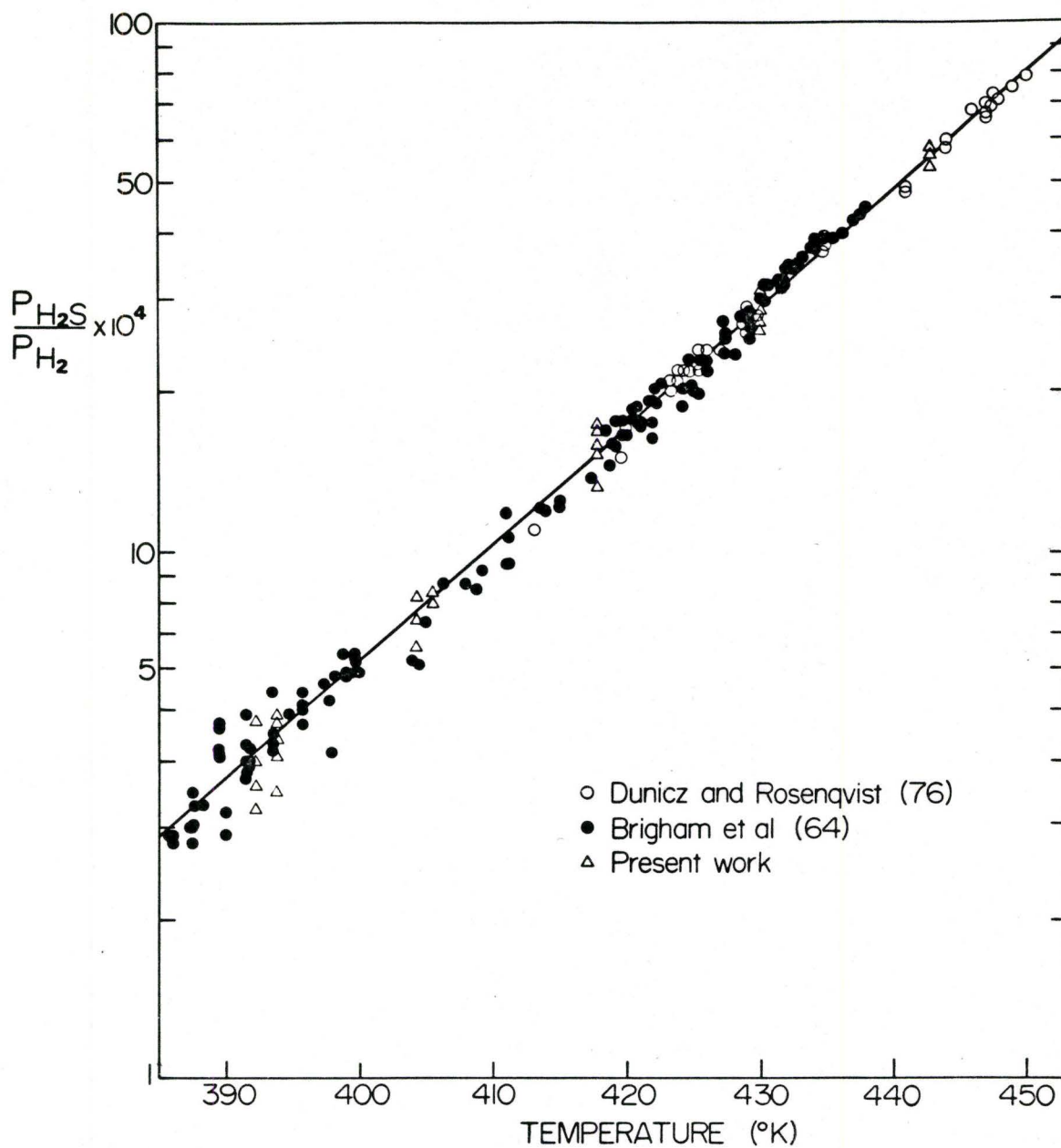


Fig. 4.2 Plot of the measured P_{H_2S}/P_{H_2} atmosphere ratio against the sulphur bath temperature in $^{\circ}K$ by several workers.

TABLE 4.2

COMPUTER PROGRAM USED TO CALCULATE SULPHUR PARTIAL PRESSURE FROM GAS ANALYSIS DATA.

PROGRAM TST (INPUT, OUTPUT, TAPE 5 = INPUT, TAPE 6 = OUTPUT)

C. A IS NUMBER OF ML. THIOSULPHATE OF 0.01N IN TITRATION
 C. PMM IS BAROMETRIC PRESSURE IN MM. OF MERCURY
 C. P ATM IS ATMOSPHERIC PRESSURE IN ATM.
 C. T K IS ROOM TEMPERATURE IN DEGREES K.
 C. VOLUME OF SAMPLING BULB IS 207.5 ML
 C. 1 ML. THIOSULPHATE = 0.00004 GRAMS OF SULPHUR
 C. R IS THE H_2S/H_2 RATIO
 400 READ (5,100) A, PMM, T K
 100 FORMAT (3F 10.0)
 P ATM = PMM/760.0
 AS = A* 4. E - 05/32.066
 $P_{H_2S} = AS* 0.08206* TK/0.2075$
 $P_{H_2} = P ATM - P_{H_2S}$
 $R = P_{H_2S}/P_{H_2}$
 $P_{S_2} = R* R* 0.00529* 0.00529$
 WRITE (6,201) A, PMM, TK, P ATM, R, P_{S_2}
 201 FORMAT (4(5X, F10.4), 2(5X, 1E16.6))
 IF(A.EQ.0.0) GO TO 99
 99 GO TO 400
 STOP
 END

examination it was found that there was considerable surface area relief arising over the polished cross sections due to the different hardness of the various constituents.

In an effort to overcome this problem the remaining specimens were nickel plated using a bath composition and conditions given in Table 4.3. A 250 ml. bath was used with a pure nickel sheet formed into a cylinder as the cathode and the specimen as the anode. The current density was controlled by the Erbach Electroplating apparatus and the bath was replenished after every second specimen. The plated specimens were then cold mounted vertically in epoxy resin inside 1" O. D. stainless steel rings and polished as before.

4.6.2 Examination

The microstructure of the specimens were examined and photographed using the Zeiss ultraflot microscope as this equipment gave the best resolution at high magnification. A selected number of specimens were examined after etching with Vilella reagent of the following composition:

- 4.5 g Picric acid.
- 22.5 ml. hydrochloric acid.
- 450 ml. ethyl alcohol.

This is a good grain boundary etchant for the alloy used. The external and subscale thicknesses on each specimen were measured on the Reichert microscope using a calibrated cross wire eyepiece equipped with a micrometer drum. The percentage of volume occupied by the subscale was found by using a point counting technique.

TABLE 4.3

Nickel Sulphamate Plating Bath Composition and Conditions.

Nickel Sulphamate	64 fl. oz/gal.
Nickel Chloride	6 oz/gal.
Boric Acid	6.5 oz/gal.
pH	3.5 - 4.0
Temperature	140 - 160°F
Current Density	80 - 120 amp/ft. ²

Information supplied by M and T Products Ltd.

4.7 Analytical Methods

4.7.1 X-ray Techniques

In an attempt to identify the constituents of the sulphidation products two X-ray techniques were used. Specimens from four out of the five different sulphur pressures used were analysed by the Debye-Scherrer powder method. The specimens from the fifth set of experiments were analysed using a Phillips X-ray fluorescent diffractometer since the scale was not suitable for the powder technique.

Samples for the Debye-Scherrer technique were prepared by scraping the external scale from the specimens, grinding it in an agate pestle and filling very fine glass capillaries with the resulting powder. Nickel-filtered copper radiation of low intensity (28kV - 15 mA) and long exposure times (up to 24 hours) was found to give better resolution of the lines on the X-ray film than higher intensity radiation. The films were analysed and compared against standards.

4.7.2 Electron Microprobe Analysis

The CAMECA MS-64 electron microprobe was used to collect information about phase compositions and the diffusion profiles of the components in the alloy and across the scale. Specimens from the metallographic examination were used for this analysis. It was necessary to deposit a thin layer of carbon on the surface of these specimens to prevent any build up of charge on the non-conductive phases present in the specimens.

Operating conditions of 15 Kv. acceleration and 100-120 nano ampere specimen current were used. Point counts were obtained for nickel, chromium and sulphur in scans from the edge of the scale

into the interior of the alloy. These counts were analysed with respect to a set of standards (NiS, Cr_7S_8 , Ni and Cr) mounted together. The results were corrected for atomic number and mass adsorption by means of a computer programme data to yield the phase composition at each point in the scan.

CHAPTER V

EXPERIMENTAL RESULTS

The data obtained from the various experimental tests described in the previous section are presented here in the form of graphs, tables and photo micrographs.

5.1 Sulphidation Kinetics

The continuous kinetic measurements carried out at sulphur potentials varying from 5.5×10^{-12} to 8.8×10^{-10} atmospheres are illustrated graphically in Fig. 5.1. in the form of weight gain in g. cm^{-2} against time in hours. At the four sulphur potentials where only the formation of chromium sulphide is thermodynamically possible the kinetics are non-linear whereas at the sulphur potential at which it is also possible for nickel to sulphidize linear kinetics are observed for the weight gain investigated. The non-linear kinetic data are plotted in the parabolic form i. e., $(\text{weight gain})^2$ vs time as in Fig. 5.2. The straight line plots obtained after the initial incubation periods indicate that the kinetics are parabolic. These results are observed only when the specimens are lowered into the reaction zone once it is at temperature and the reaction gas is flowing. Some experiments were carried out by heating the specimen in the reaction zone before passing the reaction gas and in these cases no appreciable weight gains were observed after periods of many hours. Visual observation of these specimens showed them to be slightly tarnished black.

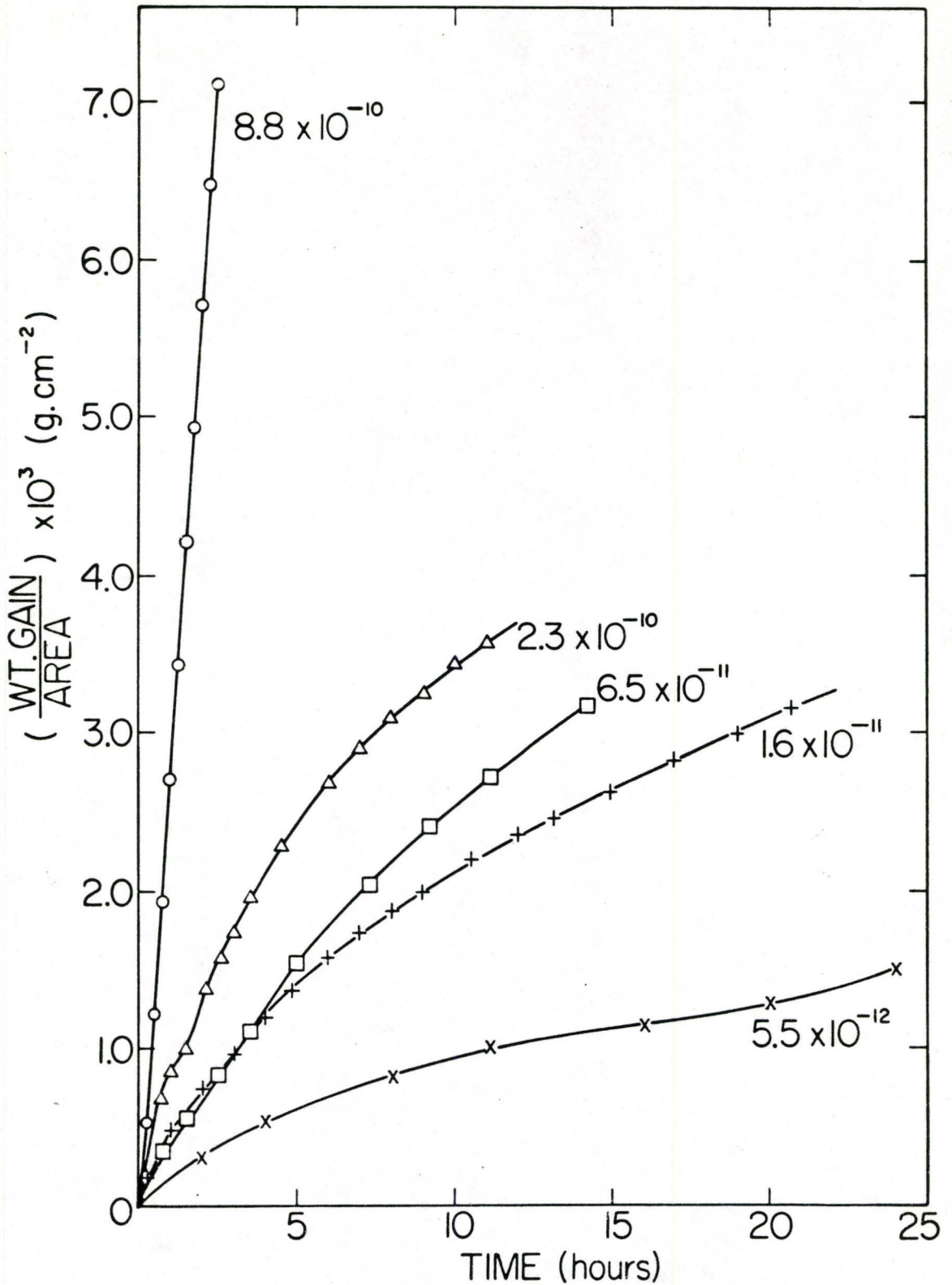


Fig. 5.1

Plot of weight gain per unit area against time for the sulphidation of a Ni - 20 w/o Cr alloy at 700°C and different sulphur potentials. The values of sulphur potential are in atmospheres.

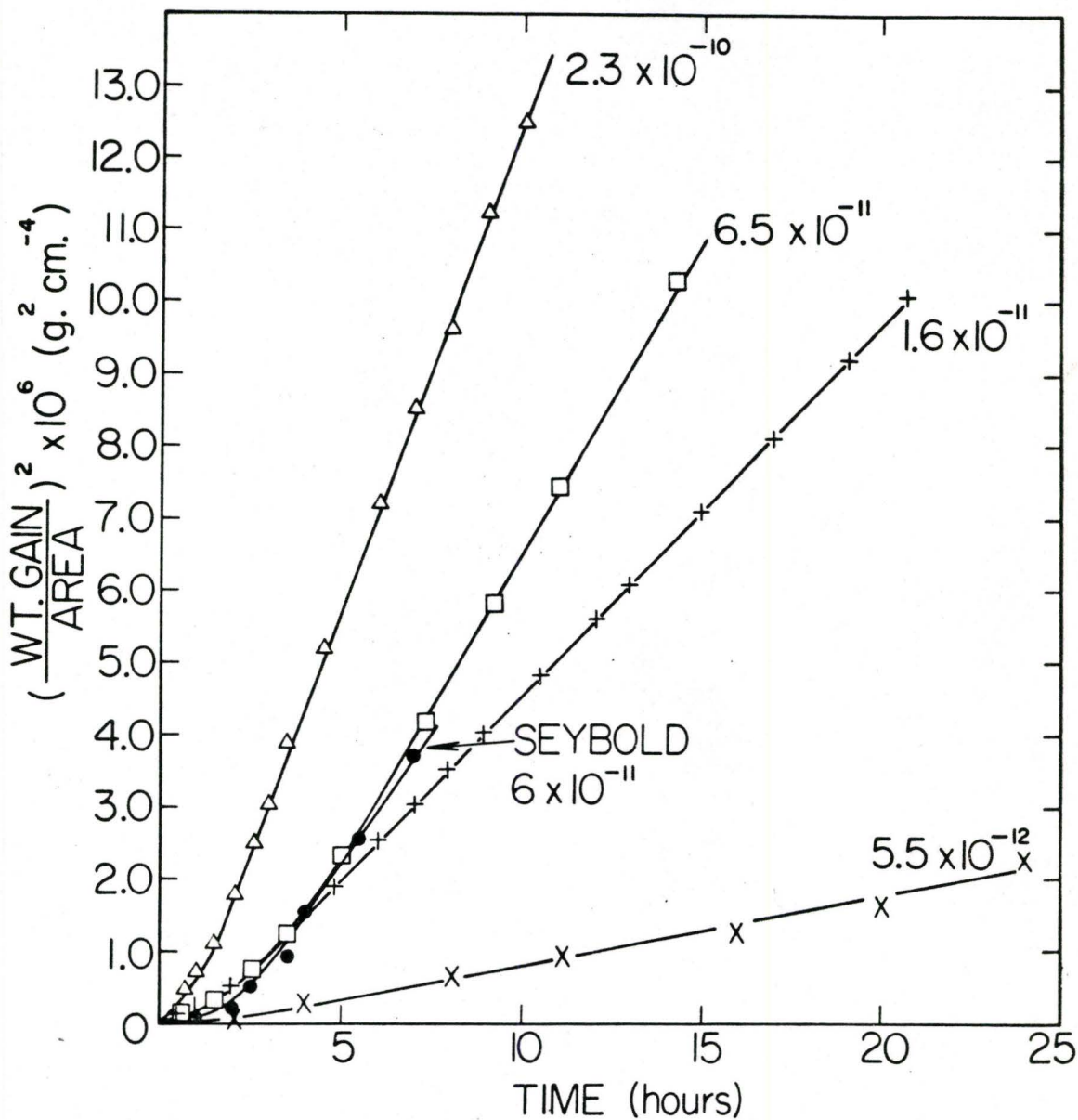


Fig. 5.2 Parabolic plot of weight gain per unit area against time for the sulphidation of a Ni - 20 w/o Cr alloy at 700°C and different sulphur potentials. Values of sulphur potential are given in atmospheres.

The parabolic rate constants, k_p , measured from the slopes of the plots in Fig. 5.2 are reported as a function of sulphur potential in Table 5.1. This data has also been plotted in Fig. 5.3 in the form of k_p vs $\log P_{S_2}$. This yields a straight line plot with a slope of 2×10^{-10} obtained by linear regression. The correlation factor for this curve is almost unity. The errors involved with the sulphur potential values obtained from Fig. 4.2 are fairly large and from these errors the error of the slope in Fig. 5.3 is estimated to be $\pm 10\%$.

The weight gains of the specimens obtained from the static experiments are listed in Table 5.2 and they compare favourably with the continuous weight gain plots in Fig. 5.1.

5.2 Metallography

The specimens sulphidized for different periods of time using the static technique were examined metallographically using an optical microscope with magnifications up to 2000X. In all cases a single layer external scale combined with a subscale was observed. The external scales were light grey, compact and soft. Difficulty was encountered in protecting the scales on polishing and in some cases nickel plating has been used to protect the edges although the scale still chipped away due to its softness.

The optical photo micrographs of the scales formed at the sulphur potentials below 5×10^{-10} atm. are shown in Figs. 5.4 to 5.7. The photo micrographs are arranged to show the external scale and subscale development with time for each sulphur potential used.

There are certain special features to note about the scales obtained. In all cases the depth of subscale penetration appears to be double the external scale thickness. The subscale particle size is very coarse but becomes finer with depth of penetration. At the lowest

TABLE 5.1

Parabolic rate constants as a function of gas composition and the sulphur potential.

$P_{\text{H}_2\text{S}}/P_{\text{H}_2}$	SULPHUR POTENTIAL P_{S_2} (atmospheres)	PARABOLIC RATE CONSTANT k_p ($\text{g}^2 \cdot \text{cm}^{-4} \cdot \text{sec}^{-1}$)
4.45×10^{-4}	5.5×10^{-12}	2.7×10^{-11}
7.56×10^{-4}	1.6×10^{-11}	1.43×10^{-10}
1.52×10^{-3}	6.5×10^{-11}	2.76×10^{-10}
2.85×10^{-3}	2.3×10^{-10}	3.75×10^{-10}

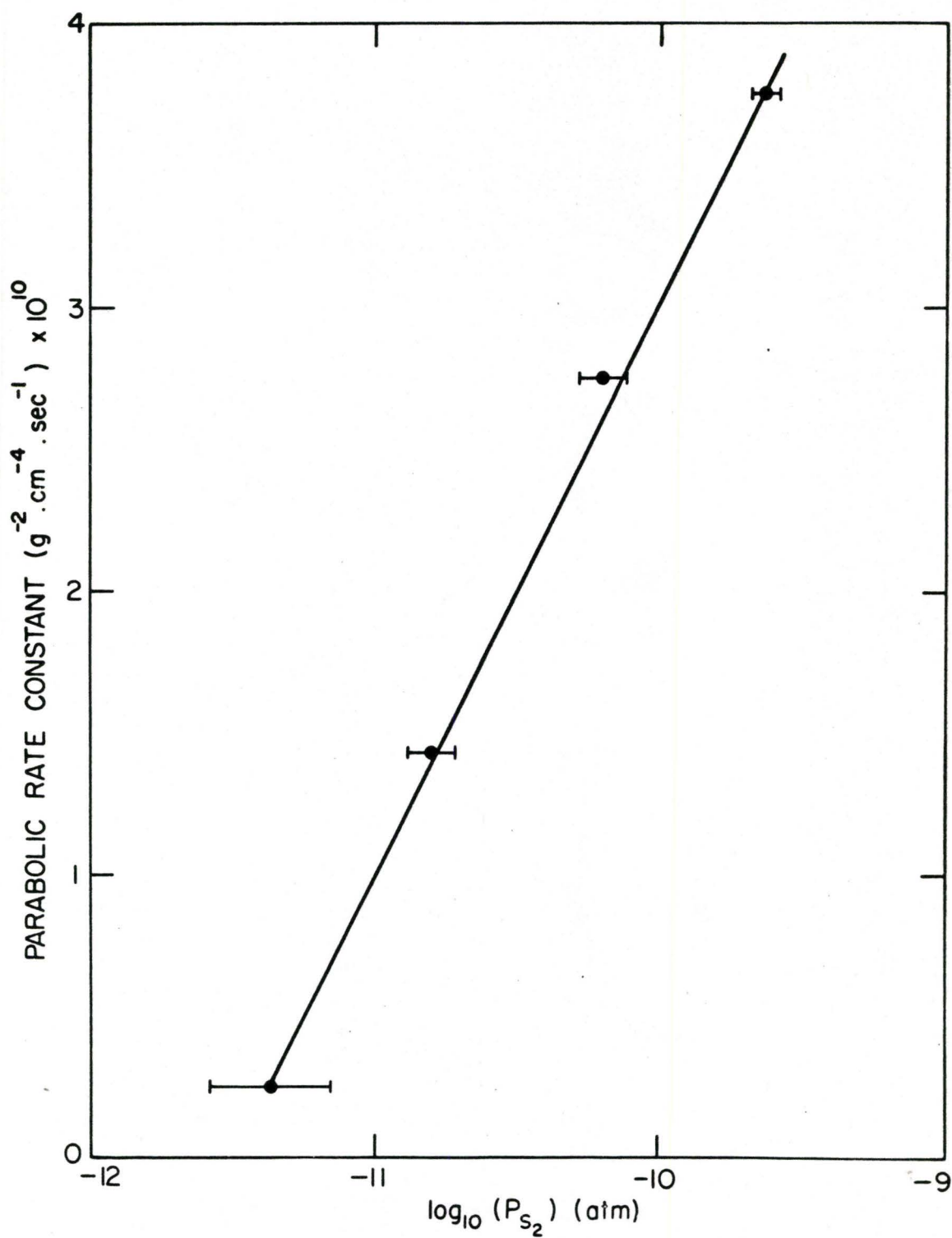


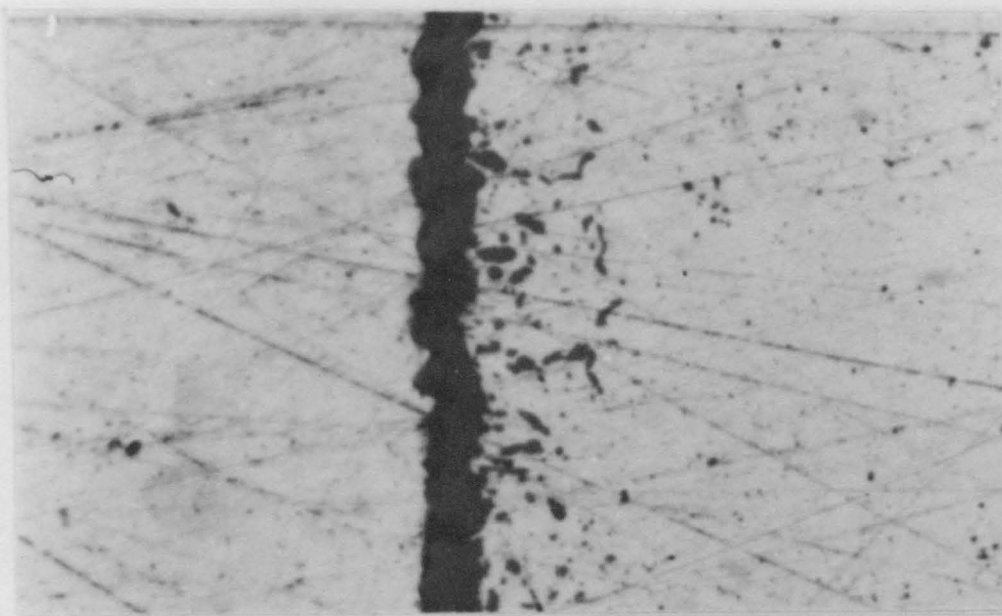
Fig. 5.3 Semilogarithmic plot of sulphur potential against parabolic rate constant, k_p .

TABLE 5.2

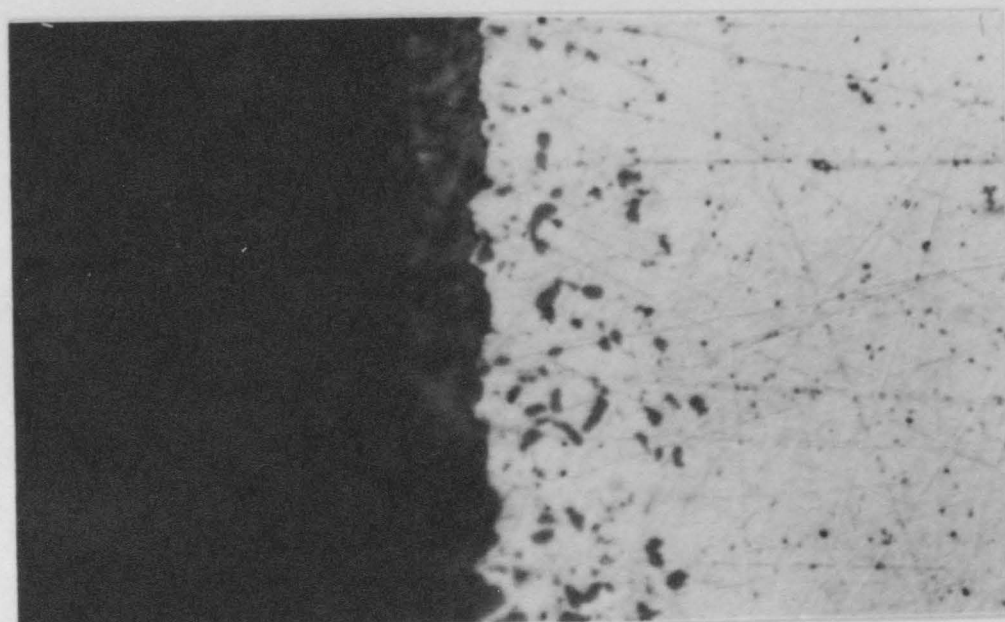
External Scale Thickness, subscale penetration, weight gain and volume fraction of subscale as a function of time.

Sulphur Potential $P_{S_2} \times 10^{-11}$ atm.	Time (hours)	Weight Gain Area ($g. cm^{-2}$).	External Scale Thickness (microns)	Subscale Penetration (microns)	Volume Fraction of Subscale
0.55	2	3×10^{-4}	2.3	5.0	25%
	4	4×10^{-4}			
	8	8×10^{-4}			
	11	1.1×10^{-3}			
	16	1.2×10^{-3}			
	20	1.3×10^{-3}			
	24	1.5×10^{-3}			
	29	1.7×10^{-3}			
1.6	1	4.5×10^{-4}	1.4	3.0	24%
	2	6.5×10^{-4}	2.2	4.6	
	4	1.1×10^{-3}	2.8	5.2	
	6	1.5×10^{-3}	3.8	8.1	
	8	1.9×10^{-3}			
	12	2.4×10^{-3}			
	15 1/2	2.9×10^{-3}	7.2	14.3	
	18 1/2	3.0×10^{-3}	8.5	15.8	
	6.5	1	5.5×10^{-4}	1.9	
2		8.0×10^{-4}	2.4	5.3	
3		1.0×10^{-3}	3.0	6.3	
4		1.3×10^{-3}	4.2	7.6	
5		1.5×10^{-3}			
6		1.8×10^{-3}			
8		2.1×10^{-3}	4.7	9.0	
12		2.8×10^{-3}	5.2	9.7	
23		1	8.0×10^{-4}	2.4	5.9
	1 1/2	1.0×10^{-3}	3.1	6.6	
	3	1.8×10^{-3}	4.0	8.3	
	4	2.1×10^{-3}	4.4	8.8	
	6	2.6×10^{-3}	5.7	10.2	
	8	3.0×10^{-3}	6.7	12.8	
	12	3.7×10^{-3}	8.5	18.5	
	16	4.1×10^{-3}			

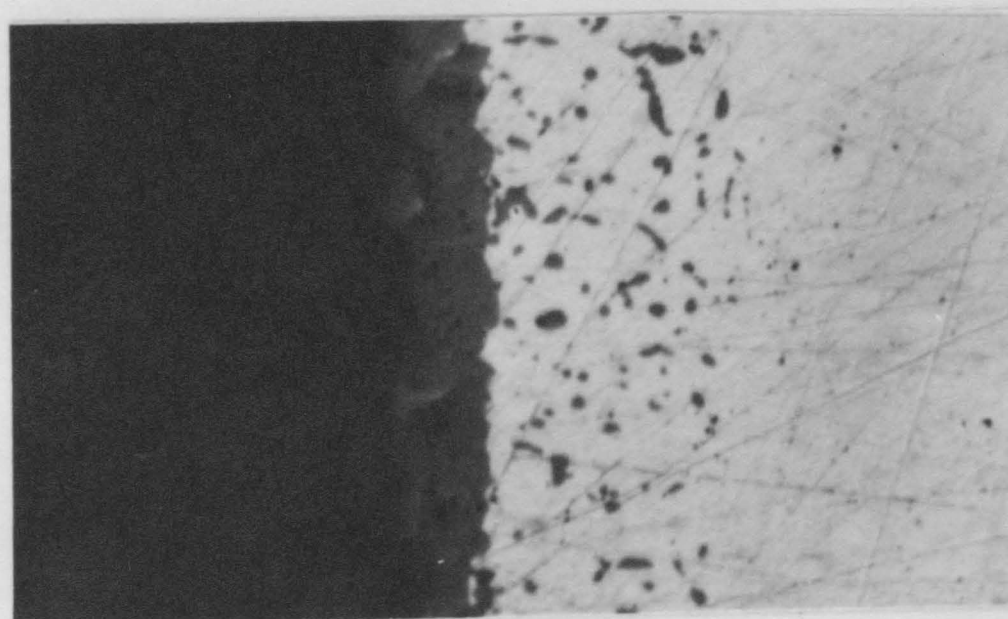
Ni plate Scale Alloy



4 HOURS

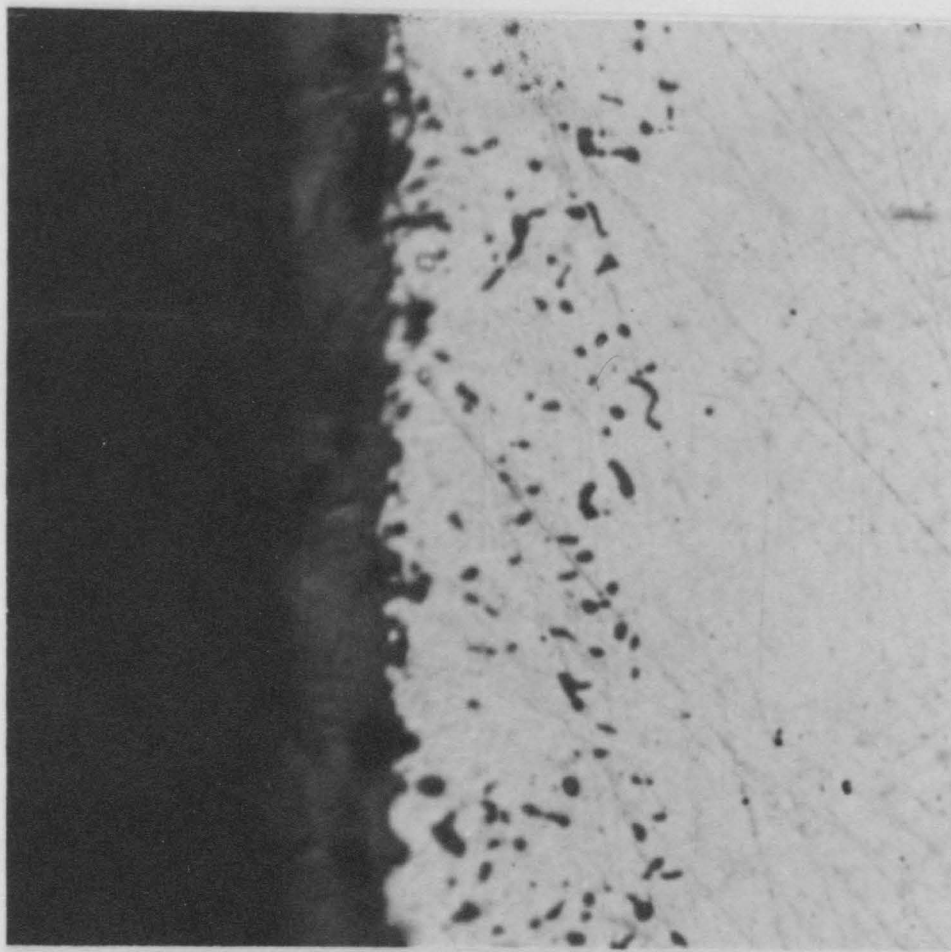


11 HOURS

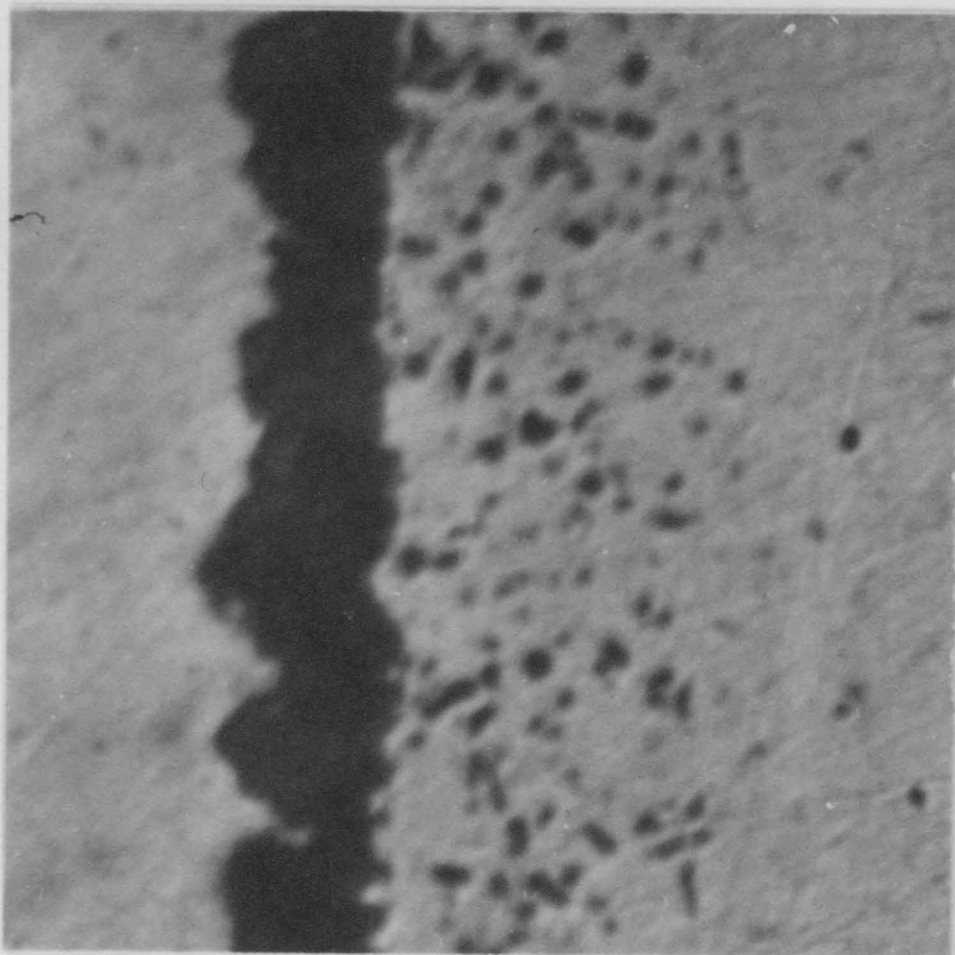


16 HOURS

Fig. 5.4 Photomicrographs of specimens sulphidized for various periods of time at a sulphur potential of 5.5×10^{-12} atmospheres. Mag. 2000X.



20 HOURS



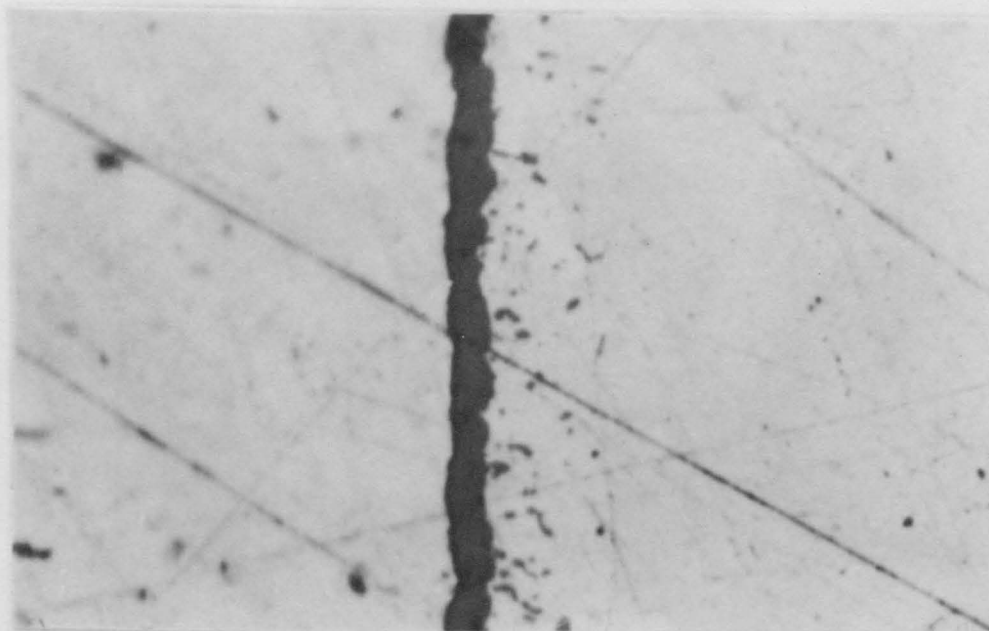
24 HOURS

Fig. 5.4 Continued. Mag. 2000X.

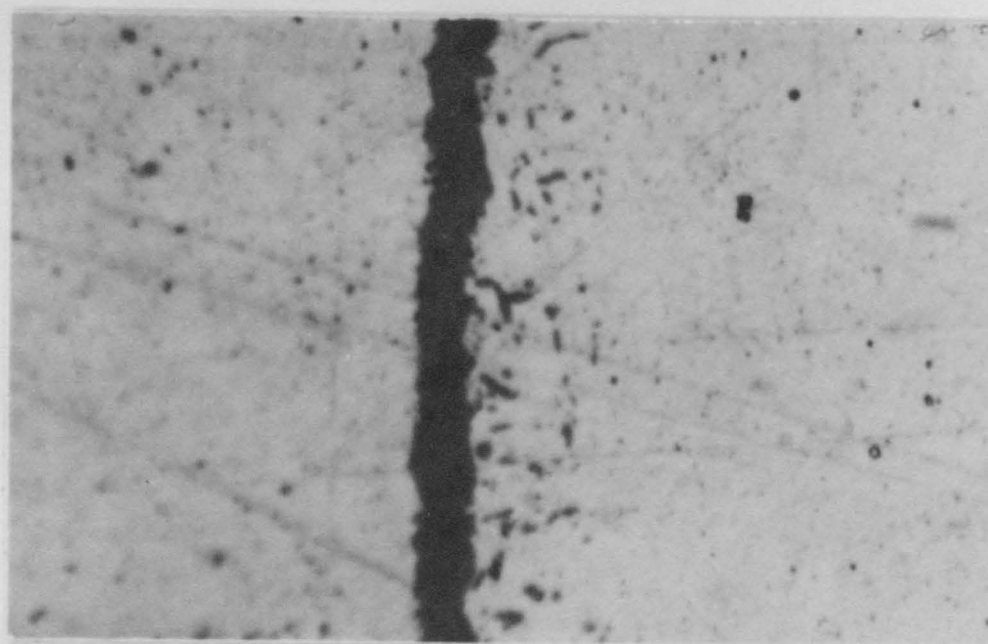
Ni plate

Scale

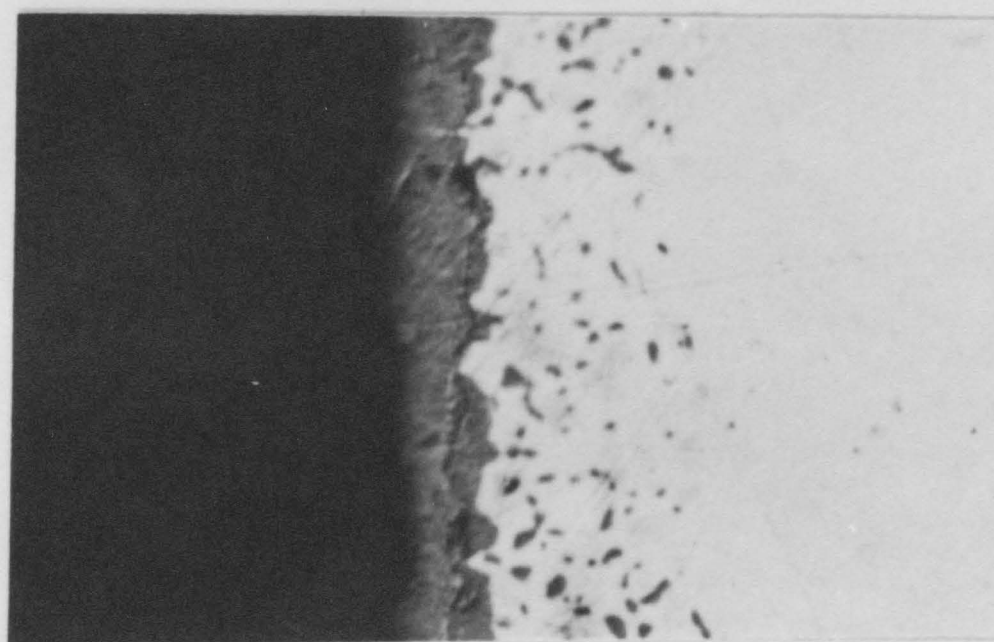
Alloy



1 HOUR



2 HOURS

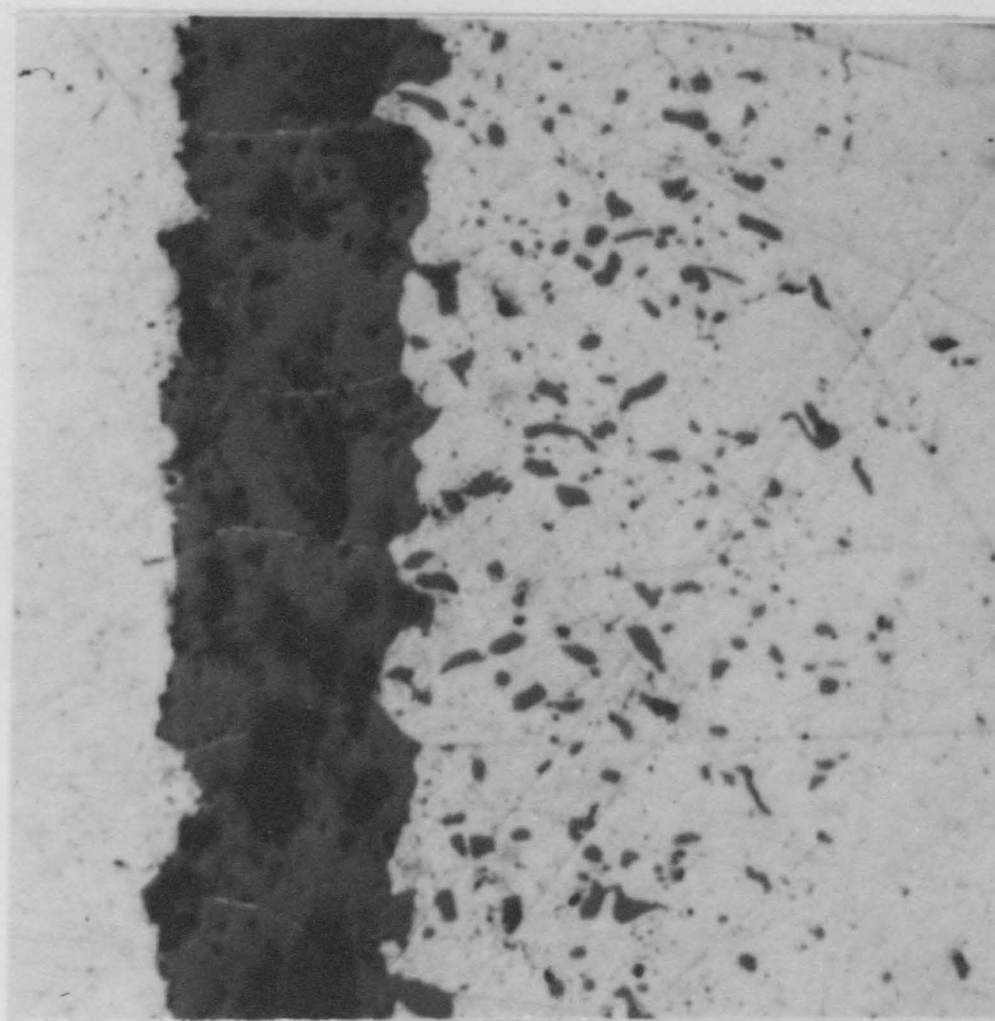


8 HOURS

Fig. 5.5 Photomicrographs of specimens sulphidized for various periods of time at a sulphur potential of 1.6×10^{-11} atmospheres. Mag. 2000X.



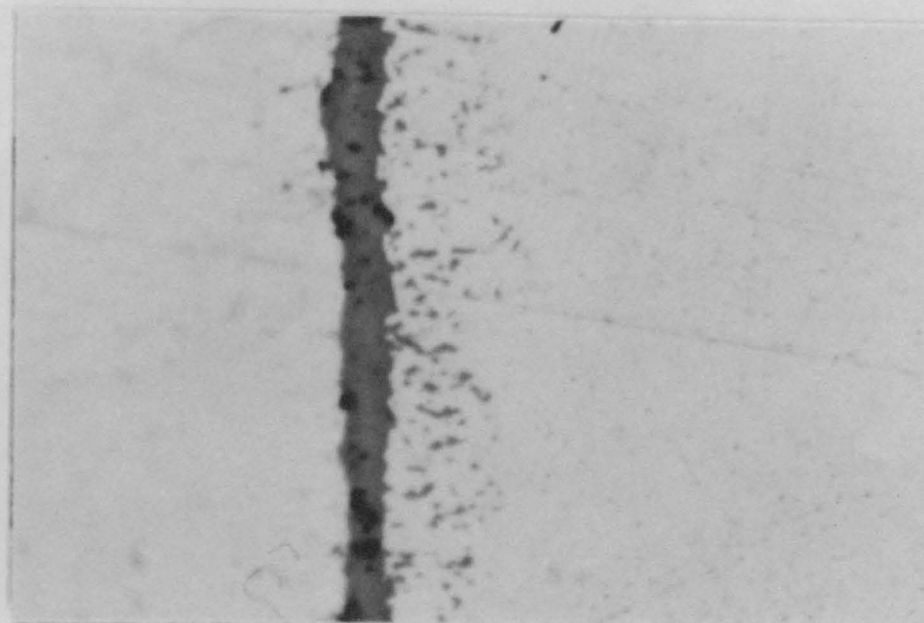
12 HOURS



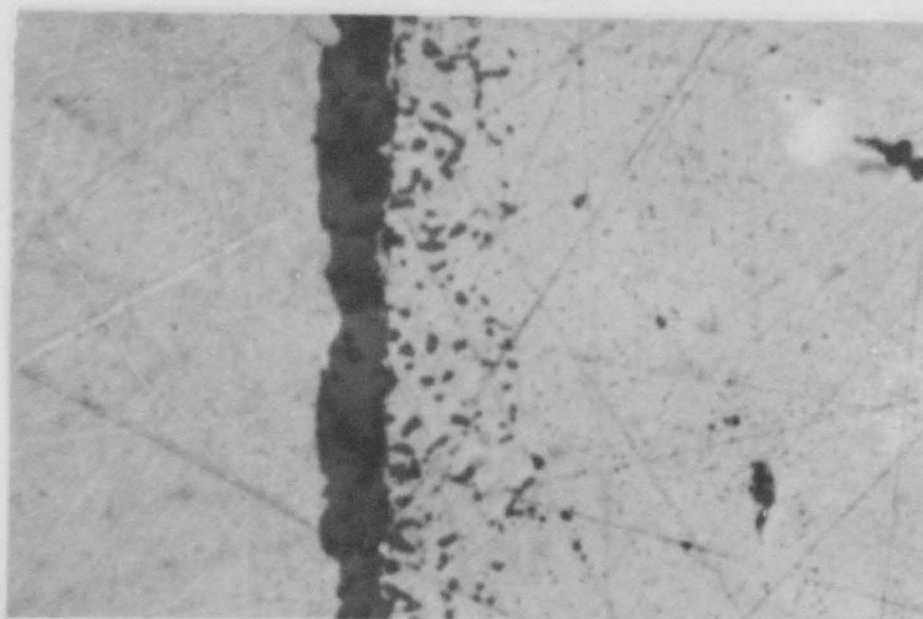
15 1/2 HOURS

Fig. 5.5 Continued. Mag. 2000X.

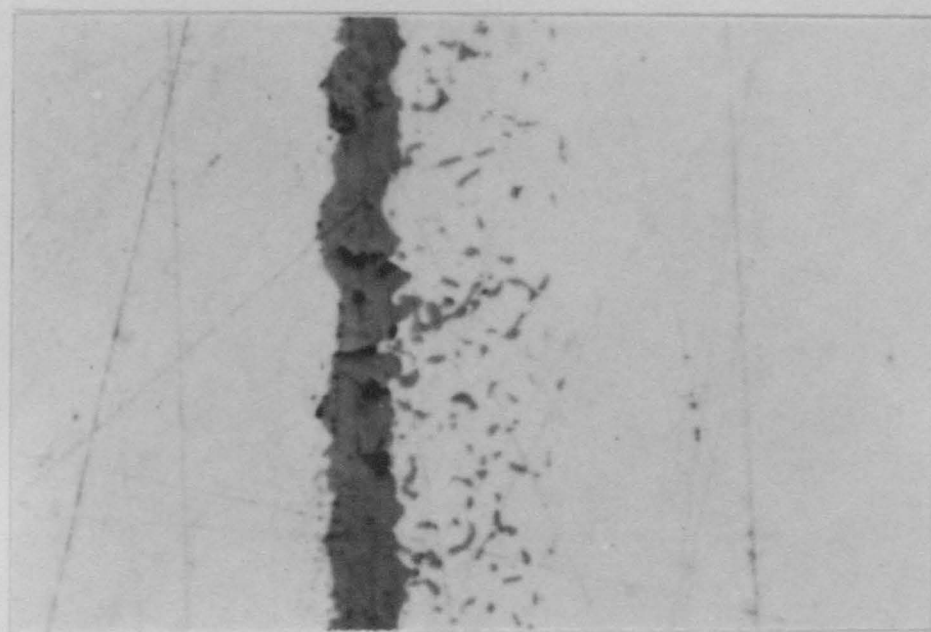
Ni plate Scale Alloy



1 HOUR

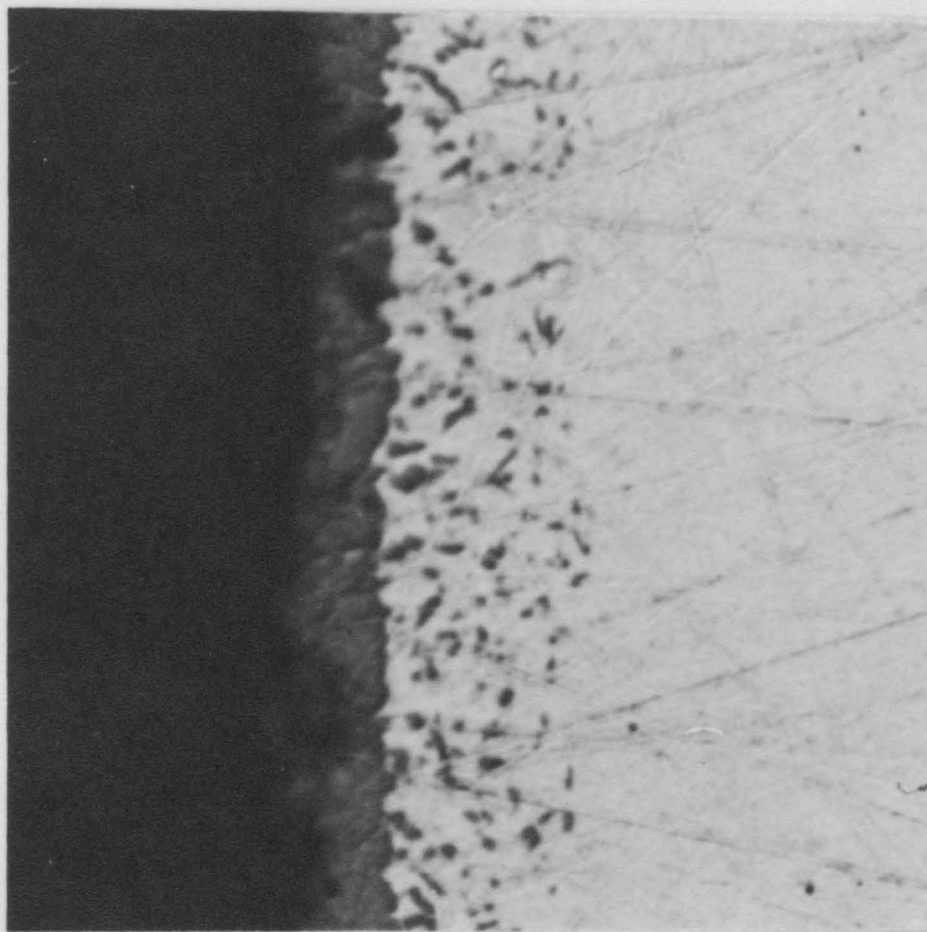


2 HOURS

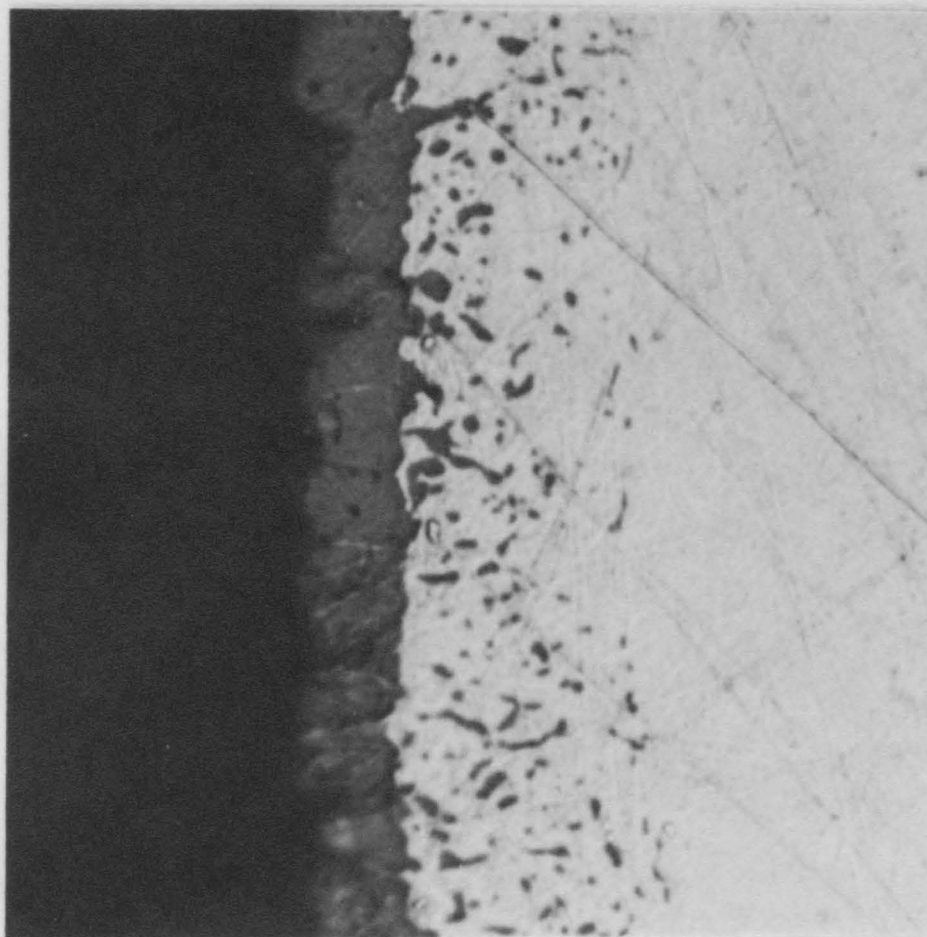


3 HOURS

Fig. 5.6 Photomicrographs of specimens sulphidized for various periods of time at a sulphur potential of 6.5×10^{-11} atmospheres. Mag. 2000X.



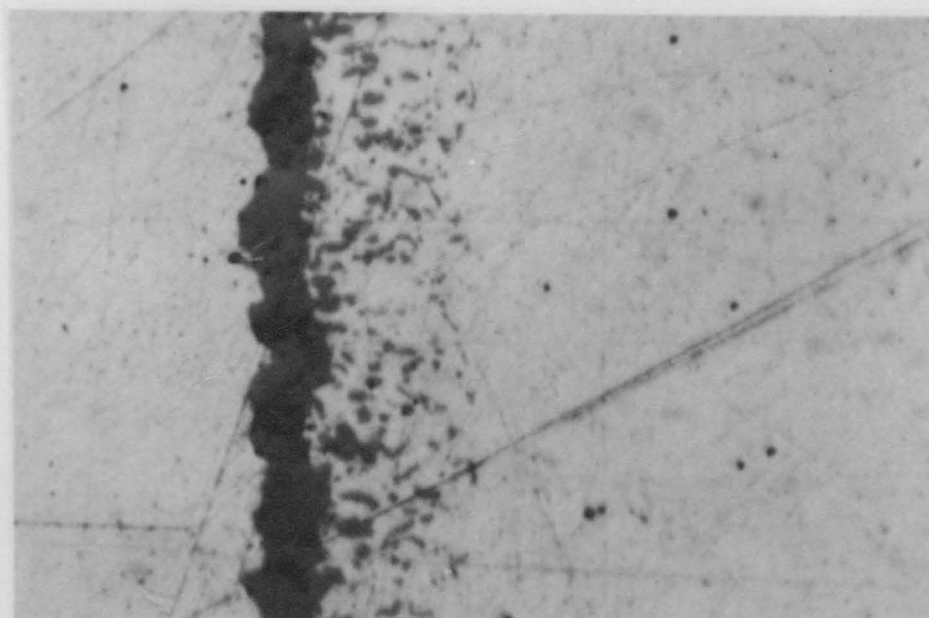
5 HOURS



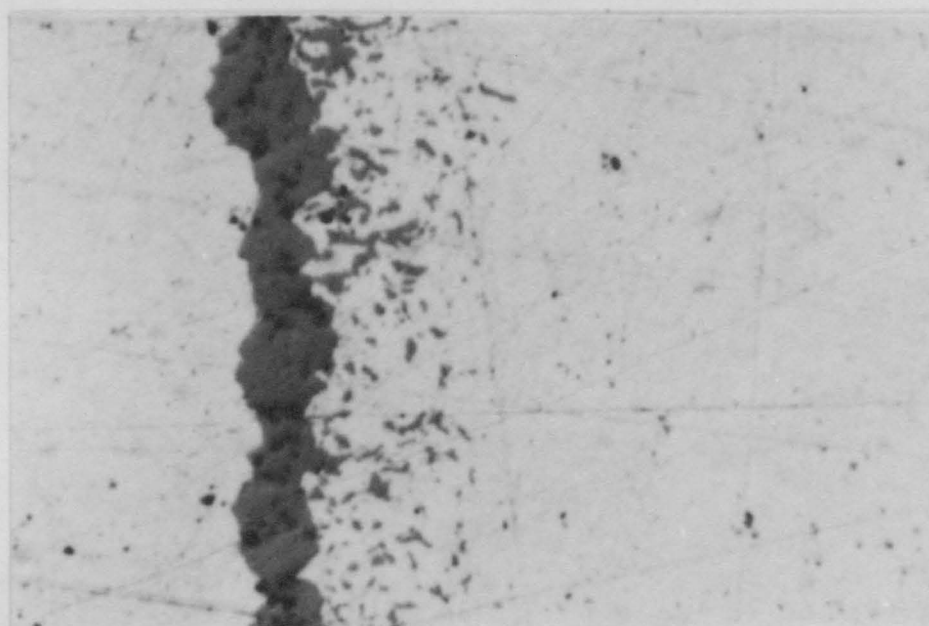
6 HOURS

Fig. 5.6 Continued. Mag. 2000X.

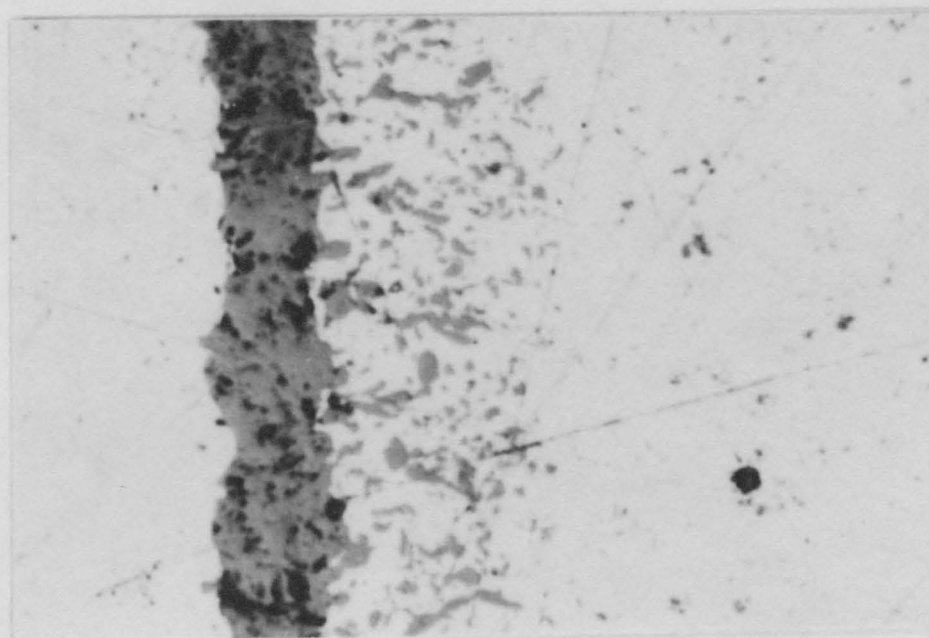
Ni plate Scale Alloy



1 HOUR

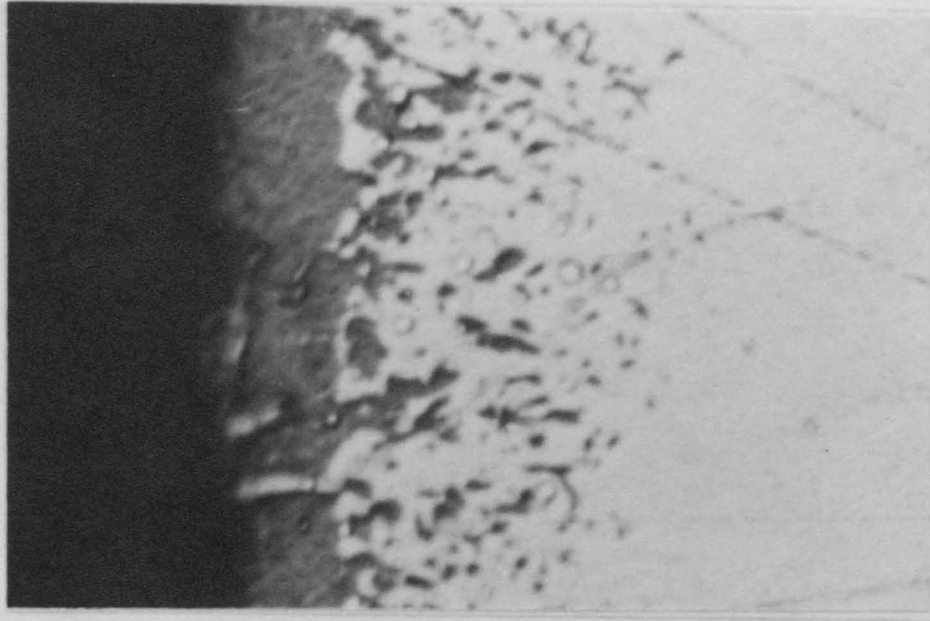


2 HOURS

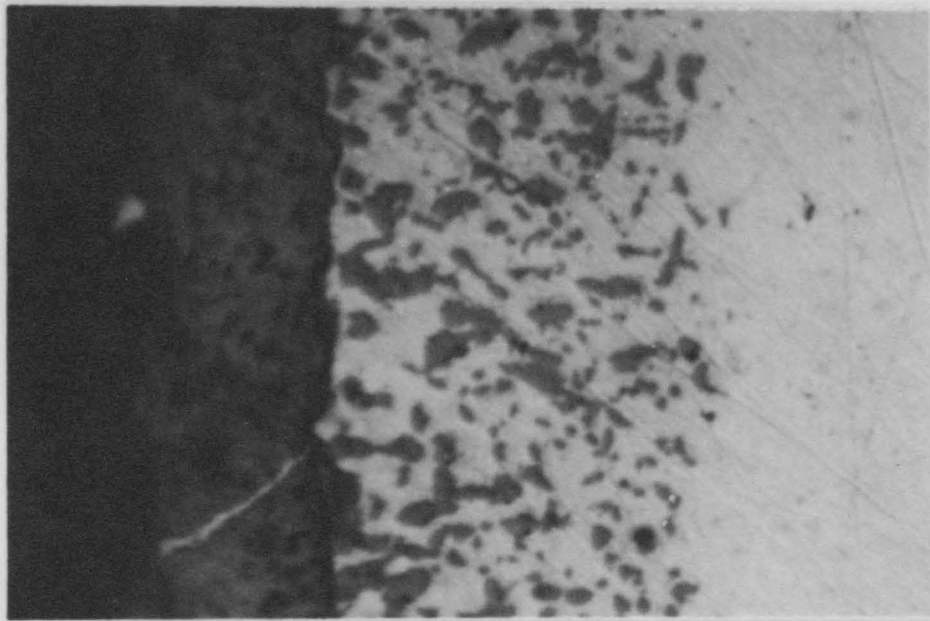


4 HOURS

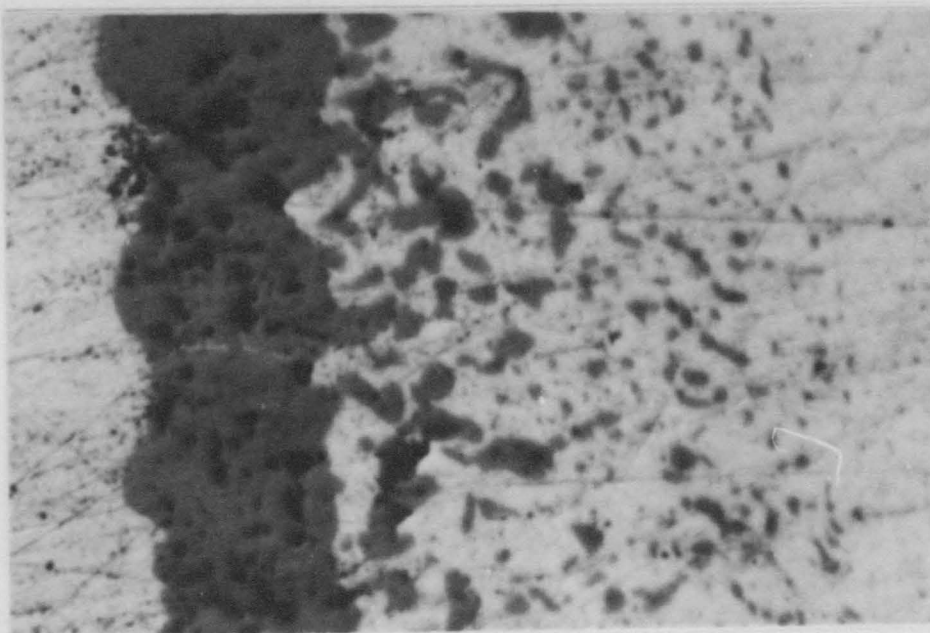
Fig. 5.7 Photomicrographs of specimens sulphidized for various periods of time at a sulphur potential of 2.3×10^{-10} atmospheres. Mag. 2000X.



6 HOURS



8 HOURS



12 HOURS

Fig. 5.7 Continued. Mag. 2000X.

sulphur potential ($P_{S_2} = 5.5 \times 10^{-12}$ atm.) the depth of subscale penetration is irregular in any one specimen but becomes more consistent with increasing sulphur potential and time. Also at this pressure an inconsistent porous layer is observed at the alloy/external scale interface as shown in Fig. 5.8.

Subscale formation has caused a morphological breakdown of the alloy/external scale interface. The extent of this breakdown appears to increase with increasing sulphur potential and time. The thicker scales also show evidence of light coloured stringers through the scales possibly at the grain boundaries. Two cases are shown in Fig. 5.9. At the lower sulphur potentials the stringers appear fine (a) and get coarser with increasing potential (b). The stringers tend to extend from the peaks of alloy at the broken down interface. Most of the stringers completely penetrate through the external scale although a few end within the layer or hook back on themselves.

A grain boundary etch was applied to one of the specimens. The results are shown in Fig. 5.10. Unfortunately, by the time the grain boundaries are revealed the subscale region is heavily etched but at least the results show that the subscale is transgranular. At points along the alloy/external scale interface the morphological breakdown is particularly severe and this may be associated with sulphide penetration at alloy grain boundaries.

A specimen sulphidized at a sulphur potential of 8.8×10^{-10} atm. is shown in Fig. 5.11. Although it is thermodynamically possible for nickel to sulphidize at this pressure the scale appears to possess the same morphology as the other specimens but with two noticeable differences. The specimens on removal from the reaction chamber possessed a light green crystalline scale compared with the light grey scales observed at the other sulphur potentials. The scales may also be denser than those previously observed as they tended to be thinner than scales of the same weight gain/unit area formed on specimens at

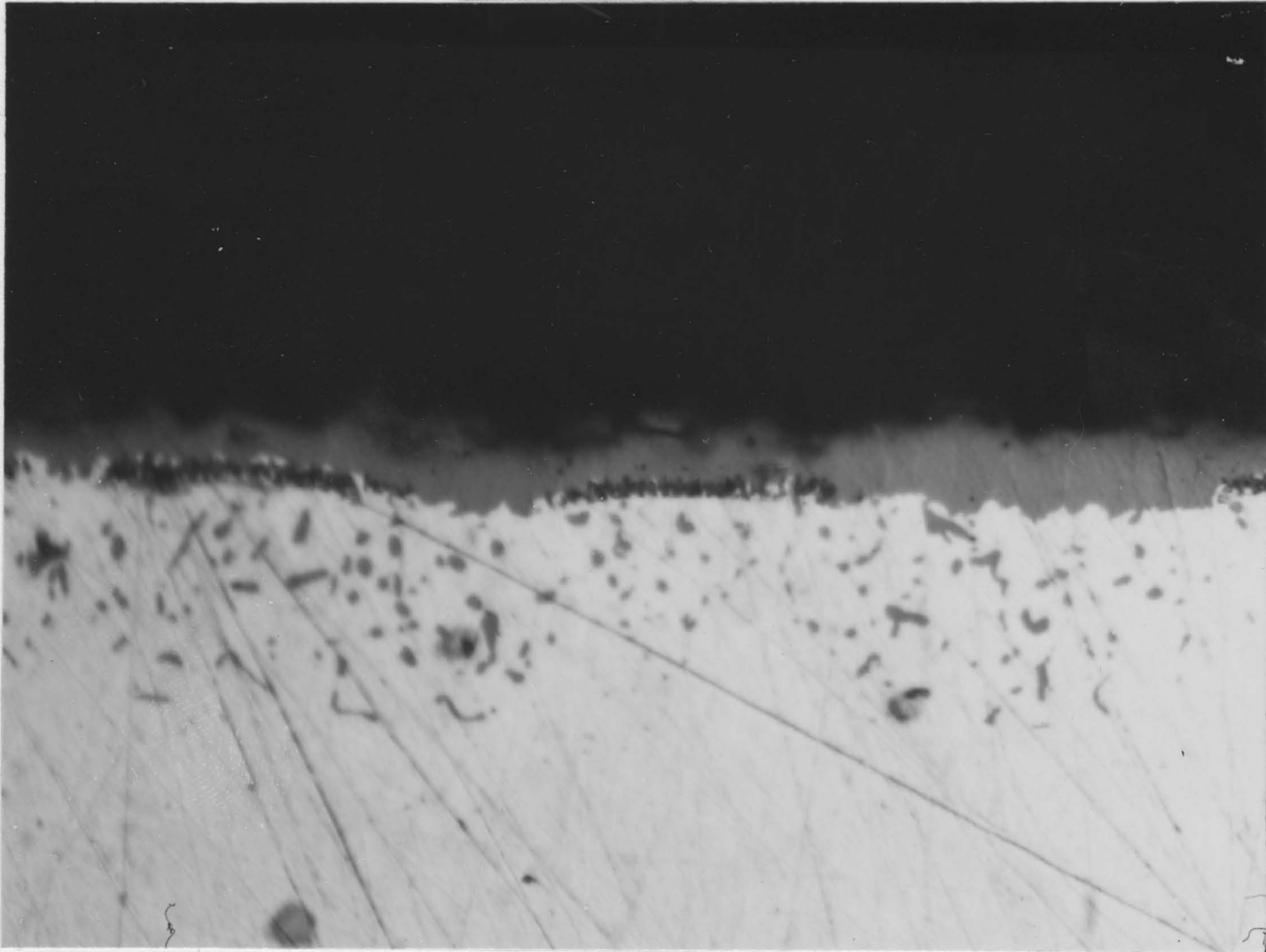


Fig. 5.8 Micrograph of specimen sulphidized at sulphur potential of 5.5×10^{-12} atm. for 16 hours showing possible porosity at alloy/scale interface. Mag. 2000X.

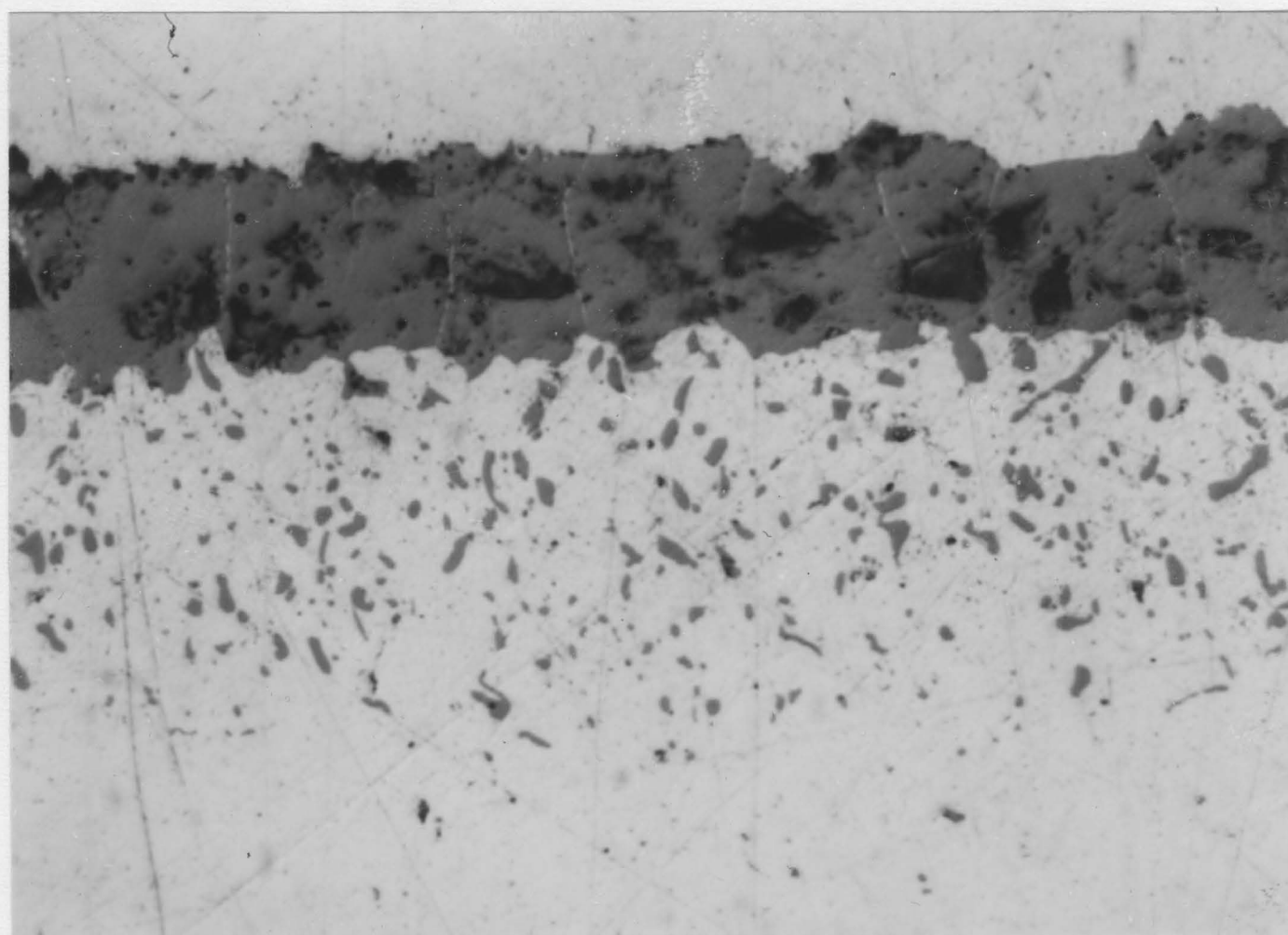


Fig. 5.9 (a) Micrograph of specimen sulphidized at sulphur potential of 1.6×10^{-11} atm. for 15 1/2 hours showing a series of fine stringers. Mag. 2000X.

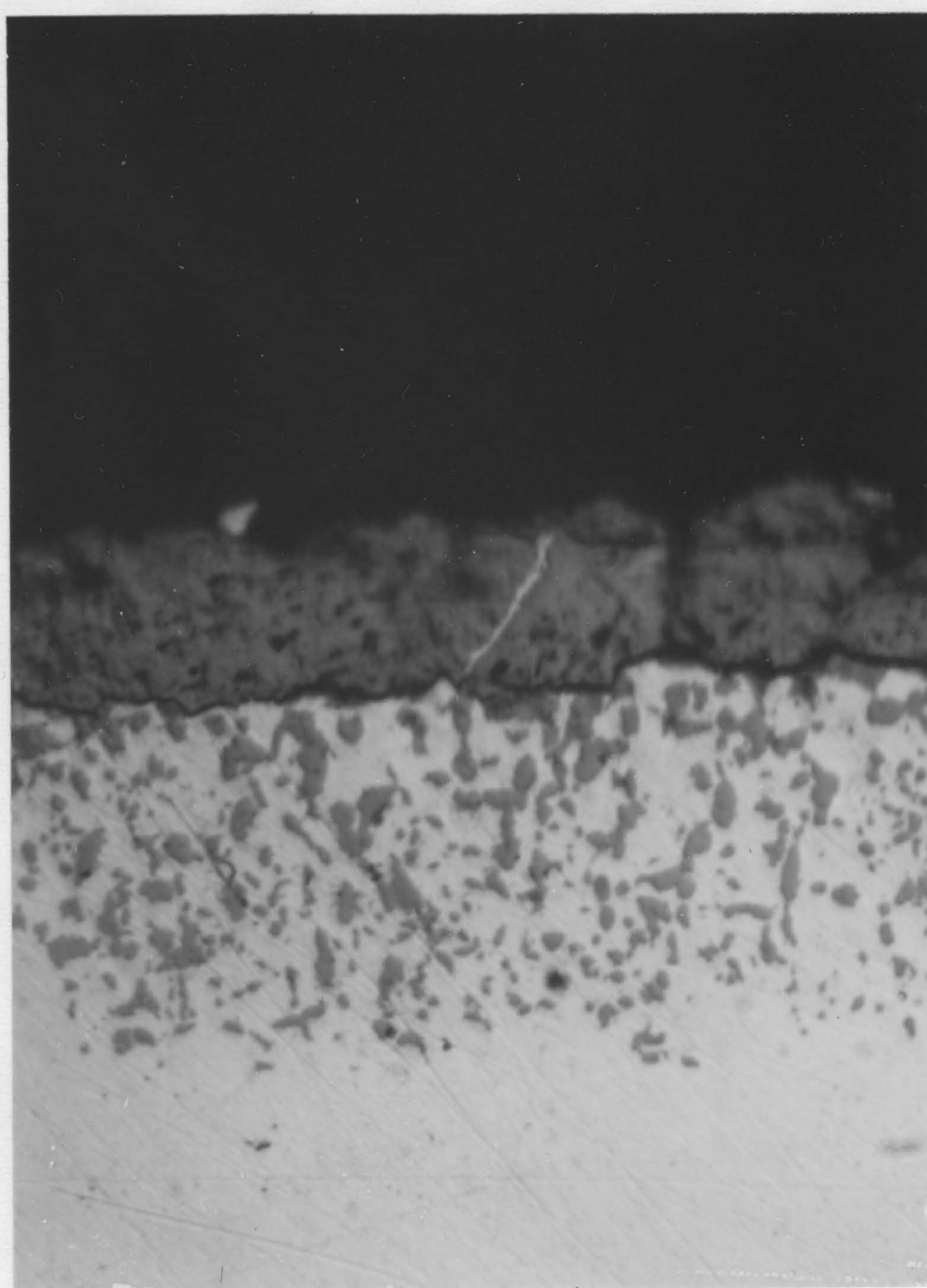


Fig. 5.9 (b) Micrograph of specimen sulphidized at sulphur potential of 2.3×10^{-10} atm. for 8 hours showing a single large stringer. Mag. 2000X.

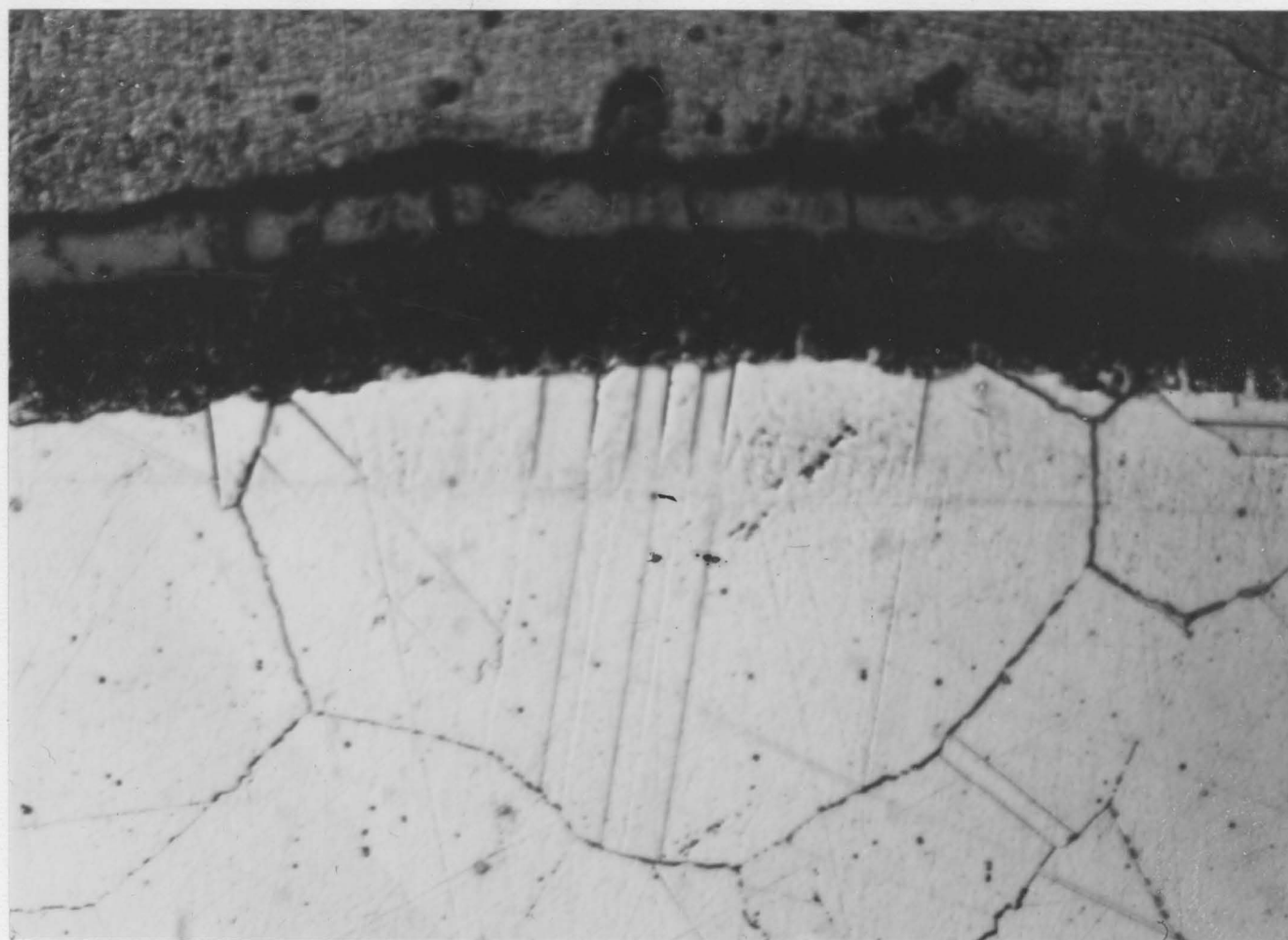


Fig. 5.10 Micrograph of sample sulphidized for 12 hours at $P_{S_2} = 2.3 \times 10^{-10}$ atm. and etched with Vilella's reagent. Mag. 600X.

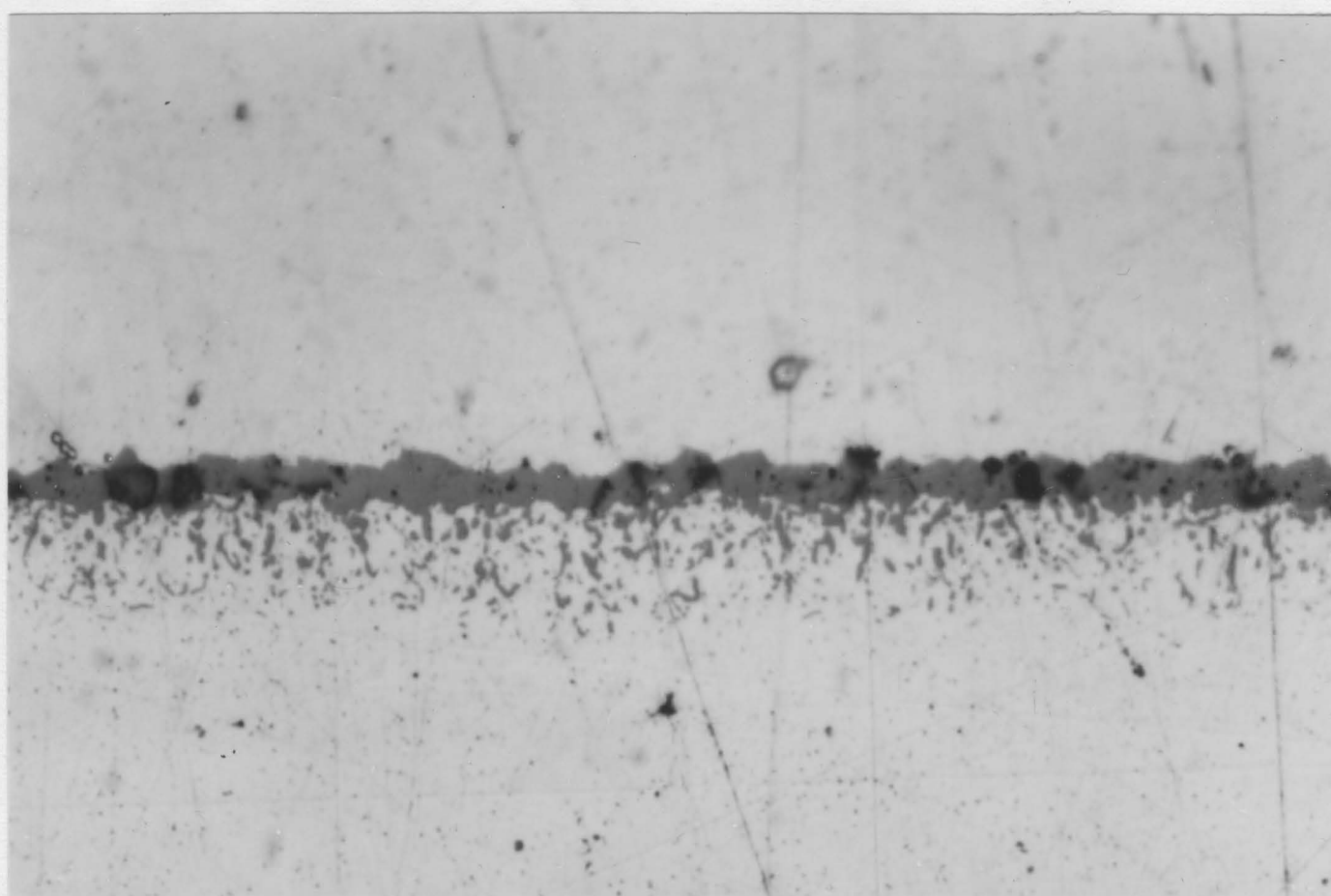


Fig. 5.11 Micrograph of specimen sulphidized for 1/2 hours at $P_{S_2} = 8.8 \times 10^{-10}$ atm. Mag. 2000X.

the lower sulphur potentials.

A presentation of the external scale and subscale growth as a function of time at one sulphur potential is given in Fig. 5.12. Scale thickness and subscale penetration were measured at 20 different points on each specimen. The average values obtained by statistical treatment have been plotted against the reaction time. The measurements are also listed in Table 5.2. The morphological breakdown of the alloy/external scale interface introduced errors into the scale thickness measurements. The original interface was considered to be halfway between the alloy peaks and the deeper points of external scale penetration. As a result of uneven external scale growth, loss of external scale outer edge and non-uniform subscale penetration the error bars in Fig. 5.12, which are proportional to the probable error, are quite large. It appears, however, that both the external scale and the subscale follow the same growth kinetics.

The volume fractions occupied by the subscale in selected specimens were measured by a point counting technique and these results are summarized in Table 5.2. Point counts on two specimens were carried out using a Quantimet 720 and gave a close comparison to the results obtained by the less sophisticated technique.

5.3 Phase Identification

Two techniques were used in an attempt to identify the phases present in the external scale. Due to the inherent difficulty in identifying the various stoichiometric forms of chromium sulphide the results from each technique alone are insufficient but when combined certain conclusions can be made.

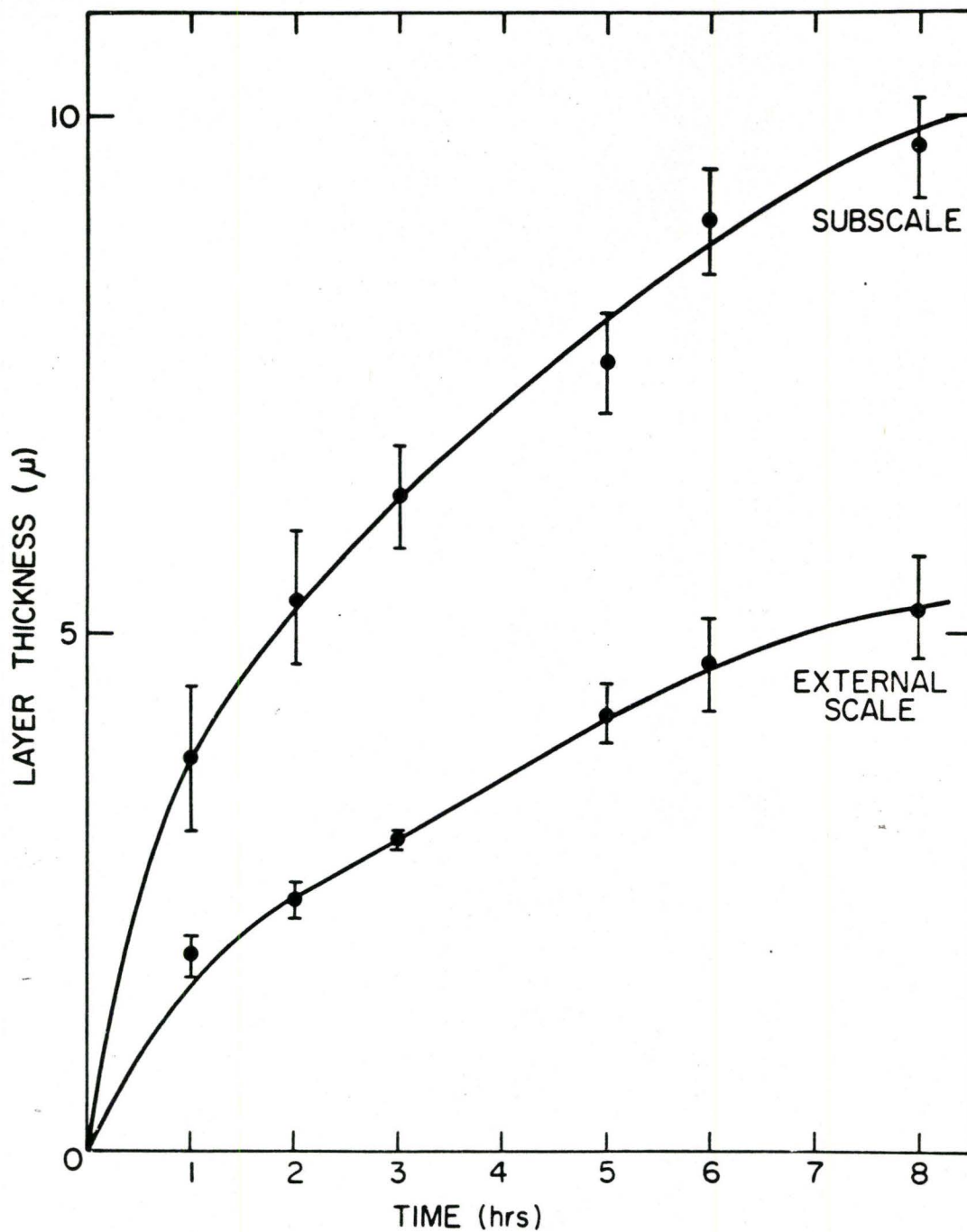


Fig. 5.12 Plot of external layer growth and subscale penetration against time for specimens sulphidized at $P_{S_2} = 6.5 \times 10^{-11}$ atmospheres.

100-10-6
100-10-4-3

5.3.1 Electron Microprobe Analysis

One specimen from each of the sulphur potentials used was examined with the electron microprobe. Scans of 1 micron steps were made from the interior of the alloy across the subscale and through the external scale. The point counts obtained were translated into the composition distance profiles shown in Figs. 5.13 to 5.17.

One micron scan steps were used because of the small scale thicknesses obtained. The electron beam spot is about 10 microns in diameter which is the same order of magnitude as the scale thickness. As a result of this the probe data obtained can only be considered as an arbitrary representation of the concentration profiles especially at the alloy/external scale interface where there is morphological breakdown.

In all cases the chromium and nickel counts in the external scale were considered to be due to sulphide. At pressures below $P_{S_2} = 5 \times 10^{-10}$ atm. all nickel inside the alloy was considered to be sulphur free. All the sulphur was considered to be combined with chromium and the chromium in the subscale region was considered to be combined with sulphur at the same ratio as in the external scale. Extra chromium counts were then treated as alloy derived. The specimen obtained at $P_{S_2} = 8.8 \times 10^{-10}$ atm. provided certain difficulties since nickel was sulphidized to a sulphide and in order to translate the point counts certain assumptions were required. All nickel counts in the alloy were considered to be sulphide free while those in the external scale were from sulphides. As long as the ratio of chromium counts to sulphur counts exceeded the ratio obtained from the chromium sulphide (Cr_7S_8) standard then the sulphur counts were derived from chromium sulphide. The chromium counts in this region were analysed according to the standard ratio. Once the sulphur counts exceed the

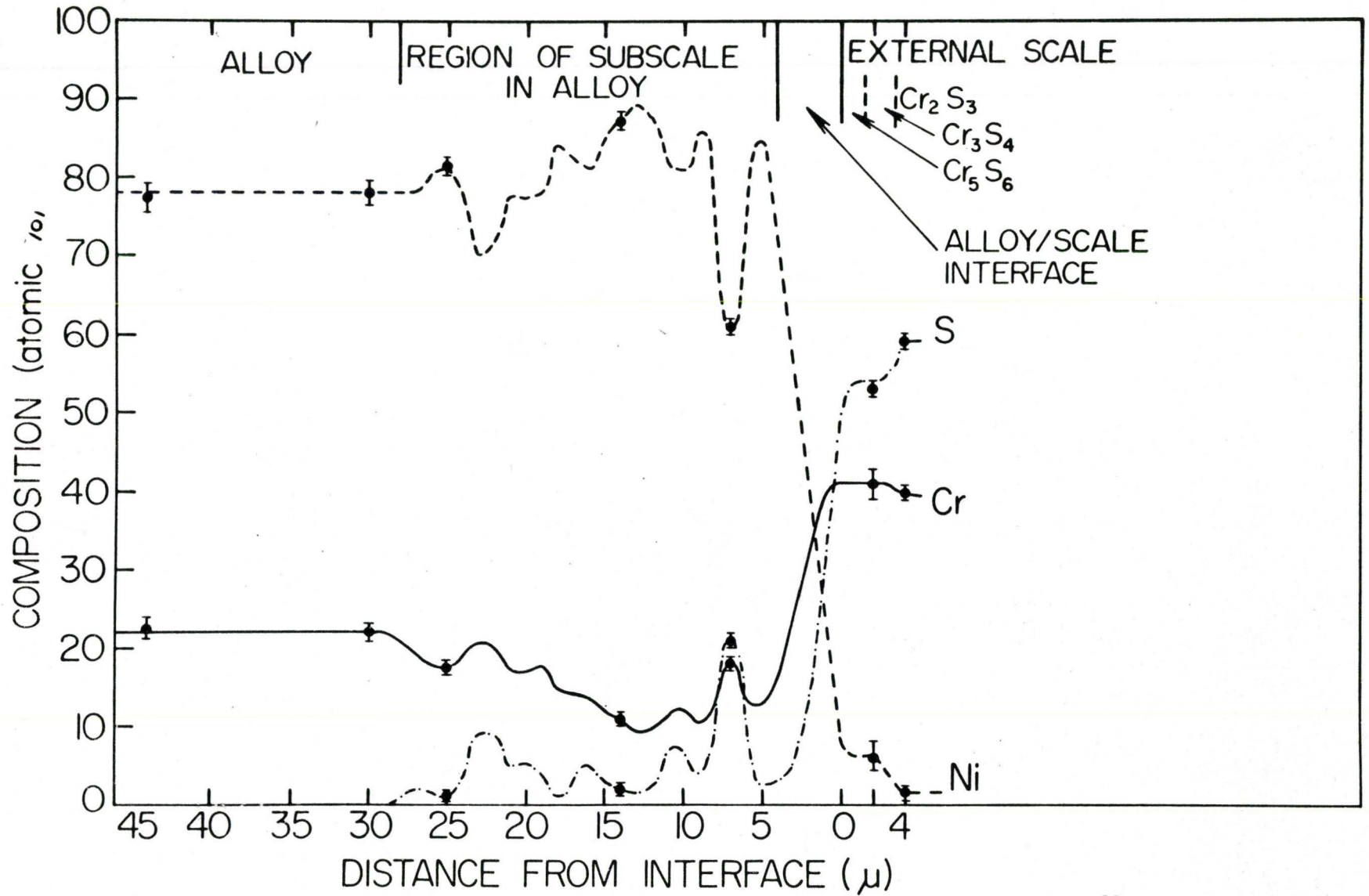


Fig. 5.13 Distribution profile after sulphidation at a sulphur potential of 5.5×10^{-12} atmospheres for 24 hours.

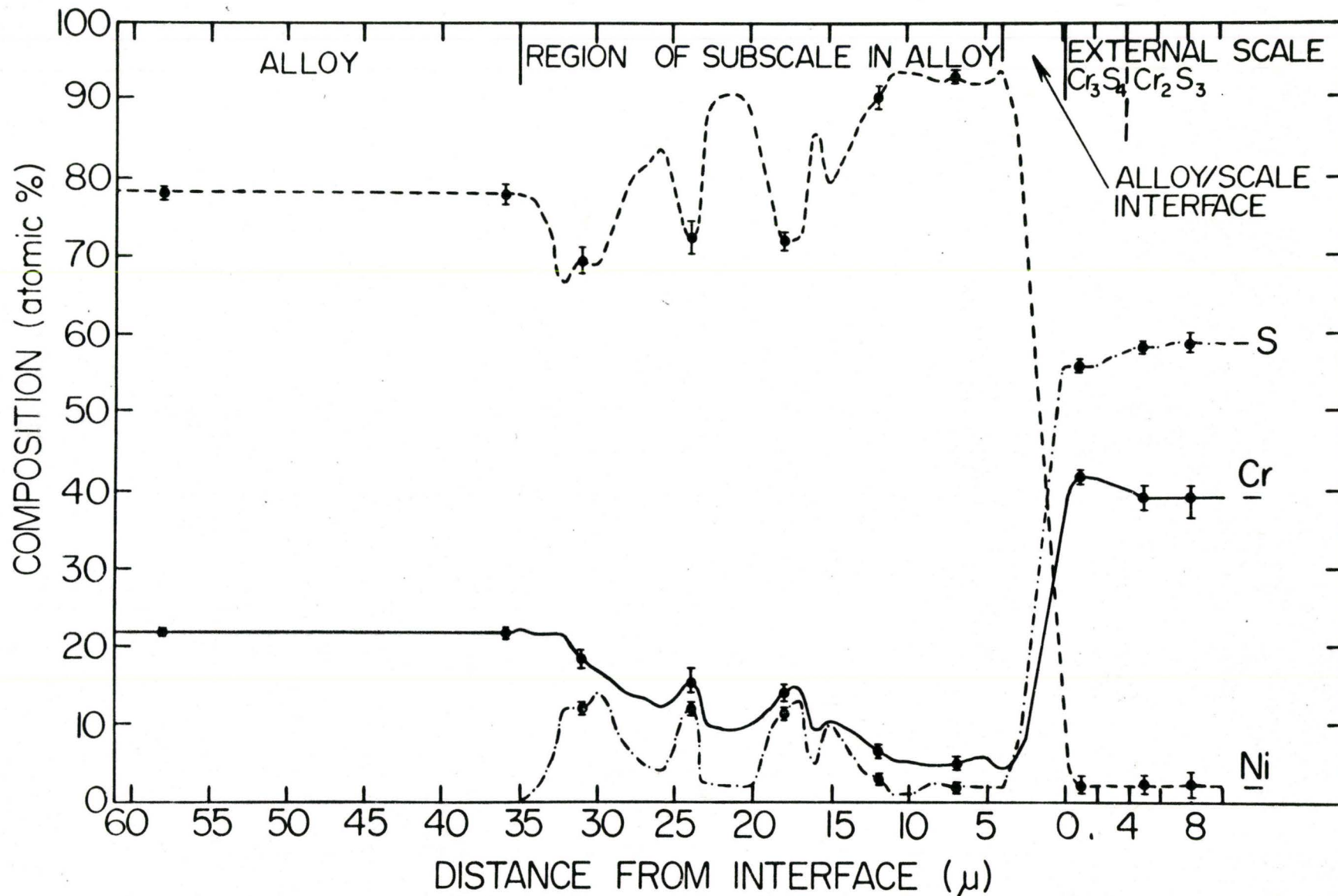


Fig. 5.14 Distribution profile after sulphidation at a sulphur potential of 1.6×10^{-11} atmospheres for 15 hours.

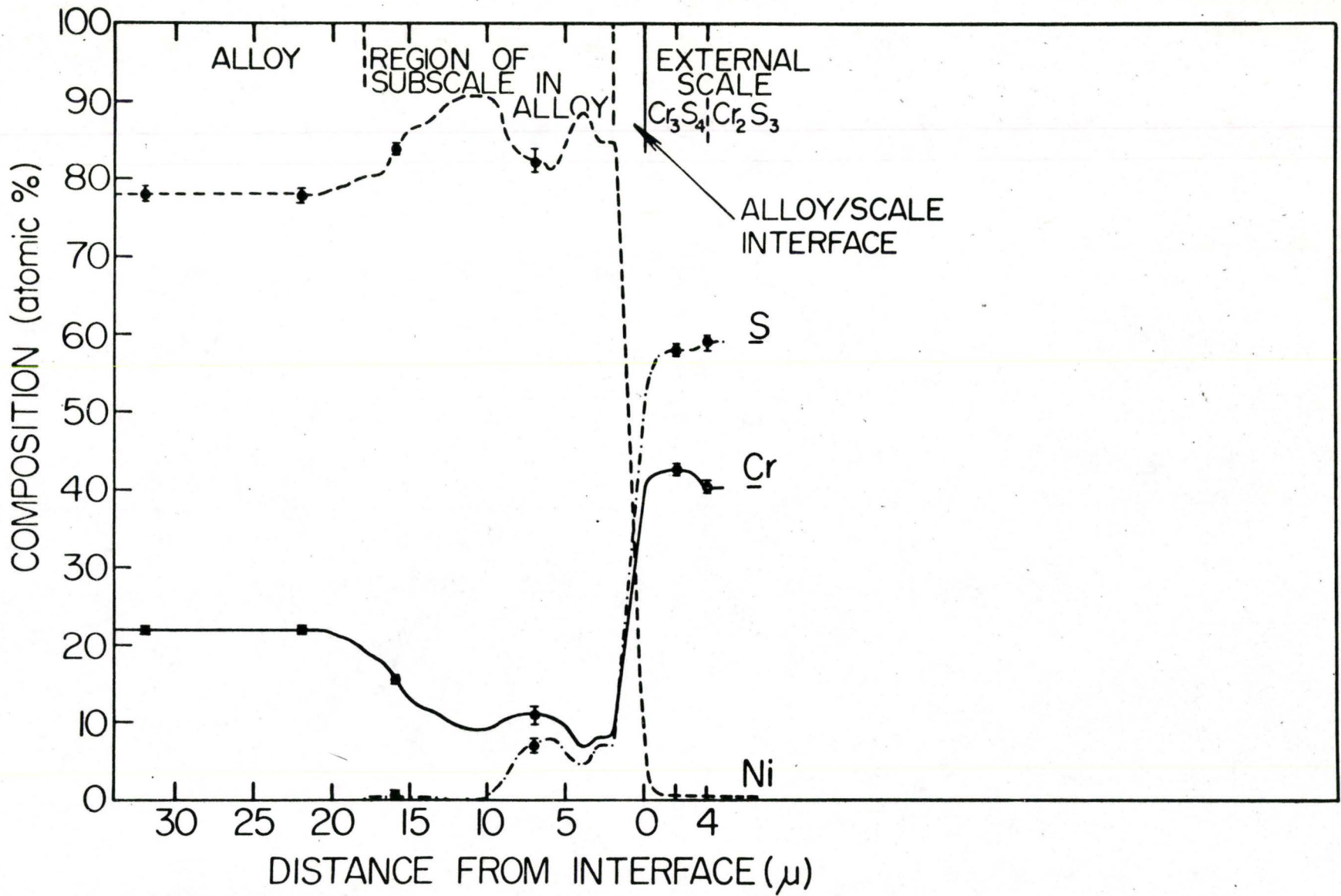


Fig. 5.15 Distribution profile after sulphidation at a sulphur potential of 6.5×10^{-11} atmospheres for 8 hours.

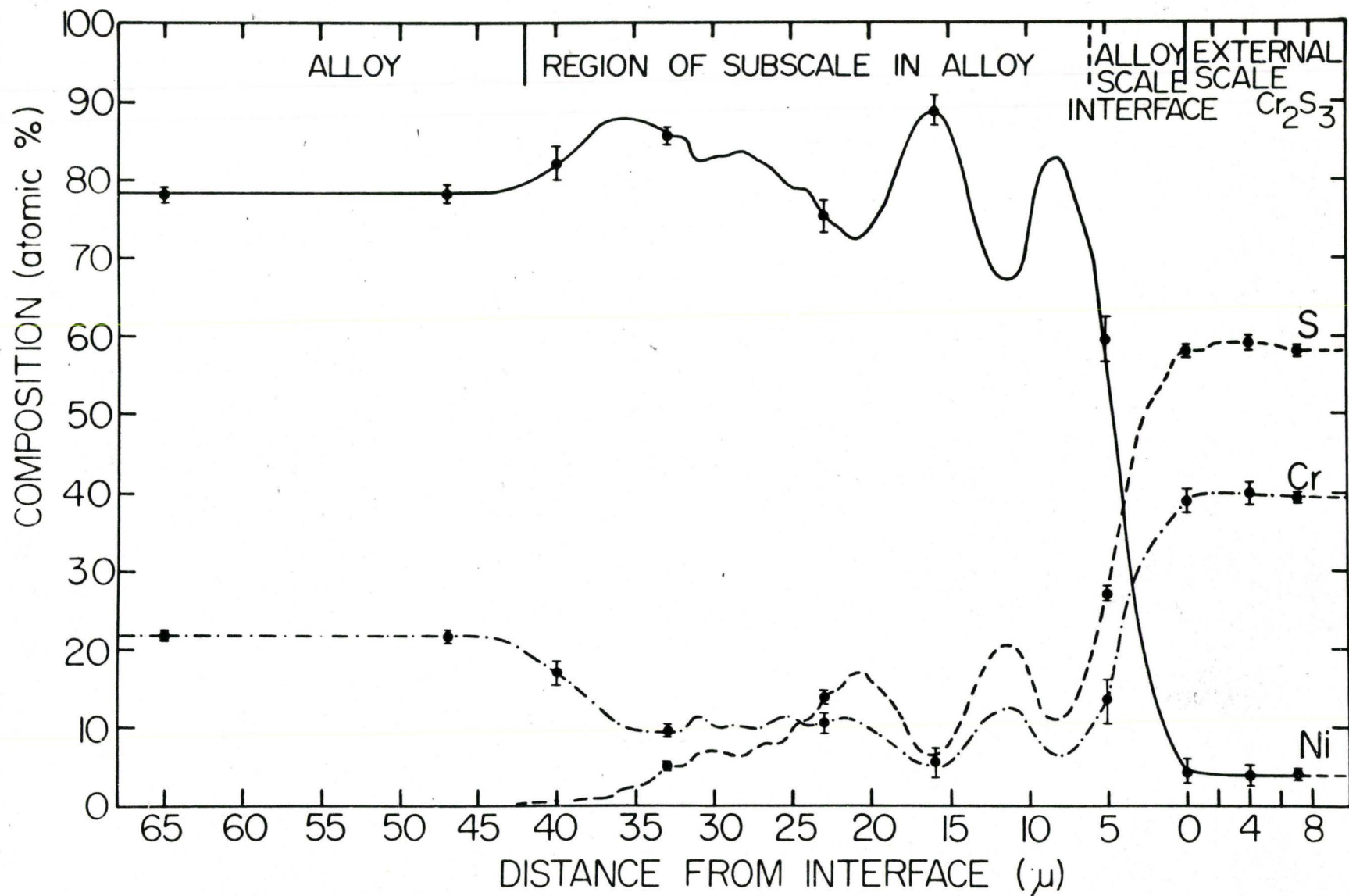


Fig. 5.16 Distribution profile after sulphidation at a sulphur potential of 2.3×10^{-10} atmospheres for 13 hours.

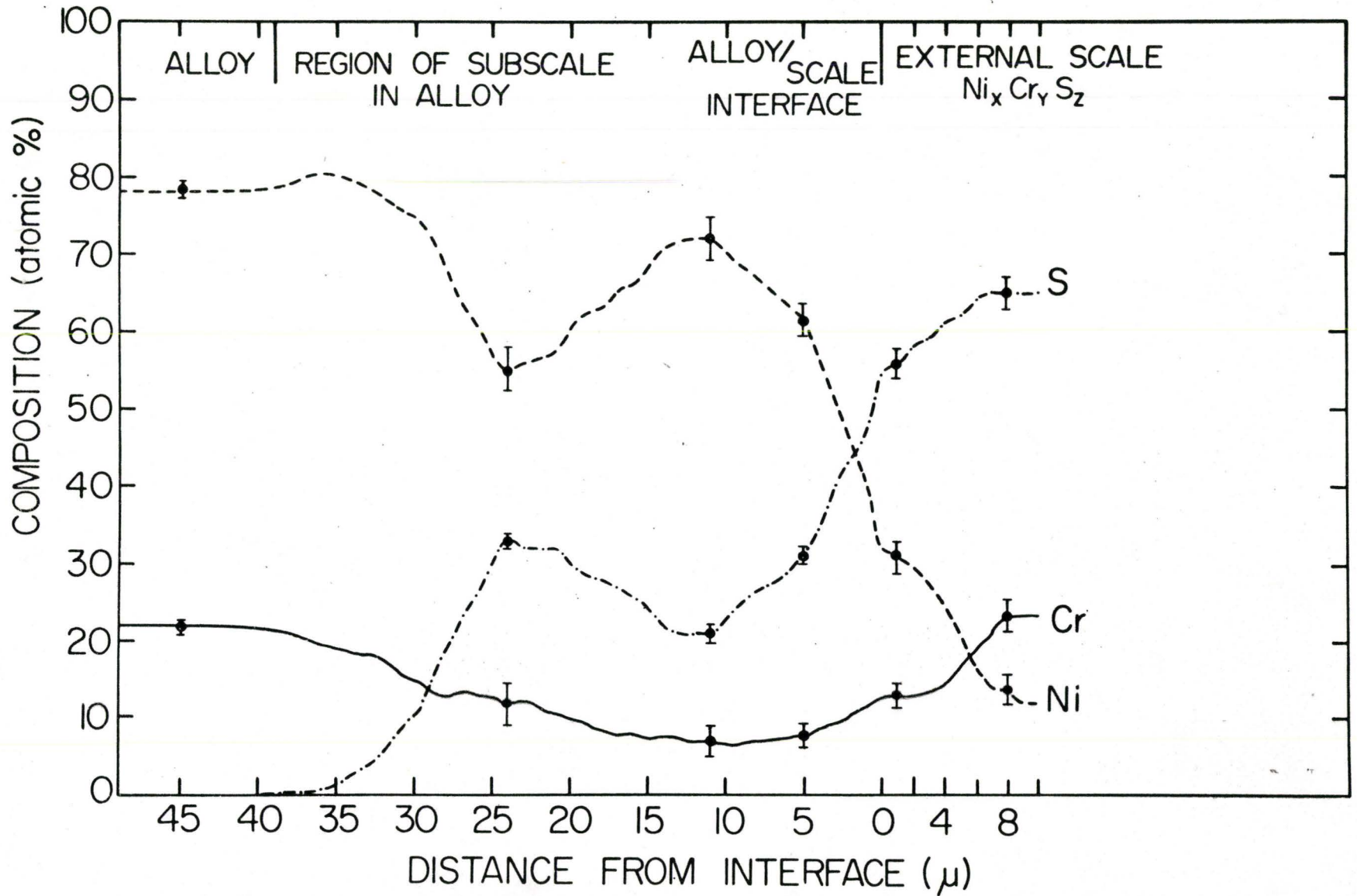


Fig. 5.17 Distribution profile after sulphidation at a sulphur potential of 8.8×10^{-10} atmospheres for 2 hours.

standard ratio all the chromium counts were considered to be from the sulphide and the sulphur counts were analysed for both chromium and nickel sulphide. The best value between the two values obtained from the two methods that matched the nickel and chromium apparent compositions was used.

The phase compositions identified in the external scales are summarized in Table 5.3. These compare favourably with the X-ray analyses following and with predictions that can be made from Fig. 3.3. Since the probe beam is larger than the subscale particle size the concentration profiles of the subscale regions are not a true representation of the situation. All that can be deduced from the data is that the peaks in the nickel curves are close to the concentration of nickel in the alloy in this region. Also, the high counts for sulphur between the peaks result from the electron beam interacting with both precipitated sulphides and the alloy. The sulphur concentration measured is much larger than its solubility in the alloy. Finally, much of the chromium is consumed in the sulphide formation.

5.3.2 X-ray Analysis

The X-ray analysis data are also summarized in Table 5.3. The specimens sulphidized at sulphur potentials below 5×10^{-10} atm. were analysed by the Debye-Scherrer powder technique using copper radiation. The specimen sulphidized at $P_{S_2} = 8.8 \times 10^{-10}$ was analysed with copper radiation on the X-ray diffractometer with a chart recorder since it was not possible to obtain a suitable powder from the scale.

Typical data from the powder technique is given in Appendix 1. There are certain problems encountered in analysing the X-ray data for chromium sulphides using A. S. T. M. cards since Jellinek⁽⁵⁰⁾ has shown that the sulphides in the range CrS to Cr_2S_3 yield very similar

TABLE 5.3

Phase Analysis of the External Scale by X-ray and Electron Microprobe Techniques.

SULPHUR POTENTIAL (atmospheres)	ELECTRON MICROPROBE ANALYSIS OF EXTERNAL SCALE		X-RAY ANALYSIS
	INSIDE	OUTSIDE	
5.5×10^{-12}	Cr _{0.41} Ni _{0.05} S _{0.54} Cr ₅ S ₆	Cr _{0.39} Ni _{0.02} S _{0.59} Cr ₃ S ₄ C ₂ S ₃	Cr ₃ S ₄
1.6×10^{-11}	Cr _{0.42} Ni _{0.02} S _{0.56} Cr ₃ S ₄	Cr _{0.39} Ni _{0.02} S _{0.59} Cr ₂ S ₃	Cr ₃ S ₄ (Cr ₂ S ₃)
6.5×10^{-11}	Cr _{0.42} Ni _{0.01} S _{0.57} Cr ₃ S ₄	Cr _{0.40} Ni _{0.01} S _{0.59} Cr ₂ S ₃	Cr ₃ S ₄ (Cr ₂ S ₃)
2.3×10^{-10}		Cr _{0.39} Ni _{0.02} S _{0.59} Cr ₂ S ₃	Cr ₃ S ₄ (Cr ₂ S ₃)
8.8×10^{-10}	Cr _{0.14} Ni _{0.28} S _{0.58}	Cr _{0.24} Ni _{0.12} S _{0.64}	No positive identification

X-ray patterns. Several stoichiometric forms of chromium sulphide are also expected to be present in any one scale. Although no absolutely clear cut identification could be made from the powder patterns obtained the best estimation possible has been made and this is well supported by the probe data and predictions that can be made from the data in Fig. 3.3.

CHAPTER VI

DISCUSSION

6.1 Introduction

A quantitative and qualitative analysis of the results obtained is discussed as two separate topics i. e., kinetics and morphology. In most cases the sulphur potentials of the hydrogen sulphide/hydrogen atmospheres used are lower than the dissociation pressure for nickel sulphide formation. As a result of this the nickel in the alloy behaves as a noble element and the product is chromium sulphide, mainly in the stoichiometric form of Cr_3S_4 , with some dissolved nickel.

The formation of the external scale and subscale observed obey parabolic kinetics when nickel is essentially noble. It is proposed that the reaction is diffusion controlled possibly by migration of chromium through the external scale although defect data of chromium sulphides is at present incomplete. It is also proposed that the diffusivity of chromium in the external scale is several orders of magnitude faster than the diffusivity of chromium in the alloy. This condition along with the fact that nickel is essentially noble is sufficient for morphological breakdown of the interface in accordance with the previously discussed Wagner mechanism⁽²⁹⁾. Thus, it is possible that diffusion of chromium in the alloy will contribute to the rate control of the process.

The formation of subscale in the alloy is discussed in terms of the theories already outlined. The data obtained from subscale penetration and volume fraction measurements are applied to a theoretical treatment of the process by Kirkaldy⁽³¹⁾. This results in an estimation

of the magnitude of the sulphur diffusivity in the alloy that satisfies the theoretical requirements for internal sulphidation.

6.2 Reaction Kinetics

6.2.1 Parabolic Kinetics

The parabolic reaction kinetics observed at sulphur potentials below 5×10^{-10} atmospheres indicate, according to the Wagner mechanism⁽¹⁹⁾, that the reaction is diffusion controlled. Whether diffusion is by cation migration via vacancies or interstitials or anion diffusion is still uncertain. The external scale has been identified as consisting of mainly Cr_3S_4 for which defect measurements have yet to be made. The detailed structure of the various stoichiometric forms of chromium sulphide has been studied by Young⁽⁵²⁾. All the sulphides have the NiAs type structure which may be described as approximately hexagonally close packed with the cations in the octohedral interstitial positions of the structure. Full occupation of the octohedral site sublattice is found only in the case of CrS. The sulphides higher than Cr_7S_8 have a cation sublattice consisting of alternately filled and partially-filled layers at right angles to the c axis. In the case of Cr_3S_4 every third cation site in the partially-filled layer is considered to be vacant and it has been proposed⁽⁷⁷⁾ that the partially-filled layers are occupied by Cr^{2+} ions whilst the completely-filled layers are occupied by Cr^{3+} ions. This description successfully accounts for the sulphide stoichiometry and its reported metallic conductivity⁽⁷⁷⁾.

According to the above description of Cr_3S_4 diffusion-controlled formation of the sulphide is expected to be via the vacancies on the Cr^{2+} sublattice which is p-type semiconducting behaviour as discussed in the theory. Since the plot of $\log k_p$ v's $\log P_{\text{S}_2}$ is non-linear the semi-

conducting behaviour of the external scale is not straightforward p-type. In fact Fig. 5.3 shows that the relationship between k_p and P_{S_2} is semilogarithmic with a positive linear slope. The significance of this relationship can be obtained by examining the mathematical formulation of the ternary diffusion model due to Wagner⁽⁷⁸⁾ for external scale formation on a binary alloy. Assuming that negligible sulphur dissolves in the alloy, the fluxes of cations of nickel and chromium in equivalents per unit area relative to the anion sub-lattice are:

$$J_{Ni (eq.)} = - \frac{D_{Ni} (1 - \epsilon)}{V_{eq.}} \frac{\partial \ln a_{Ni}}{\partial x} \quad (6.1)$$

$$J_{Cr (eq.)} = - \frac{D_{Cr} \epsilon}{V_{eq.}} \frac{\partial \ln a_{Cr}}{\partial x} \quad (6.2)$$

where $1 - \epsilon / V_{eq.}$ and $\epsilon / V_{eq.}$ are the local concentrations of nickel and chromium cations, respectively, in equivalents per unit volume. The activities of the elements nickel, chromium and sulphur and their sulphides are interrelated by

$$\mu_{Ni}^{\circ} + RT \ln a_{Ni} + \left(\frac{Z_{Ni}}{Z_S} \right) (\mu_S^{\circ} + RT \ln a_S) = \mu_{Ni(S)}^{\circ} + RT \ln a_{Ni(S)} \quad (6.3)$$

$$\mu_{Cr}^{\circ} + RT \ln a_{Cr} + \left(\frac{Z_{Cr}}{Z_S} \right) (\mu_S^{\circ} + RT \ln a_S) = \mu_{Cr(S)}^{\circ} + RT \ln a_{Cr(S)} \quad (6.4)$$

Now equations 6.1 and 6.2 can be rewritten by expressing the activities of nickel and chromium in the scale in terms of sulphur activity and the local equivalent fraction of chromium sulphide (ϵ). On application of the Gibbs-Duhem relationship

$$(1 - \epsilon) d \ln a_{Ni(S)} + \epsilon d \ln a_{Cr(S)} = 0 \quad (6.5)$$

equations 6.1 to 6.4 can be solved to give

$$J_{\text{Ni (eq.)}} = - \frac{D_{\text{Ni}} (1 - \epsilon)}{V_{\text{eq.}}} \left(\frac{\partial \ln a_{\text{Ni(S)}}}{\partial \epsilon} \frac{\partial \epsilon}{\partial x} - \frac{Z_{\text{Ni}}}{Z_{\text{S}}} \frac{\partial \ln a_{\text{S}}}{\partial x} \right) \quad (6.6)$$

$$J_{\text{Cr (eq.)}} = - \frac{D_{\text{Cr}} \epsilon}{V_{\text{eq.}}} \left(\frac{\partial \ln a_{\text{Cr(S)}}}{\partial \epsilon} \frac{\partial \epsilon}{\partial x} - \frac{Z_{\text{Cr}}}{Z_{\text{S}}} \frac{\partial \ln a_{\text{S}}}{\partial x} \right) \quad (6.7)$$

The sum of the fluxes of nickel and chromium at any distance x through the scale is related to the thickening of the scale by the equation

$$(J_{\text{Ni (eq.)}} + J_{\text{Cr (eq.)}}) V_{\text{eq.}} = \frac{d X_{\text{S}}}{dt} = \frac{k_r}{X_{\text{S}}} \quad (6.8)$$

Any distance, x , through the scale is defined such that

$$y = \frac{x}{X_{\text{S}}} \quad (6.9)$$

On substituting equations 6.6, 6.7, and 6.9 into equation 6.8 the following first order differential equation is obtained.

$$\begin{aligned} & D_{\text{Ni}} (1 - \epsilon) \left(- \frac{\partial \ln a_{\text{Ni(S)}}}{\partial \epsilon} \frac{d \epsilon}{dy} + \frac{Z_{\text{Ni}}}{Z_{\text{S}}} \frac{d \ln a_{\text{S}}}{dy} \right) \\ & + D_{\text{Cr}} \epsilon \left(- \frac{\partial \ln a_{\text{Cr(S)}}}{\partial \epsilon} \frac{d \epsilon}{dy} + \frac{Z_{\text{Cr}}}{Z_{\text{S}}} \frac{d \ln a_{\text{S}}}{dy} \right) = k_r \end{aligned} \quad (6.10)$$

Certain assumptions may be made about some of the parameters in equation 6.10 from observations of the external scale. Firstly, it is assumed that the nickel and chromium activities through the scale have very little variation, the sulphur activity being the controlling factor. Thus, equation 6.10 reduces to

$$k_r = (D_{Ni} + (D_{Cr} - D_{Ni}) \epsilon) \frac{Z_m}{Z_S} \frac{d \ln a_S}{dy} \quad (6.11)$$

where Z_m is the valency of both nickel and chromium which is assumed to be the same.

Since the concentration of nickel in the scale is very small the value of ϵ approaches unity so equation 6.11 may be rewritten as

$$k_r \approx D_{Cr} \epsilon \frac{Z_{Cr}}{Z_S} \frac{d \ln a_S}{dy} \quad (6.12)$$

This is equivalent to the parabolic rational rate constant for ambipolar diffusion in a binary system as derived by Wagner⁽¹⁹⁾ and given as equation 2.18. On integration of equation 6.12 the parabolic rational rate constant of the reaction controlled by chromium diffusion may be written as

$$k_r = C_{eq.} \int_{P_{S_2(i)}}^{P_{S_2(o)}} D_{Cr}^* \left(\frac{Z_{Cr}}{Z_S} \right) \cdot d \ln P_{S_2}^{1/2} \quad (6.13)$$

where D_{Cr}^* is the effective cation diffusion coefficient through the external scale, and $C_{eq.}$ is the equivalent concentration of cations in the sulphide in equivalents cm^{-3} .

From the above expression

$$\frac{d k_r}{d \ln P_{S_2}} = \frac{C_{eq.}}{2} \cdot \frac{Z_{Cr}}{|Z_S|} \cdot D_{Cr}^* \quad (6.14)$$

The parabolic reaction rate constant, k_p , is related to the parabolic rational rate constant by

$$k_p = k_r \cdot EW \cdot \rho \cdot 2. \quad (6.15)$$

where E. W. is the equivalent weight of sulphur

ρ is sulphide density.

Thus the slope of Fig. 5.3 is given by

$$\text{Slope} = \frac{d k_p}{d \log_{10} P_{S_2}} = 2.303 \cdot C_{eq.} \cdot EW \cdot \rho \cdot \frac{Z_{Cr}}{|Z_S|} \cdot D_{Cr}^* \quad (6.16)$$

Assuming the valency of both the anions and cations is 2 then equation 6.16 gives a value of $D_{Cr}^* = 1.5 \times 10^{-11} \text{ cm}^2 \text{ sec}^{-1}$ which means that the effective diffusivity of chromium ions across the external scale is considered constant.

Although the external scale has been identified as mainly Cr_3S_4 other stoichiometric forms of chromium sulphide are expected to be present to a lesser degree. As a result the concentration profile of chromium across the scale is not continuous but changes in steps at phase boundaries as shown by the probe results in Fig. 5.13 to 5.17. Although the concentration profile is not continuous it is proposed that the cation activity gradient is and, with the assumption that the scale is a semi-infinite medium, this would explain the apparent constant value for D_{Cr}^* obtained.

The lack of thermodynamic data on the chromium-sulphur system makes it difficult to make a completely quantitative application of the relationships between the rate of sulphidation of pure chromium and that of the alloy as proposed by Wagner⁽²⁸⁾ and given in equations 2.21 and 2.22. The parabolic rate constant obtained for the alloy in this work is approximately 1/20 of the value obtained by Lifshin et al⁽⁷⁾ for pure chromium obtained under very similar conditions. By applying this value to equation 2.22 it appears that X, the mole fraction of chromium in the alloy at the alloy-sulphide interface, approaches

X_{eq} , the mole fraction of chromium in the alloy that would be in equilibrium with chromium sulphide at the applied sulphur potential. From this it seems that the growth rate is equally determined by the interdiffusion process in the chromium depleted alloy layer, as shown by the microprobe results, as well as chromium diffusivity in the scale. Unfortunately, the Wagner analysis does not consider the case of simultaneous external and internal sulphidation. As will be shown later, since there is morphological breakdown and internal sulphidation the diffusivity of chromium in the alloy is expected to be several orders of magnitude lower than its diffusivity in the external sulphide scale. Thus the chromium concentration gradient through the subscale determines to some degree the flux of chromium entering the external scale and hence has an effect on its rate of formation. The diffusion of sulphur in the alloy is expected to be faster than that of chromium so that, with the low solubility product of chromium and sulphur to form the sulphide, internal sulphidation is given. This subscale acts as a sink for chromium and decreases the concentration of chromium through the subscale until a balance between internal and external scale formation is obtained. Thus, subscale formation should have an effect of reducing the over-all rate of attack.

6.2.2 Linear Reaction Kinetics

At a pressure above $P_{S_2} = 5 \times 10^{-10}$ linear kinetics were observed for the weight gain followed. It is felt that if the reaction were followed for a longer period of time parabolic reaction kinetics would be observed since the scale obtained was compact and pore-free. The model for this behaviour is a combination of short circuit and lattice diffusion of reactants, especially the nickel which is present to a much larger extent than previously observed.

At the other sulphur pressures where parabolic kinetics were observed the reactions were preceded by a region of slow non-parabolic kinetics due to some phase boundary reaction such as adsorption control of the gas at the scale/gas interface which might be expected at these low sulphur potentials. The reaction could also be controlled by the reaction at the metal/scale interface.

In the case where the specimen was preheated before sulphidation the reaction was inhibited by an oxide film formation on specimen surface as explained by Romeo and Spacil⁽⁵⁷⁾.

6.3 Morphology

6.3.1 The External Scale

The observed external scale stoichiometry from the microprobe results for samples sulphidized at sulphur potentials below 5×10^{-10} atmospheres is plotted against $\log_{10} P_{S_2}$ in Fig. 6.1. This curve is compared with equilibrium studies carried out by Young⁽⁵²⁾. It appears from this comparison that the stoichiometries of the chromium sulphides obtained exist at a lower sulphur potential than expected from the equilibrium studies. The composition of the outer edge of the external scale, as obtained by the microprobe analysis, is used for this comparison as it is the part of the scale in equilibrium with the measured reaction sulphur potentials. The X-ray analysis gives the general stoichiometry of the whole scale and is therefore not relevant.

It appears that the presence of nickel in the external scale in quantities up to 5 atom % has the effect of stabilizing the chromium sulphides i. e., it lowers the sulphide dissociation pressure. It is known⁽⁵⁾ that the presence of chromium in nickel sulphide has the

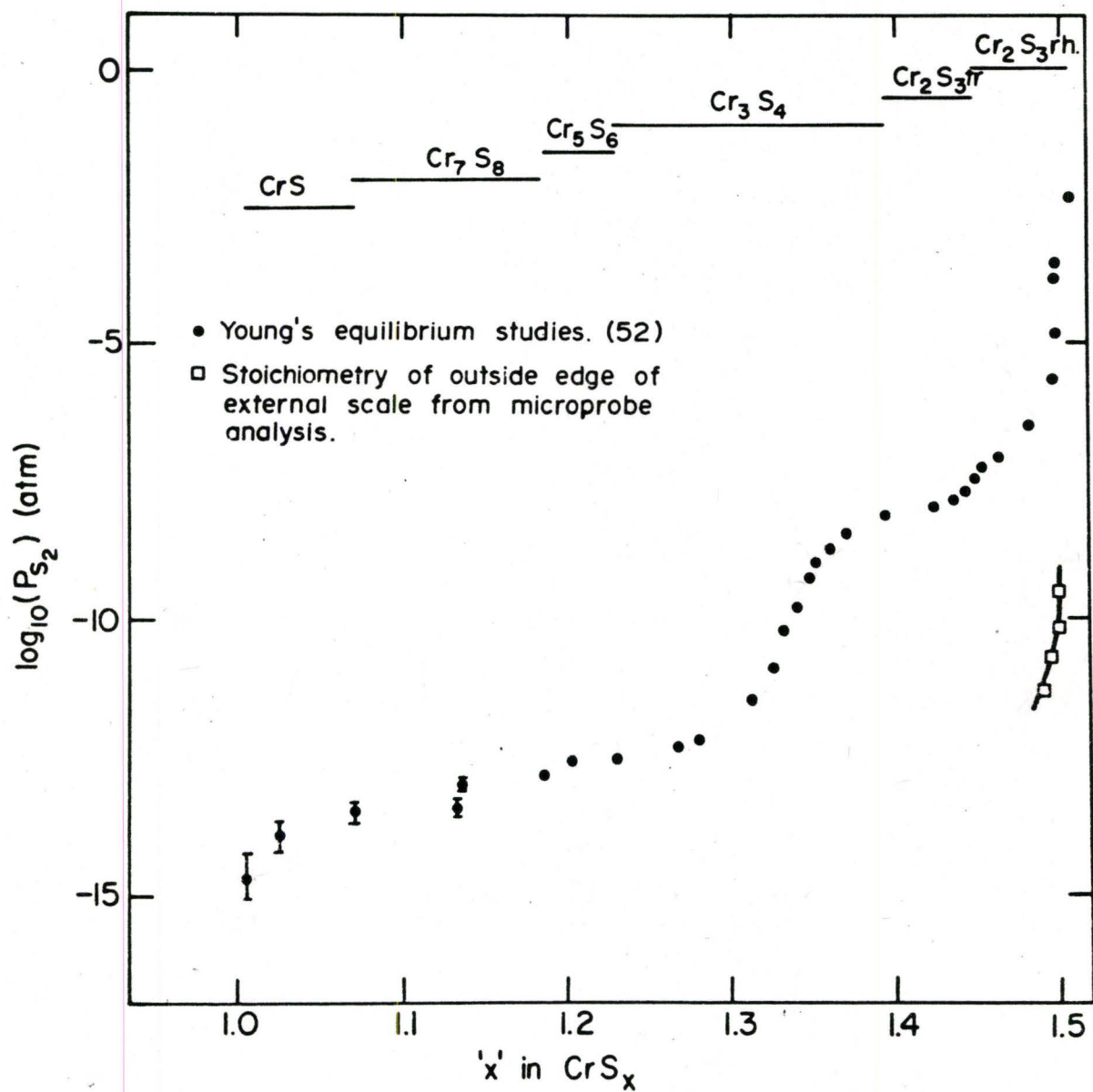


Fig. 6.1 Plot of external scale stoichiometry against sulphur potential compared with Young's⁽⁵²⁾ equilibrium studies.

same effect. In order to explain how this model works the Ni-Cr-S isothermal ternary phase diagram for 700°C given as Fig. 3.4⁽⁵⁸⁾ has been converted into a tentative phase diagram of sulphur potential against alloy composition as a mole fraction. The result is Fig. 6.2. The expected composition path for the reaction is shown as the broken line. From this diagram the expected scale identity is Cr₃S₄ with some Cr₂S₃ towards the higher sulphur potential at the scale outer interface.

In the case where the sulphur potential is such that the nickel may also sulphidize the single layer scale obtained could not be positively identified by X-ray analysis but is assigned a tentative composition of Ni Cr₂ S₅ as given by the microprobe analysis (Fig. 5.17). It seems from this that the scale is probably a solid solution of Cr₂ S₃ and nickel as shown by the region where the composition path ends in Fig. 6.2.

In all cases the external scale observed is grey and compact except at the lowest sulphur potential when an intermittent dark layer is observed at the alloy-scale interface as shown in Fig. 5.8. Unfortunately, this layer has not been identified and any deductions must be made from visual observations. The grey compact scales are thinner in the regions of the darker layers than where the dark layers do not exist. It is possible that this dark layer that occupies between 10 and 20% of the interfacial area is a porous sulphide. The porosity could be caused by metal migration and vacancy condensation due to the slow reaction rate.

The external scale thickness measurements can be used to calculate an approximate value for the diffusivity of chromium in the scale. It is assumed that the scale is a semi-infinite single phase and there is non-steady state diffusion. Under these conditions

$$x = 2 \sqrt{D_{Cr}^* t} \quad (6.17)$$

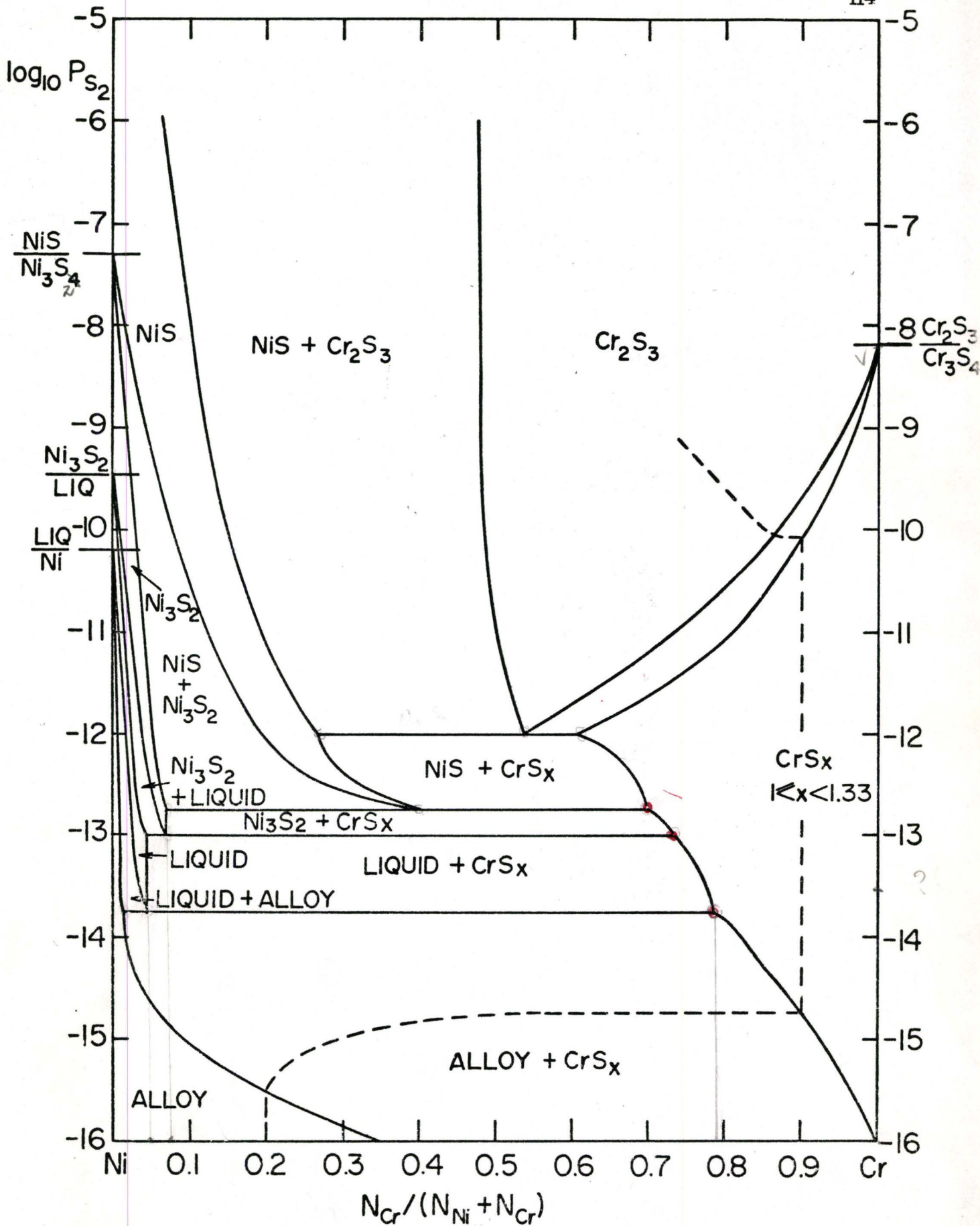


Fig. 6.2 Plot of sulphur potential ($\log_{10} P_{S_2}$) against alloy composition as a mole fraction to give a $\log_{10} P_{S_2}$ tentative phase diagram for the Ni-Cr-S system at 700°C .

where x is scale thickness.

At $P_{S_2} = 2.3 \times 10^{-10}$ it was found that D_{Cr}^* has an approximate value of $8 \times 10^{-12} \text{ cm}^2 \text{ sec}^{-1}$ which is of the same order as the value calculated from the slope of Fig. 5.3.

6.3.2 Morphological Breakdown

Monma et al⁽⁷⁹⁾ have found that the diffusivity of chromium in the Ni-19.9% Cr alloy obeys the following relationship at elevated temperature.

$$D_{Cr}^{\text{Alloy}} = 1.9 \exp \frac{-67700}{RT} \text{ cm}^2 \text{ sec}^{-1} \quad (6.18)$$

This gives a value of 1.5×10^{-15} at 700°C . Since the experimental conditions are such that nickel does not sulphidize and remains in the alloy then chromium is the only diffusing species. It has been shown that the diffusivity of chromium in the external scale is several orders of magnitude greater than its diffusivity in the alloy. As discussed in section 2.3.3 (c) the external scale/alloy interface is likely to be unstable if the chromium diffuses through the scale faster than it does through the alloy. By applying the data obtained to equation 2.24 the following approximate result is obtained

$$\frac{X_{Cr}}{1 - X_{Cr}} \frac{(D_{Cr}/V)_{\text{alloy}}}{(D_{Cr}^*/V)_{\text{sulphide}}} \approx \frac{1}{9} \cdot \frac{10^{-15}}{10^{-11}} < 1 \quad (6.19)$$

which satisfies the Wagner necessary (but not sufficient) condition for instability of the planar interface. Unfortunately, the more comprehensive model for interface instability proposed by Coates and Kirkaldy⁽⁸⁰⁾ cannot be tested due to the lack of data obtained.

The morphological breakdown of the interface under these experimental conditions can be compared to the planar interface obtained by Romeo et al⁽⁵⁾ at the higher sulphur potentials. In their case the nickel was free to diffuse out through the inner chromium sulphide scale to the outer nickel sulphide layer which acts as a sink. In this case the alloy interdiffusion coefficient must be greater than the diffusivity of the nickel in the inner sulphide layer.

6.3.3 Internal Sulphidation

The formation of subscale is expected to follow parabolic kinetics as first proposed by Rhines et al⁽⁸¹⁾ and later Wagner⁽³⁰⁾. The mathematical treatments by Wagner are for planar interfaces and do not apply exactly to cases where morphological breakdown of the interface occurs, but they do show the importance of the rate of sulphur diffusion into alloy. A better treatment of the situation has been made by Kirkaldy⁽³¹⁾ and is relevant to the situation where simultaneous external scale and subscale is formed with breakdown of the interface. This has been discussed in section 2.3.3. (d) and equation 2.28 is particularly relevant in order to establish an approximate value for the diffusivity of sulphur in the alloy.

The subscale penetration data for specimens sulphidized at a potential of 6.5×10^{-11} atm. plotted in Fig. 5.12 is replotted in Fig. 6.3 as a function of $\sqrt{\text{time}}$ in hours. This shows that the subscale formation does in fact obey parabolic kinetics. Now equation 2.28 can be rewritten as follows:

$$P(x, t) = \frac{D_s^{\text{Alloy}} - D_{\text{Cr}}^{\text{Alloy}}}{D_{\text{Cr}}^{\text{Alloy}}} C_s \operatorname{erf} c \frac{k_1}{2 \sqrt{D_{\text{Cr}}^{\text{Alloy}}}} \quad (6.20)$$

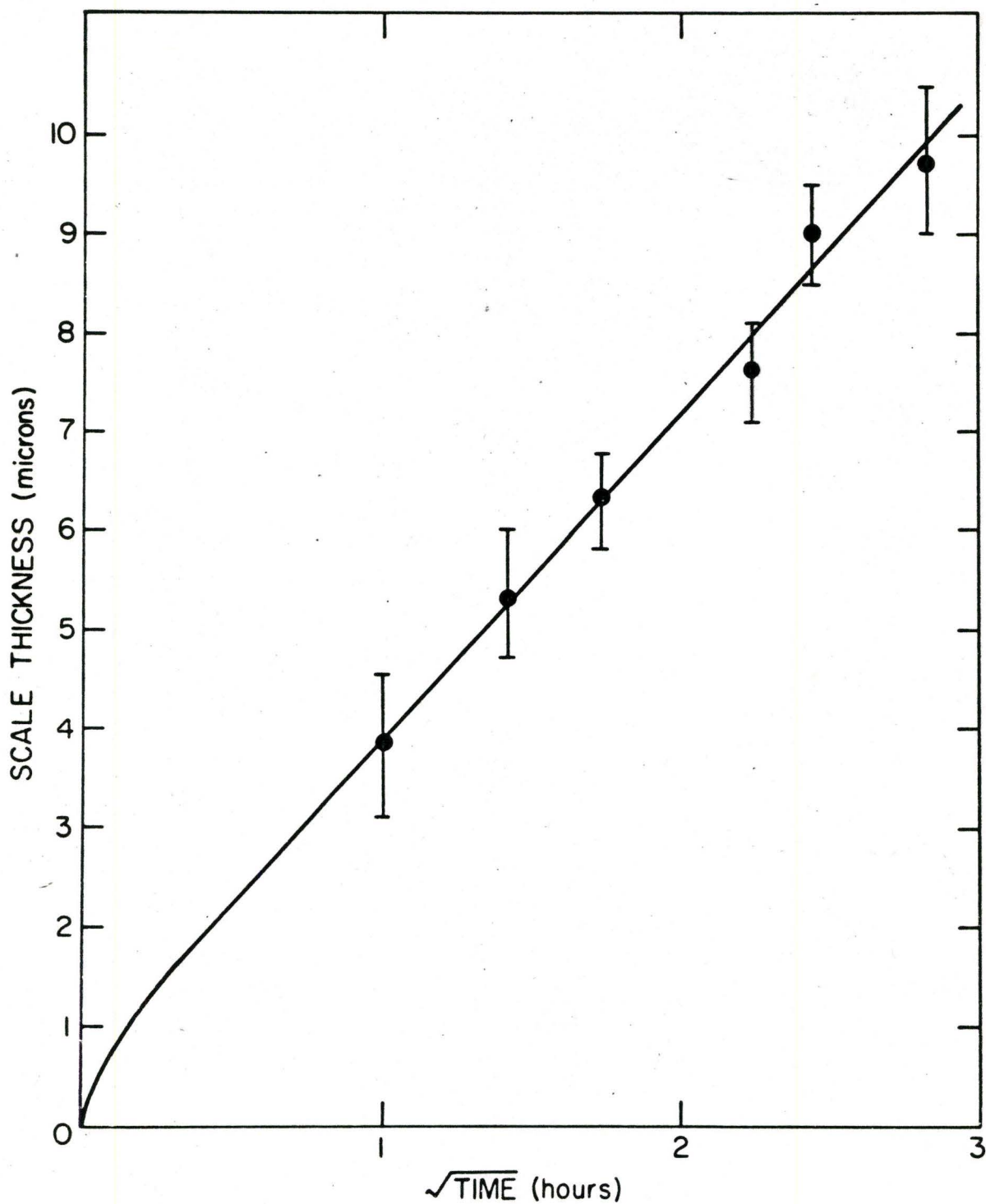


Fig. 6.3 Plot of subscale penetration against the square root of time for specimens sulphidized at a sulphur potential of 6.5×10^{-11} atm.

where $P_{(x,t)}$ is volume fraction occupied by subscale sulphide at penetration depth x after time t .

D_S, D_{Cr} are diffusivities of S and Cr in the alloy resp.

C_S is solubility of sulphur in pure nickel

k_1 is parabolic rate constant for subscale formation and is equal to x/\sqrt{t} .

The following parameters are known or have been approximately calculated: $P_{(x,t)}$, D_{Cr}^{Alloy} , C_S and k_1 . Thus on introducing these known parameters into equation 6.20 it has been found that the diffusivity of sulphur in the alloy has an approximate value of $1 \times 10^{-12} \text{ cm}^2 \text{ sec}^{-1}$. A test for the Kirkaldy treatment using the relationship for penetration depth $X_P = 2 \sqrt{D_{Cr}^{Alloy} t}$ yields a value for D_{Cr}^{Alloy} in the order of $10^{-11} \text{ cm}^2 \text{ sec}^{-1}$. The Wagner treatment given as equation 2.29 yields a value for $D_S^{Alloy} \approx 10^{-11} \text{ cm}^2 \text{ sec}^{-1}$. This treatment considers the sulphur diffusivity as the controlling factor for subscale penetration and since the alloy throughout the subscale region is chromium depleted the latter treatment is probably more valid.

The value of sulphur diffusivity in the alloy can be compared with the value for chromium diffusivity calculated previously as approximately 1.5×10^{-15} . Thus, the diffusivity of sulphur into the alloy is several orders of magnitude faster than the counter diffusion of chromium. This is a necessary condition for the 'in situ' precipitation of internal sulphide. The following model is proposed to explain the mechanism of the subscale formation obtained. Since the subscale has a vague dendritic appearance with the formation of large irregular sulphide particles the sulphur is believed to diffuse into the alloy via preferred paths such as grain boundaries, dislocations and subgrain boundaries to a greater extent than through the grains as a whole. These preferred diffusion paths also act as preferred sites for nucleation and growth of the sulphide particles so a majority of the sulphide will precipitate at these points by chromium diffusion towards them. The solubility product of chromium and sulphur in the alloy is expected to be very low and the precipitated sulphide to be

fairly unstable so that the particles will grow by an Ostwald ripening effect thus creating the vague dendritic appearance.

In an effort to satisfy the thermodynamics for internal sulphidation a tentative composition path has been plotted on the ternary phase diagram for the Ni-Cr-S system at 700°C and is represented in Fig. 6.4. Since the composition path cuts the tie lines in the region that represents the CrS/Alloy interface the conditions for internal precipitation of sulphide are satisfied. The point at which the traverse is made represents the volume fraction of internal precipitate.

6.3.4 External Scale Stringers

It has been noted that stringers appear in the external scales after long periods of growth. Although these stringers have not been identified they are believed to be almost pure nickel as they emanate from the alloy peaks of the broken-down external scale/alloy interface. Since these stringers appear to be associated with the scale grain boundaries it is proposed that they are formed by a 'squeeze' mechanism. It is felt that as the break-down of the interface proceeds with time the alloy is forced down low resistance paths such as grain boundaries by sulphide formation which occupies a greater volume than the consumed chromium from the alloy.

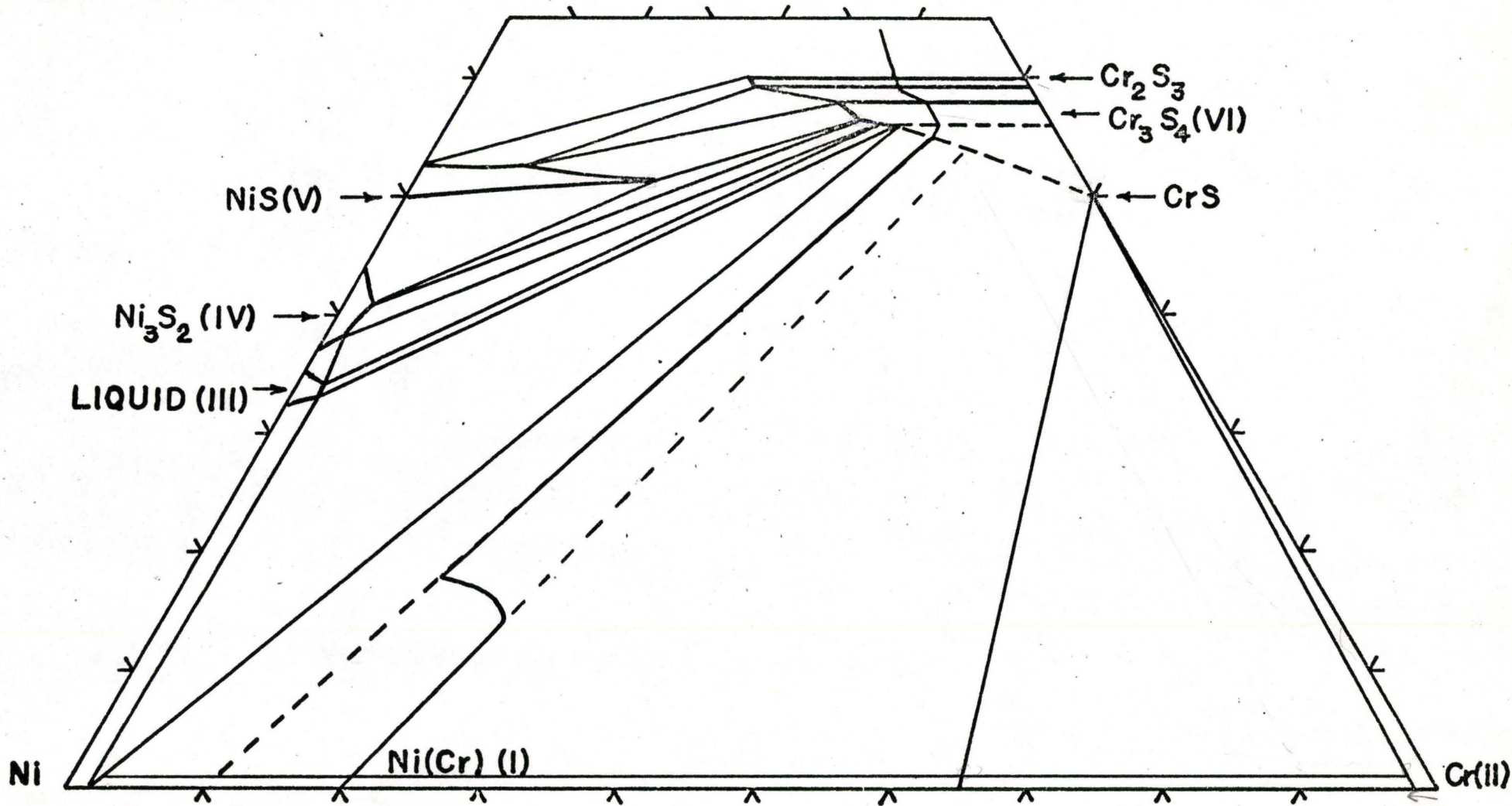


Fig. 6.4 700°C isotherm of Ni-Cr-S phase diagram showing tentative composition path.

CHAPTER VII

SUMMARY

1. At sulphur potentials below 5×10^{-10} atmospheres the reaction kinetics are parabolic with rates approximately 1/20 of those observed for pure chromium at similar potentials.
2. The reaction appears to be controlled by the rates of diffusion of chromium through both the external scale and the alloy.
3. The parabolic reaction rate varies semilogarithmically with sulphur potential the positive slope of which yields a constant value for chromium diffusivity in the order of $1.5 \times 10^{-11} \text{ cm}^2 \text{ sec}^{-1}$.
4. At a sulphur potential above 5×10^{-10} atmospheres the reaction kinetics are linear but since the reaction product is compact the kinetics are expected to become parabolic.
5. At all sulphur potentials the reaction product consists of a grey, compact, pore-free external scale and a subscale with morphological break-down of the external scale/alloy interface.
6. At sulphur potentials below 5×10^{-10} atmospheres the external scale is identified as mainly Cr_3S_4 with traces of dissolved nickel up to 5% and higher and lower sulphides to a lesser degree.
7. The dissolved nickel in the external scale appears to stabilize

the chromium sulphides i. e. , lower their dissociation pressures.

8. The diffusivity of chromium in the external scale (in the order of $10^{-11} \text{ cm}^2 \text{ sec}^{-1}$) is several orders of magnitude greater than the diffusivity of chromium in the alloy ($10^{-15} \text{ cm}^2 \text{ sec}^{-1}$) which satisfies the Wagner conditions for morphological breakdown.
9. Volume fraction measurements of the region occupied by subscale when applied to theoretical predictions for internal sulphidation yield a value of sulphur diffusivity in the alloy in the order of $10^{-11} \text{ cm}^2 \text{ sec}^{-1}$ which, since it is faster than the diffusivity of chromium in the alloy and its solubility is very low, satisfies conditions for subscale formation.
10. At a sulphur potential above 5×10^{-10} atmospheres the external scale has an apparent composition of NiCr_2S_5 and this is more dense than the chromium sulphides obtained at lower sulphur potentials.

CHAPTER VIII

FUTURE WORK

A comprehensive study of the kinetics and morphology for the sulphidation of the 80% Ni - 20% Cr alloy at elevated temperature (700°C) over a wide range of sulphur potentials is now fairly complete. Although the mechanisms of this reaction are still uncertain work on basic thermodynamic, diffusion and defect data as well as structural studies are in progress.

The formation of subscale at the low sulphur potentials where nickel behaves as an essentially noble alloy element eliminates any benefit gained from the slow formation of a compact, protective external scale of chromium sulphide. It appears that the next step is to study the effect of adding a third element to the alloy in an attempt to obtain improved sulphidation resistance either by selective sulphidation of the third element or by forming an external scale with the third element in solid solution.

Aluminium is certainly one element that should be considered as this is already in use for some turbine blade applications. Molybdenum and vanadium are also elements that have the potential of giving added resistance as reported by Strafford and Hampton⁽⁵⁶⁾. Once again basic information for these systems is expected to be sparse and initial studies will only report kinetic and basic morphological information.

APPENDIX

X-RAY ANALYSIS DATA

Typical measurements of the Debye-Scherrer powder photograph lines are listed in the table below and are compared with the standard A. S. T. M. data card information for Cr_3S_4 and trigonal Cr_2S_3 . The relative intensities of the lines are given as s (strong), m (medium) and blank (weak). The data for the lower sulphur potential is very close to Cr_3S_4 whereas the high potential data, although close to Cr_3S_4 , possesses some Cr_2S_3 characteristics.

SAMPLE LINE	DATA FOR ASTM FILE d (Å)		STANDARD	ASTM DATA
	5.5×10^{-12} atm.	2.3×10^{-10} atm.	Cr_3S_4	Cr_2S_3 (trig.)
1	5.62 m	5.57 m	5.64 m	5.56
2	5.27	5.18	5.27	5.17
3	2.97 s	3.26	5.21 m	3.01
4	2.63 s	2.96 m	2.97s m	2.97
5	2.60 s	2.63 s	2.642 s	2.62 s
6	2.52	2.58 s	2.606 m	2.505
7	2.20	2.51	2.531	2.12
8	2.07 m	2.18	2.198	2.052 m
9	2.05 s	2.04 s	2.076 m	2.036 s
10	2.03 s	2.01 s	2.059 s	1.714 m
11	2.02 m	1.71 s	2.032 s	1.579 m
12	1.72 m	1.57 m	2.021 m	1.311 m
13	+	1.31 m	1.718 m	
14	very weak lines	+ many weak lines	1.713 m	

REFERENCES

1. S. Mrowec, T. Werber, and M. Zastawink, *Corrosion Sci.*, 6, 47 (1966).
2. P. Hancock, *First International Conference on Metallic Corrosion*, London, 1961, p.193 (1962).
3. A. Davin, D. Coutsouradis, M. Urbain and L. Habraben, *Ind. Chim. Belge*, 30, 340 (1965).
4. A.U. Seybolt, *Trans. A.I.M.E.*, 242, 1955, (1968).
5. G. Romeo, W.W. Smeltzer and J.S. Kirkaldy, *J. Electrochem. Soc.*, 118, 740 (1971).
6. G. Romeo, W.W. Smeltzer and J.S. Kirkaldy, *ibid*, 118, 1336, (1971).
7. E. Lifshin, A. V. Seybolt and J.B. Hudson, *General Electric Co.*, Report No. 70-C-134 (April 1970).
8. O. Kubaschewski and B. E. Hopkins, *Oxidation of Metals and Alloys*, London, Butterworths, 1962.
9. U.R. Evans, *The Corrosion and Oxidation of Metals*, London, Edwin Arnold, 1960.
10. K. Hauffe, *Oxidation of Metals*, New York, Plenum Press 1965.
11. P. Kofstad, *High Temperature Oxidation of Metals*, New York, Wiley, 1966.
12. J. Bénard, *Oxidation des Métaux*, Paris, Gauthier-Villiers, 1962-4.
13. K.N. Strafford, *Met. Rev.*, 138, 153 (1969).
14. J. Berkowitz, *Elemental Sulphur: Chemistry and Physics*, Chapter 7, 1962: New York and London (John Wiley).

15. R. D. Freeman, Oklahoma State University Research Found. Rep. (60), 1962.
16. H. J. T. Ellingham, J. Soc. Chem. Ind., 63, 125 (1944).
17. F. D. Richardson and J. H. E. Jeffes, J. Iron and Steel Inst., 171, 165 (1952).
18. O. Kubaschewski, E. L. Evans, and C. B. Alcock, Metallurgical Thermochemistry, Oxford Inc. (Pergamon Press) 1967.
19. C. Wagner, Z. Phys. Chem. (B), 21, 25 (1933).
20. M. Lafitte and J. Benard, Compt. Rend. 242, 518 (1956).
21. W. Biltz, Z. Anorg. Chem. 228, 275 (1936).
22. N. B. Pilling and R. E. Bedworth, J. Inst. Metals, 29, 529 (1923).
23. F. P. Fehlner and N. F. Mott, J. Oxid. of Metals, 2, 59 (1970).
24. R. C. Logani and W. W. Smeltzer, Trans. Can. Met. Quart., 10, 149 (1971).
25. C. Wagner, 'Pittsburg International Conference on Surface Reactions', p. 77, 1948, Pittsburgh (Corrosion Publishing Co.).
26. J. Moreau and J. Benard, L'Oxydation des Metaux, Vol. 1, 318, Gauthier-Villars, Paris 1962.
27. G. C. Wood, Oxidation of Metals, 2, 11 (1970).
28. C. Wagner, J. Electrochem. Soc., 99, 369 (1952).
29. C. Wagner, *ibid*, 103, 571 (1956).
30. C. Wagner, Z. Electrochem. 63, 772 (1959).
31. J. S. Kirkaldy, Can. Met. Quart., 8, 35 (1971).
32. L. Onsager, Ann. N. Y. Acad. Sci., 46, 241 (1945-46).
33. J. S. Kirkaldy "Advances in Materials Research", Vol. 4, H. Herman, ed. Wiley N. Y. 1970.

34. J. S. Kirkaldy and D. G. Fedak, *Trans. AIME*, 224, 490, (1962).
35. J. S. Kirkaldy and L. C. Brown, *Can. Met. Quart.*, 2, 89 (1963).
36. D. E. Thomas, *J. of Metals*, 3, 926 (1951).
37. C. Wagner, *Corrosion Sci.*, 8, 889 (1968).
38. S. Zelouf and G. Simkovich, *Trans. AIME.*, 245, 875 (1969).
39. G. N. Lewis and M. Randall, 'Thermodynamics' p. 173, McGraw Hill, N. Y. (1961).
40. T. Rosenqvist, *J. I. S. I.*, 176, 37 (1954).
41. G. Kellerud and R. A. Yund, *J. of Petrology*, 3, 126 (1962).
42. K. Hauffe and H. G. Flindt, *Z. Physikal Chem.*, 200, 199 (1952).
43. L. Czerski, S. Mrowec, T. Werber, *J. Electrochem. Soc.*, 109, 273 (1962).
44. A. Dravnieks, *ibid*, 102, 435 (1955).
45. K. Hauffe and A. Rahmel, *Z. Physical Chem.*, 199, 152 (1952).
46. I. Pfeiffer, *Z. Metallkunde*, 49, 267 (1958).
47. J. E. Dutrizac and T. R. Ingraham, *Can. Met. Quart.* 8, 119 (1969).
48. A. Brückman, S. Mrowec and T. Werber, *Fiz. metal. metalloved*, 20, 702 (1965).
49. A. El Goresy and G. Kellerud, *Carnegie Institution Yearbook*, p. 182 (1966-67).
50. F. Jellinek, *Acta Cryst.* 10, 620 (1957).
51. P. N. Smith, private communication.
52. D. Young, private communicate.
53. T. Kamigaichi, *J. Sci. Hiroshima Univ.*, 24, 371 (1960).
54. V. I. Arkorov, V. N. Konev, and V. P. Pavlova, *Fiz. Metal. Metalloved*, 9, 701 (1960).

55. A. Davin and D. Coutsouradis, *Cobalt*, 17, 23, (1962).
56. K.N. Strafford and A.F. Hampton, *J. Less Common Metals*, 21, 305 (1970).
57. G. Romeo and H. S. Spacil, private communication.
58. J. S. Kirkaldy, G. Bolze, D. McCutcheon and D. J. Young, submitted to *Met. Trans.* (Sept. 1972).
59. G. Romeo and W. W. Smeltzer, *J. Electrochem. Soc.*, 119, 1267 (1972).
60. K.N. Strafford and A. F. Hampton, *J. Less Common Metals*, 25, 435 (1971).
61. C. J. Bechtold and H. C. Vacher, *Trans. A. I. M. E.* 221, 14 (1961).
62. J. Romanski, *Corrosion Sci.*, 8, 67 (1968).
63. T. Rosenqvist and B. L. Dunicz, *Trans. A. I. M. E.*, 194, 604, (1952).
64. R. J. Brigham, H. Neumayer and J. S. Kirkaldy, *Can. Met. Quart.*, 9 525 (1970).
65. W. A. West and A. W. C. Menzies, *J. Phys. Chem.* 33, 1880 (1929).
66. L. A. Morris and W. W. Smeltzer, *Acta. Met.*, 15, 1591 (1967).
67. F. C. Ochsner, *Product Engineering*, 19, 126 (1948).
68. L. A. Morris, Ph. D. Thesis, McMaster University, Hamilton, Ontario (1965).
69. J. D. Hager, Ph. D. Thesis, MIT, Cambridge, Mass. (1966).
70. D. Yuan and F. A. Kroger, *J. Electrochem. Soc.*, 118, 841, (1971).
71. J. A. N. A. F. Thermochemical Tables, p. 13168370 (1964) U. S. Dept. of Com., Nat. Bur. St.
72. C. W. Bale and J. M. Toguri, *J. Thermal Analysis*, 3, 153 (1971).

73. H. Braune, S. Peter and V. Neveling, *Z. Naturforsch.*, 69, 32 (1951).
74. A. G. Gaydon, *Dissociation Energies and Spectra of Diatomic Molecules*, J. Wiley and Sons, N. Y. (1947).
75. G. St. Pierre and J. Chipman, *J. Am. Chem. Soc.*, 74, 1023 (1952).
76. B. L. Dunicz and T. Rosenqvist, *Analytical Chem.*, 24, 404 (1952).
77. R. J. Bouchard and A. Wold, *J. Phys. Chem. Solids*, 27, 591 (1966).
78. C. Wagner, *Corrosion Sci.* 9, (1969).
79. K. Monma, H. Suto and H. Oikawa, *J. Japan, Inst. Metals*, 28, 188 (1964).
80. D. E. Coates and J. S. Kirkaldy, *Trans. A. S. M.* 62, 426 (1969).
81. F. N. Rhines, W. A. Johnson and W. A. Anderson, *Trans., T. M. S-AIME*, 147, 205 (1942).